FUNDAMENTAL STUDY OF SILICATE SUBSTITUTED NANOSTRUCTURED CALCIUM PHOSPHATES (NANOSICAPS) AND 3-D SCAFFOLDS FOR NON-VIRAL GENE DELIVERY

by

Sudhanshu Shekhar

B.S. Biotechnology, Christ University, 2010

M.S. Regenerative Medicine, Manipal University, 2012

Submitted to the Graduate Faculty of

Swanson School of Engineering in partial fulfillment

of the requirements for the degree of

Doctor of Philosophy

University of Pittsburgh

2018

UNIVERSITY OF PITTSBURGH

SWANSON SCHOOL OF ENGINEERING

This dissertation was presented

by

Sudhanshu Shekhar

It was defended on

October 16, 2018

and approved by

Bryan N. Brown, Ph.D., Assistant Professor, Department of Bioengineering

Julie A. Phillippi, Ph.D., Assistant Professor, Department of Cardiothoracic Surgery

Steven R. Little, Ph.D., William Kepler Whiteford Endowed Professor, Department of Chemical and Petroleum Engineering

Dissertation Director: Prashant N. Kumta, Ph.D., Edward R. Weidlein Chair Professor, Department of Bioengineering, Chemical and Petroleum Engineering, Mechanical Engineering and Materials Science

FUNDAMENTAL STUDY OF SILICATE SUBSTITUTED NANOSTRUCTURED CALCIUM PHOSPHATES (NANOSICAPS) AND 3-D SCAFFOLDS FOR NON-VIRAL GENE DELIVERY

Sudhanshu Shekhar, Ph.D.

University of Pittsburgh, 2018

Nanostructured calcium phosphate (NanoCaPs) particles are biocompatible and non-toxic bioceramics widely studied owing to their structural and compositional similarity to the mineralized tissue architecture of native bone. They are therefore considered as an ideal choice for gene delivery applications in bone tissue engineering. However, NanoCaPs are typically characterized by variable transfection, short shelf life due to particle aggregation, and difficulties associated with endosomal escape. The objectives of this dissertation were therefore crafted to develop strategies to circumvent, if not eliminate, some of the limitations that have previously stymied the success of NanoCaPs as a non-viral gene delivery vector for bone tissue engineering applications.

A modified version of NanoCaPs containing critical concentration of silicate ions substitutions were synthesized, aptly called NanoSiCaPs. Fundamental understanding of the influence of silicate ion substitutions in the NanoCaPs lattice structure was conducted using various materials characterization techniques. *In-vitro* transfection results indicated, a two-fold increase in transfection levels exhibited by NanoSiCaPs, owing to the enhanced dissolution kinetics and

ability to limit particle aggregation. Subsequently, two different strategies were developed to achieve scaffold mediated gene delivery via generation of plasmid DNA bound to NanoSiCaPs (NanoSiCaPs complexes, NC). First, a novel and simple coating methodology was developed using NCs adsorbed on Ti-surfaces coated with polyelectrolyte. Surface characterization results indicated successful generation of the nanoceramic coating on the Ti-surfaces. Additionally, it was demonstrated that the Ti-polyelectrolyte-NC assemblies contribute to surface mediated gene transfection, without eliciting any cytotoxicity. Second, a lyophilization technique was developed that enabled long-term storage of the NCs under ambient conditions, without inducing either a significant change in particle size or loss in gene transfection efficiency. Subsequently, a 3-D gene delivery system comprising fibrin hydrogels and lyophilized NCs was developed. *In-vitro* transfection results indicated that gene expression mediated via synthesized gels can be meticulously controlled by modulating the amounts of fibrinogen and NCs utilized in the synthesis of the gels. In conclusion, the studies demonstrate creation of next generation NanoCaP vectors, NCs and their implementation in the development of 3-D scaffolds serving as effective gene delivery agents as well as functional scaffolds for bone tissue repair and regeneration.

TABLE OF CONTENTS

LIST OF TABLES

LIST OF FIGURES

PREFACE

To my uncle:

Dr. Rudra Pratap

Thank you for your inspiration.

This work would not have been possible without the guidance of my committee - Dr. Julie A. Phillippi, Dr. Bryan N. Brown and Dr. Steven R. Little. Special thanks to Dr. Abhijit Roy and Dr. Abhinav Acharya for their continued feedback and advice at many steps along the way. Thank you to the Department of Bioengineering for your support over the many years. Thank you Dr. Prashant N. Kumta for taking me as a graduate student and giving me the opportunity to work in your laboratory. Thank you for entrusting me with the gene delivery project and giving me freedom to explore roles beyond my primary research in lab.

A huge thank to all my friends I have made here in the city of Pittsburgh who have supported me throughout this process. Thanks to all the Dr. Kumta lab members. I have learnt a lot from working with everyone in the lab.

Of course, I could not have made it through without the love and support from my parents Rana Pratap Singh and Dewanti Singh. Thank you for always believing in me and giving me the independence to follow my passions. And finally, a big thank you to my partner Babes Maust, aka Ruth Maust for your love and support.

1.0 INTRODUCTION

1.1 BONE TISSUE

Bone tissue is a dynamic, highly vascularized tissue that provides essential mechanical and structural support to the body. Due to its high degree of vascularization, bone tissue is constantly undergoing phases of resorption (via osteoclasts) and reformation (via osteoblasts) [1]. Bone healing involves a complex set of events encompassing many genetic and molecular triggers, morphogens, signaling molecules, and transcriptional regulators that act in concert during specific stages of bone tissue remodeling process [2]. However, healing capacity of bone in some situations might be limited or insufficient to heal large bone defects. Without medical intervention, the response of the body is relatively limited and is mainly restricted to repair processes, and repair in most scenarios does not lead to the restoration of normal structure and function [3]. Therefore, biomaterial-based tissue engineering strategies for regeneration of damaged bone tissues are being developed and evaluated that may enable the repair of tissues with high complexity, while avoiding excessive inflammation and an immune response to the medical implants [3].

1.2 TISSUE ENGINEERING AND REGENERATIVE MEDICINE

Tissue engineering is a multifaceted discipline combining the fields of materials science, bioengineering, pharmacy, life sciences and medicine towards the development of biological substitute materials, systems and devices, with a common goal to induce regeneration of damaged or diseased organs within the body [4-6]. The field of tissue engineering thus ranges from controlling cellular responses to material implants, manipulating the healing micro environment for tissue growth and implant integration, to developing a fundamental understating of many biological processes that guide tissue regeneration [4, 7]. Traditional tissue engineering approaches involved use of either or both, a biomaterial scaffold that allowed cell infiltration, proliferation and subsequent regeneration; or cell therapy, where autologous or allogenic cells are implanted at defect sites to stimulate repair [5, 7].

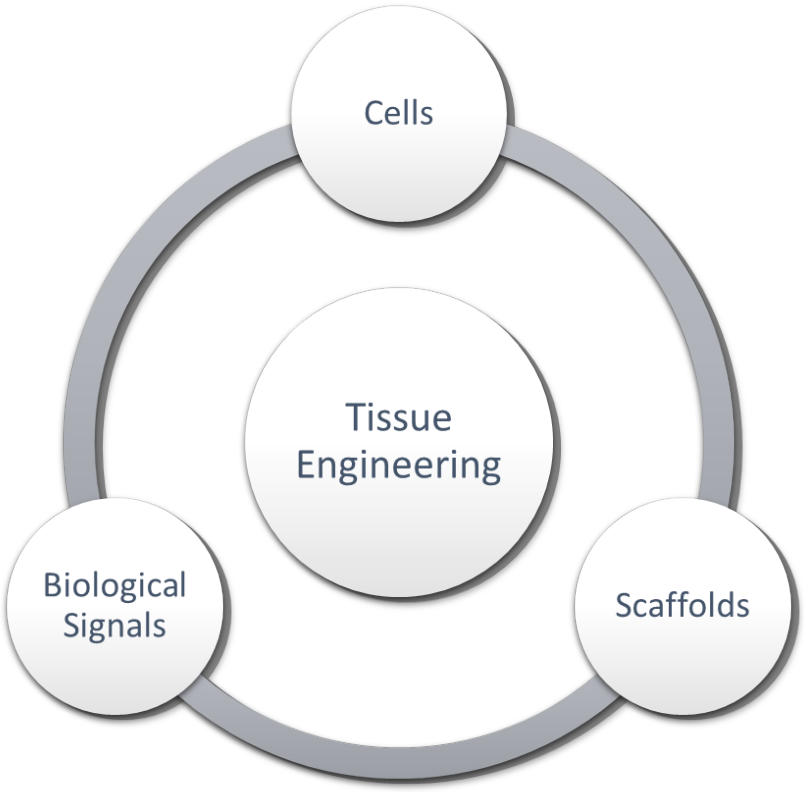

Figure 1.1. Tissue engineering strategies

More recently, an innovative approach has evolved that involves incorporation of regenerative stimuli into biomaterial scaffolds to enhance the regenerative response to host cells, termed as in-situ tissue engineering [7]. This approach involves incorporation of growth factors [8, 9], cytokines [10, 11], genetic factors [12, 13] in the biomaterial scaffold to induce specific cellular response for host tissue regeneration (Figure 1.1).

1.2.1 Bone tissue engineering

In the U.S., more than 15 million people suffer from bone fractures annually. Defects may occur due to injuries, infections, tumors, or degenerative diseases [3]. Delayed healing or non-union occurs in 5-10% of all fractures and 20% of high impact fractures [14]. This impaired healing is

caused by the body's inability to regenerate the bone, and complication due to poor healing leads to prolonged hospitalizations and result in high health care costs [3, 14]. In addition, non-union fractures especially those in anatomical locations suffering from a low blood supply such as the distal radius or scaphoid bone, do not have optimal therapies [14]. Therefore, bone regeneration therapies continue to require optimization and improvement because many of the skeletal disorders remain untreated. Current treatment of bone injuries typically involves using autologous or allogenic bone grafting methods but have several limitations, such as donor site morbidity, risk of infection, and disease transmission [15]. Naturally derived or synthetic bone graft substitutes made of metals, ceramics and polymers are also clinically employed as potential treatment options to improve the overall bone healing outcomes, but lack the osteogenic capacity of auto-grafts [16]. In addition to excellent biocompatibility and biomechanical properties, successful bone healing outcome using synthetic grafts also depends on other critical factors such as favorable osteoconduction, osteoinduction, and vascularization [16]. Therefore, control over cellular and tissue interaction with biomaterials is garnering importance. Moreover, these biomaterials are implanted more frequently in geriatric population suffering from other major health problems, which interfere with the natural healing response around implants [15]. Successful healing of fractures requires integration of engineered tissue with surrounding host tissues and involves combined input from signaling generated by intercellular communications, cell-matrix interactions, and growth factors [7]. Therefore, design of biomaterial scaffold loaded with therapeutics that allow for spatio-temporal release within the defect site thus remains to be one of the imperative clinical need in the field of bone tissue engineering.

1.2.2 Gene therapy for bone tissue engineering

Popular bone tissue engineering strategies involve the delivery of external factors such as therapeutic proteins or genes to promote the repair or regeneration of tissues [3]. Protein-based therapies utilize cytokines or growth factors to directly target the wound site [15]. On the other hand, gene therapy exploits the advantage of the intrinsic production capability of proteins by the resident cells at or near the target site after successful delivery and expression of genes of interest [14]. Therefore, delivering genes can encode the therapeutic cytokines or growth factors, and can achieve the same effect as protein therapy. Moreover, the production of therapeutic proteins via its genetic counterpart can potentially be more sustained than administering the proteins locally that tend to denature rapidly, thus limiting its activity once delivered into the body [7]. Due to short half-lives and rapid degradation, supraphysiological levels of proteins (in milligrams) are administered for relevant clinical outcomes which may result in side effects [17, 18], for example high doses of recombinant BMP-2 protein can result in soft tissue swelling, radiculitis and ectopic bone formation [19]. On the other hand the delivery of genes will not be hindered by its stability or short half-lives issues since the carrier will ensure that the genetic information is well protected by the binding, condensation and packaging ability of the carrier [20]. In this respect, gene therapy appears to be more attractive, reliable and cost effective than protein therapy [14]. However, it is a well-known fact that the main obstacle toward achieving successful gene therapy is not the identification of therapeutic genes, but rather, the lack of a suitable gene delivery technique that is non-toxic, non-immunogenic and efficient [21].

1.3 GENE DELIVERY

Gene delivery is a technique used to introduce genetic information (DNA, RNA) to cells directing the synthesis of a specific protein. Typically, the "genetic information" or exogenous gene categorized as nucleic acid payloads can be divided into two groups based on their mechanism of action: (i) genome-editing systems like clustered regularly interspaced short palindromic repeats (CRISPR-Cas9), Zinc finger nucleases (ZFNs), transcription activator-like effector nucleases (TALENs); and (ii) transiently acting such as plasmid DNA (pDNA), messenger RNA (mRNA), micro RNA (miRNA), small interfering RNA (siRNA) or small hairpin RNAs (shRNA), and antisense oligonucleotides (AONs) [21]. Genome editing systems are commonly used in treatment of genetic disorders through permanent genetic modification in the human genome through gene correction, disruption, and whole gene-insertion [21]. Recently, several CRISPR based techniques have been developed and approved by FDA for immune-oncology and oncology therapies and others are likely to be approved within few years to treat retinal degeneration and hemophilia [22]. On the other hand, transiently acting systems are commonly employed for tissue engineering application since the expression of gene is required for a short period for regeneration of the damaged tissue [14].

Among numerous nucleic acid payloads, the most common transient expression dependent systems comprise circular, double-standard DNA constructs, termed as plasmids or plasmid DNA (pDNA) [21]. These plasmids contain several basic components to drive gene expression such as origin of replication, promoter, gene of interest, terminator, regulatory signals, antibiotic resistance gene, and the remaining base pairs termed as plasmid back bone [7].

Once inside the cells, pDNA is transcribed to mRNA in the nucleus of the cells following which gene of interest is subsequently translated to protein in the cytoplasm of the cells [7]. Use

of pDNA in gene therapy is common due to its rapid clearance from the body thereby reducing off-target side effects and cytotoxicity [23, 24]. Moreover, the cost of production of pDNA in large amounts with high purity for clinical application is relatively low as compared to production of recombinant proteins [25, 26]. However, due to the various biological characteristics of super-coiled pDNA, which include its large size (~3000 kDa) and net negative zeta-potentials of -30 to -70 mV owing to its phosphodiester back-bone [27, 28], plasmids are prevented from readily crossing the plasma membrane [29]. They are thus, considered inefficient for gene transfection. Physical methods of introducing pDNA to cells such as DNA injection [30, 31], gene gun administration [32, 33], electroporation [31, 34-36] have been developed but these methods are not widely used due to its feasibility and potential to cause damage to cells. Targeted and efficient delivery of pDNA therefore requires a more sophisticated delivery system that is discussed in the following section.

1.3.1 Gene delivery vectors

Vectors for gene delivery typically comprised of viral and non-viral types. Viral vectors are widely used in gene therapy applications, with approximately 70% of clinical trials carried out so far for gene therapy treatments utilized viral vectors such as lentiviruses, adeno-viruses, adeno-associated viruses and retroviruses [37]. Viral vectors are generally preferred for gene therapy applications since they are capable of transduction of non-dividing cells (lentiviruses) and inserting genetic payload in the host chromosome (retroviruses), driving long term gene expression [38]. Although viral vectors are extremely efficient and capable of delivering genetic payloads to cells with high specificity, they do suffer from several inherent shortcomings such as small capacity for packaging DNA, safety concerns (such as insertional mutagenesis and

associated carcinogenesis), and difficulty associated with production of large number of viruses [27, 37, 39-43]. Nevertheless, development of viral vectors in recent years has substantially advanced the gene-delivery technology and lead to development of Food and Drug Administration (FDA)-approved gene therapeutics, Kymriah and Yescarta, both anti-CD19 chimeric antigen receptor (CAR) T-cell therapies for B-cell cancers [44]. Approval of Kymriah and Yescarta has led to renewed excitement within the field with the hope that these therapies will pave way for approval of more gene therapeutics. It seems likely that treatment of genetic disorders will be approachable with gene editing systems like CRISPR/Cas9, using viral vectors where a long-term expression is needed to combat a persistent condition [38, 44]. However, for tissue engineering applications where an initial stimulation or transient expression is enough to promote cell proliferation and differentiation, viral vectors are not necessary [7, 45]. In addition, for the purpose of bone tissue engineering, transient gene expression-the type of expression achieved using non-viral vectors- is desirable because it limits the amount of newly formed bone and decreases the chances for bone malformation [14].

Recent advances in materials science and nanobiotechnology has led to the development of next generation synthetic, non-viral vectors that exhibit low immunogenicity and toxicity compared to the viral counterparts [46]. Non-viral vectors also permit high genetic payloads and incur low cost of production on a large scale [47, 48]. Examples of common non-viral vectors include lipids (liposomal or non-liposomal), and cationic polymers [28, 49-59], branched cationic polymers termed as dendrimers, and co-precipitates of purified DNA and CaP (hydroxyapatite) [60-69]. Numerous synthetic transfection reagents have been commercialized for in vitro gene transfer, for example the liposomal transfection reagents Lipofectamine (Invitrogen, USA), the non-liposomal lipid transfection reagent FuGENE HD (Roche,

Switzerland), the dendrimer-based transfection reagent Superfect (Qiagen, USA), the polyethyleneimine (PEI)-based transfection reagent, jetPEI (Polypus-transfection, USA) and the calcium phosphate transfection reagent, Profection (Promega, USA) [70]. In addition, some non-viral transfection reagents have recently been optimized for in vivo gene transfer and commercialized (e.g. in vivo jet PEI) [39]. Among the non-viral systems, lipid and polymer-based vectors display higher transfection efficiency over other systems, but their use in tissue engineering applications is still limited for their associated toxicity [27]. Ideally, for tissue engineering applications scaffolds are loaded with non-viral vectors with or without cells and are expected to allow for spatio-temporal release of vectors. Given that non-viral systems face challenges in the successfully delivery of pDNA to cells, scaffolds are generally loaded with substantial amounts of non-viral vectors to achieve desired therapeutic effect. However, use of lipid and polymer based non-viral vectors in large amounts is limited due to their potential side effects to the surrounding tissue [39]. Therefore, safer and more efficient non-viral systems are still being sought.

1.4 CALCIUM PHOSPHATE BASED GENE DELIVERY SYSTEMS

Among all the various non-viral gene delivery systems currently under investigation [62, 71-81], calcium phosphate (CaP) mediated gene transfection is considered to be an attractive option due to its ability for *in-vitro* transfection of a wide variety of mammalian cells with little or no toxicity [82]. Furthermore, nanostructured calcium phosphate biomaterials are of special interest for bone tissue engineering applications as they share chemical/crystallographic similarities to inorganic components of bone [83]. Several CaP phases exist and among those hydroxyapatite

(HA), $Ca_{10}(PO_4)_6$ $(OH)_2$; Ca/P = 1.67) and tricalcium phosphate (TCP, $Ca_3(PO4)_2$, Ca/P = 1.5) are the most widely used due to their close structural similarity to the mineralized matrix of natural bone [84-89]. Among these, HA phase is also one of the most stable phases that can be generated under physiological conditions. As such, it has been the model system that has been widely studied thus far for non-viral gene delivery applications [27].

Hydroxyapatite (HA) can be either pure or calcium-deficient. Pure HA, $Ca_{10}(PO_4)_6(OH)_2$, has the stoichiometric Ca to P ratio of 1.67 [68]. Stoichiometric HA can be prepared hydrothermally by solid-state reactions at either 375 °C or > 900 °C or by sintering apatite precipitated from very basic conditions (pH > 11) above 900 °C [68]. However, these synthesis methods are not suitable for biological applications since they require the use of such high temperatures and non-physiological conditions. As a result, aqueous based approaches have been developed to synthesize HA. These approaches yield calcium deficient or nonstoichiometric Ca/P (i.e. Ca/P < 1.67) [68]. Typically, for gene delivery applications, a solution comprised of $CaCl_2$ and pDNA is added drop wise to an equal volume of a HEPES buffered phosphate solution (pH ~ near physiological) comprised of HEPES, NaCl and Na_2HPO_4. Conventional CaP synthesis procedures involved manual mixing of these precursor solutions that typically results in complexes with variable particle sizes that tend to aggregate rapidly, which when implemented in gene transfection experiments often result in low and variable transfection efficiencies.

Particle aggregation is unfavorable since it ultimately reduces the ability of these complexes to be internalized by cells, thus limiting the gene transfection ability of the CaP vectors [67]. Optimal calcium and phosphate concentrations in the precursor solutions, which determine the Ca/P ratio and controlled mixing of the two solutions, can produce particles within the size range of 50-100nm [67, 68]. Smaller sized particles are also known to exhibit a higher

specific surface area, since specific area is defined as $3/r\rho$, where r is the radius of the particle and ρ is the density of the particle (assuming a spherical morphology). Radius being inversely proportional to the specific surface area implies that smaller particles have higher surface area thereby capable of higher DNA loading during the precipitation of CaP particles. Therefore, efforts have been made to optimize the synthesis technique to generate nanostructured calcium phosphate pDNA complexes, aptly called NanoCaPs.

1.4.1 Nanostructured calcium phosphate pDNA complexes (NanoCaPs)

To overcome the problems associated with existing manual method of mixing precursor solution for generation of CaP particles, Olton et al reported a novel synthesis technique for generation of consistent, nano-sized, mono-dispersed CaP-pDNA particles, termed as NanoCaPs [67]. The authors demonstrated the significance of optimizing both the stoichiometry (Ca/P ratio) of the CaP particles as well as the mode in which the calcium and phosphate precursor solutions are mixed. NanoCaPs synthesized using Ca/P ratio of 130 and a controlled mixing flow rate of 13.4µl/s exhibited transfection efficiencies ~25 fold greater than conventional HA using literature methods [67, 69]. However, to become clinically relevant NanoCaP vectors must better tolerate the challenges of a physiological environment that impede the clinical translation of this gene delivery technology. There are numerous extracellular and intracellular barriers that must be overcome to achieve efficient gene transfection, which are discussed in the following sections.

1.5 BARRIERS TO SUCCESSFUL NANOCAPS MEDIATED GENE DELIVERY

Irrespective of the type of non-viral vector employed, a gene-delivery vector must navigate through numerous barriers to achieve efficient gene transfection as shown in Figure 1.2. They are broadly categorized into: (1) extracellular barriers; (2) intracellular barriers [21]. Besides these barriers there are manufacturing considerations that also play a critical role in determining the feasibility of clinical application of the gene delivery vector.

1.5.1 Extracellular barriers

There are numerous extracellular barriers a non-viral gene delivery vector faces, however the significance of those barriers depends on the route of administration of these vectors. For clinical translation, a key issue to be considered in practice, is whether administration should be intravenous or direct injection to the target tissue. Direct injection lacks specificity and requires repeated administration of vectors at the target site, whereas intravenous delivery of vectors faces several barriers for the application to be effective [27]. One of the main factors limiting the effectiveness of intravenous delivery of non-viral gene delivery vectors is the colloidal instability of these complexes in the extracellular space [21, 27]. Colloidal instability arises due to the high ionic strength in the extracellular space, and the presence of serum components. In addition to colloidal instability, non-viral vectors are prone to rapid clearance by non-parenchymal cells, rapid degradation of the DNA by plasma nucleases, accumulation or deposition in organs such as the skin, lung, and intestines [27]. Additionally, even in the case of direct delivery, the complexes may suffer from inflammation, immune response, and the rapid degradation of the DNA by plasma nucleases, before it could enter the target cells [27]. Therefore, introduction of

scaffold materials is one way of overcoming such hurdles in systemic and local delivery of vectors, as scaffold would provide protection to the vector complex, and ensure stable and controlled release of the complexes over time.

1.5.2 Intracellular barriers

Once the gene delivery vector reaches the cell surface after overcoming all the extracellular barriers, it must gain entry to the cell through endocytosis (Figure 1.2). Olton et al demonstrated that cellular uptake of NanoCaPs is mediated by both clathrin- and caveolae- dependent endocytosis [66]. In general, CaP based vectors once inside the endosome compartments undergo acid-triggered dissolution (pH 6.0-6.5, early endosomal pH) that results in a massive proton influx creating an osmotic pressure across the endosomal membrane, followed by its rupture and finally release of pDNA from the vesicles in the cytosol for nuclear translocation [27]. Therefore, changes in NanoCaPs dissolution kinetics to enable early release from endosomes thereby escaping lysosomal degradation pathway can help overcoming one of the intracellular barriers. Additionally, pDNA once in the cytosol, must make its way into the nucleus of the cell via nuclear pore complex for the transcription of transgene [21]. It is currently accepted that non-viral vectors heavily rely on cell division during which nuclear membrane breaks down and pDNA released from vectors is randomly incorporated in daughter nuclei. However, for non-dividing cells, the presence of nuclear envelope poses a significant challenge [27]. In these instances, nuclear localization sequences (NLS) are incorporated into the vector-DNA complexes or in the pDNA backbone to direct the plasmid to the nucleus via active transport [90-92].

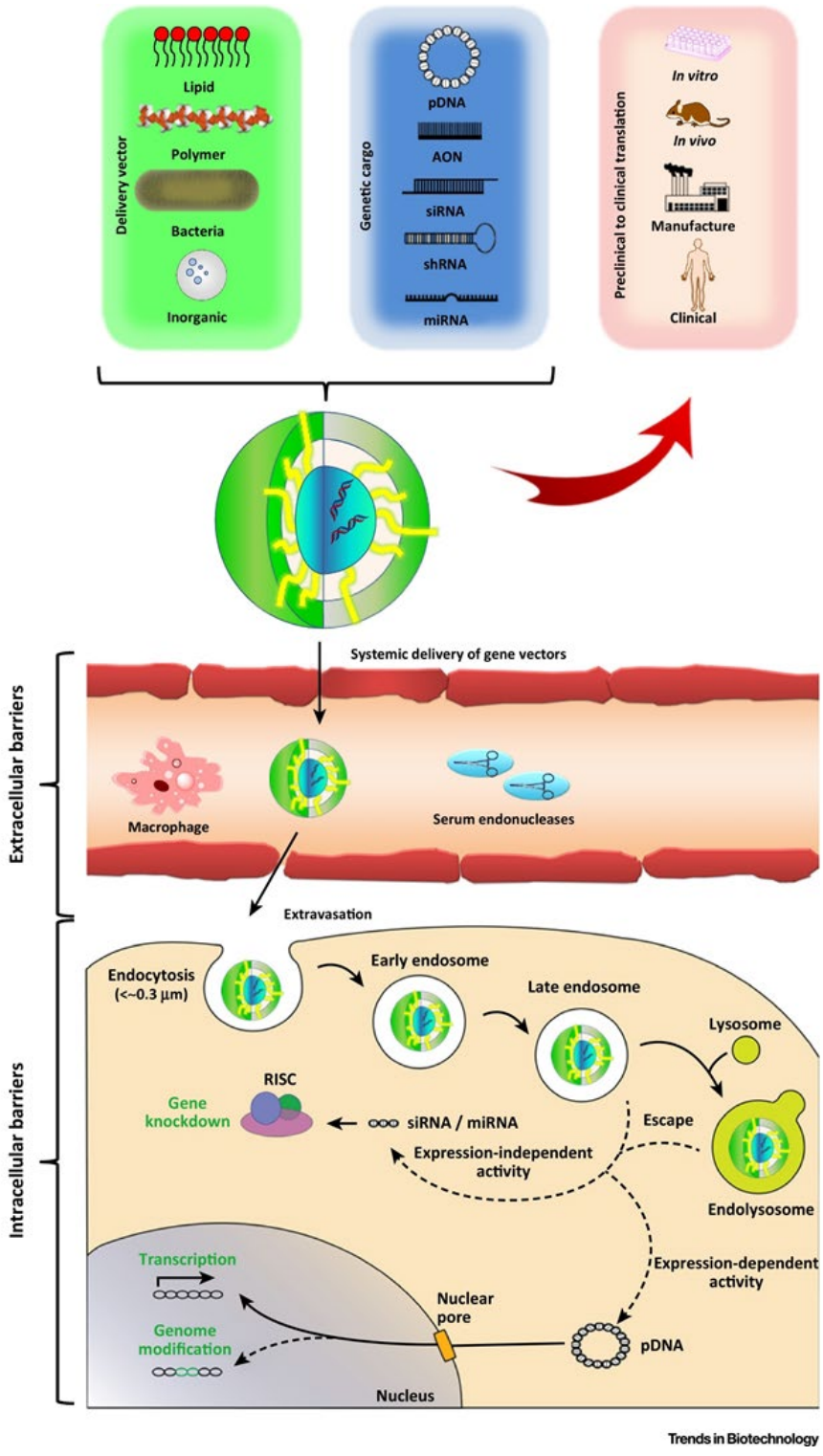

Figure 1.2. Barriers to non-viral gene delivery.

Reproduced with permission [21].

1.6 STRATEGIES TO OVERCOME BARRIERS FOR NANOCAPS MEDIATED GENE DELIVERY

The following section will lay down the fundamentals behind the strategies employed for current research work that will circumvent, if not eliminate, some of the limitations that have previously stymied the success of NanoCaPs as a gene delivery vector for bone tissue engineering applications.

1.6.1 Ionic substitution in NanoCaPs

CaP particles have an inherent propensity to aggregate rapidly with time in dispersing media due to low surface charge (around -20mV) [93]. Rejman et al. have reported that particles <100 nm are readily endocytosed by cells [94]. The expected uncontrolled growth and aggregation of CaP particles however, expectedly results in lower levels of gene expression. There are, however reports on stabilizing the growth of CaP particles by coating with lipid [95], adsorption of chitosan on growing CaP aggregates to prevent particle aggregation and provide stability to the gene delivery vector [96]. On the other hand, there are reports in literature showing cationic substitution of magnesium and strontium, and anionic substitution of carbonate and fluoride into the calcium phosphate-based gene delivery systems contributing to enhanced transfection efficiency [97-102]. This increase in transfection efficiency due to substitution with cations or anions is attributed to the possible reduction in particle aggregation and faster dissolution of the endocytosed particles. Notably, one of the most crucial intracellular barrier for CaP based vectors is escape from endosomes and release of the functional plasmid DNA in the cytosol [103]. Plasmid DNA that escapes endosomes effectively, escaping lysosomal degradation,

successfully make their way to the nucleus through the nuclear pore complex or get distributed during cell division [27].

Since escaping endosomes effectively is crucial for the CaP based vectors, putatively, this makes it even more pertinent to fine tune the dissolution characteristics of nanostructured CaPs (NanoCaPs) by incorporation of various cations and anions, as reported in the literature [99, 104-107]. Furthermore, the motivation for ionic substitution of CaPs arises from the fact that the natural bone mineral is composed of not only calcium and phosphate moieties, but also carbonate, sodium, magnesium, potassium, zinc, barium, copper, aluminum, iron, fluoride, chloride, and silicon ions [108, 109]. Thus, investigating the influence of ionic substitution on NanoCaPs mediated gene delivery would be an efficient strategy to alter its materials properties thereby enhancing its transfection abilities.

1.6.2 Freeze drying of NanoCaPs

While ionic substitution of NanoCaPs will influence the material properties of the vector complex and potentially increase the transfection efficiency when used in aqueous suspension, long term storage of these particles in aqueous medium will lead to particle aggregation and ultimately resulting in poor transfection results. Furthermore, to be clinically relevant, it is ideal to develop a technique that will allow for long-term storage of NanoCaPs under ambient conditions, which would also enable shipment of pre-made NanoCaPs, while maintaining its transfection abilities. Lyophilization is a very attractive way to achieve dried pharmaceuticals in general and DNA-based formulations [110]. However, the freeze-drying process involves two stresses, freezing and drying, that are known to be damaging to macromolecules and nanoparticulate structures, unless appropriate stabilizers are used [111, 112].

Lyoprotectants are additives which serve as stabilizing agents during freeze-drying. These additives effectively stabilize vector complexes due to their ability to both replace water as well as their ability to form stable glasses [110, 113]. Notably, several studies have shown use of monosaccharides, disaccharides, oligosaccharides and polysaccharides as a stabilizing agent for freeze drying of polyplexes and lipoplexes vectors [113-117]. Thus, use of a stabilizing agent will serve to maintain the native environment of the NanoCaPs complexes in the lyophilized state, thus minimizing the particle aggregation while maintaining efficient levels of gene expression. Changes to the materials properties of NanoCaPs and development of technique that allows for long term storage of the particles would enhance the gene transfection prowess of these vectors, however for bone tissue engineering application their incorporation in scaffolds is necessary.

1.6.3 Surface mediated gene delivery

Segmental bone defects are critical sized bone defects that are not amenable to healing by the inherent regenerative capacity of bone [118] due to the large defect size. Treatment of segmental bone defects is at present typically accomplished using autologous or allogenic bone grafting methods [118]. Naturally derived or synthetic bone graft substitutes made of metals, ceramics and polymers are also clinically employed as potential treatment options to improve the overall healing outcomes but lack the osteogenic capacity of auto-grafts. In addition to excellent biocompatibility and biomechanical properties, successful bone healing outcome using synthetic biomaterials also depends on other critical factors such as favorable osteoconduction, osteoinduction, and vascularization [3]. Additionally, the surface of implanted biomaterials is in direct contact with the host bone and soft tissue, and plays a critical role in determining the

biocompatibility, functional compatibility and tissue integration of implants [119]. Therefore, control over cellular response towards biomaterial surfaces is garnering importance. Moreover, these biomaterials are implanted more frequently in geriatric population suffering from other major health problems, which interfere with the natural healing response around implants. Thus, it is necessary for implant surfaces to evoke a controlled cellular and tissue interfacial response for better tissue integration of biomedical implants.

Various strategies have been employed to improve osseointegration property of implants namely, florid modification, micro-arc oxidation treatment, electrolytic and heat treatment as well as alkali treatment, etc [120]. Coating of implants with a thin layer of calcium phosphate has also proven to be an effective approach to providing the base material with good biocompatibility and good osteoconductivity owing to its similarity with native bone structure [121]. Interestingly, numerous studies have focused on creating calcium phosphate composite layers immobilizing DNA on the surfaces of base materials [122-124]. These resulting composite layers are endowed with useful characteristic of both osteoconductive bioceramics and transfection reagents; they thus provide a biocompatible surface to support cell attachment, spreading, and proliferation, and can stimulate the cell effectively via surface-mediated gene transfer. Therefore, development of a user-friendly technique that allows adsorption of NanoCaPs on surfaces of biomaterials commonly utilized for bone tissue engineering would further expand the applications of NanoCaPs as a non-viral gene delivery technology. Techniques commonly employed for surface mediated gene delivery and their limitations are discussed in Chapter 4.0 .

1.6.4 Three-dimensional polymeric scaffolds for gene delivery

Gene expression mediated via non-viral gene delivery is transient in nature as the delivered pDNA does not integrate in the host genome and is randomly distributed during cell division, and/or degraded over time. Therefore, to be able to attain a long-term therapeutic effect, the sustained expression of the transgene should be implemented. Surface mediated gene transfer, as discussed in the previous section, is one of the ways of achieving scaffold mediated gene delivery. However, release of vector complexes from the bulk of the scaffold material still presents a significant challenge. The proposed solution lies in the utilization of three-dimensional (3-D) scaffolds to accomplish what the NanoCaPs alone cannot achieve. Typically, polymeric, biodegradable, and highly porous biomimetic extracellular matrix materials are engineered to mimic the bone microstructure comprised of crystalline/amorphous CaP and polymer/CaP composite with or without growth factors [125-127]. Hydrogels are a class of biomaterials that have a great scaffolding potential in many tissue engineering applications owing to their tissue-like water content, high biocompatibility in general, mechanical properties that parallel the properties of soft tissues, efficient transport of nutrients and waste, powerful ability to uniformly encapsulate cells, growth factors and genetic material, and ability to be injected as a liquid that gels in-situ [15, 128-130]. Furthermore, injectable hydrogel formulations can be utilized to infiltrate porous metallic and ceramic biomaterials commonly used for bone tissue engineering. Naturally derived polymers, such as chitosan, gelatin, collagen, and fibrin are commonly employed for scaffold design to support bone formation because of their biocompatibility and biodegradability [15, 127, 131].

Hydrogels, as a 3-D scaffold is intended to serve multitude of purposes. **First**, the 3-D scaffold serves as templates for the infiltration, attachment, and proliferation of cells and

subsequent tissue formation in three dimensions. **Second**, the scaffold acts as a protective shield to prevent the embedded factors from the harsh external environment such as low pH and enzyme degradation, thereby overcoming extracellular barriers. **Third**, the scaffold provides the sustained release of embedded factors over time to allow long-term therapeutic effects. **Finally**, in the case of NanoCaPs, by entrapping and distributing NanoCaPs complexes over a 3-D volume, the aggregation of NanoCaPs complexes can potentially be reduced or eliminated since the interactions between the individual NanoCaPs particles are less likely to occur.

Therefore, with all the strategies discussed to circumvent the limitations faced by NanoCaPs mediated gene transfection, we are now prepared to present the overall goal of this dissertation.

2.0 SPECIFIC AIMS

The overall goal of this dissertation is to create new class of NanoCaPs gene delivery vectors via ionic substitution. We hypothesize that alteration of materials properties of NanoCaPs will confer superior transfection abilities on the synthesized nanoparticles. Additionally, by developing methodologies that enable sustained gene expression achieved through creation of modified NanoCaPs complexes would help in creation of functional scaffolds for bone tissue repair and regeneration. Accordingly, three specific aims have been formulated.

2.1 SPECFIC AIM 1

Synthesize silicate substituted calcium phosphate nanoparticles (NanoSiCaPs), perform materials characterization, and assess in-vitro gene delivery efficiency of the substituted NanoSiCaPs system. A modified version of NanoCaPs will be developed by substituting different amounts of silicate in lieu of phosphate through aqueous precipitation method. The synthesized silicate substituted NanoCaPs/HA (NanoSiCaPs/SiHA) will be characterized using different materials characterization techniques. We hypothesize that substitution of silicate in NanoCaPs will alter its material properties thereby affecting its transfection ability and pDNA binding efficiency. Therefore, we would also investigate the in-vitro gene delivery efficiency of

synthesized NanoSiCaPs, in addition to pDNA binding efficiency, and morphology of the nanoparticles.

2.2 SPECIFIC AIM 2

Synthesize polyelectrolyte NanoSiCaPs complex assemblies (PNA) on titanium substrates for surface mediated gene delivery. A technique will be developed to adsorb NanoSiCaPs complexes on Titanium (Ti) substrates by dip coating method. We hypothesize that using the electrostatic interaction between negatively charged NanoSiCaPs complexes and positively charged polymer coated Ti-surfaces, we can obtain a nanoceramic coating that can achieve surface mediated gene transfection. Surface composition and microstructure of the coated Ti surfaces will be assessed using different materials characterization techniques. The substrates will be assessed for their in-vitro transfection efficiency, cell attachment and viability.

2.3 SPECIFIC AIM 3

Formulate and synthesize a 3-D gene delivery system using fibrin hydrogels to encapsulate lyophilized NanoSiCaPs complexes, for achieving increased stability and longer shelf life. The lyophilization technique would be developed that allow long term storage of NanoSiCaPs complexes. We hypothesize that by determining optimum conditions for freeze-drying of NanoSiCaPs complexes, long-term storage of these complexes is possible while maintaining particle stability and transfection efficiency. Additionally, incorporation of lyophilized

NanoSiCaPs in fibrin gels would further limit particle aggregation and provide sustained gene expression. Optimum conditions for lyophilization of NanoSiCaPs will be determined. A fibrin gene delivery system with NanoSiCaPs will be synthesized and the role of different components utilized in the synthesis of this gene delivery system will be assessed.

In order to distinguish between the calcium phosphate used in different applications, the use of CaPs as gene delivery vectors will henceforth be referred to as NanoCaPs or NanoSiCaPs while calcium phosphate in the bulk will be referred to as HA or SiHA throughout the text of this dissertation to avoid any confusion. Additionally, NanoCaPs or NanoSiCaPs with pDNA will be referred to as NanoCaPs or NanoSiCaPs complexes.

3.0 SYNTHESIS AND CHARACTERIZATION OF SILICATE SUBSITITUTED CALCIUM PHOPSHATE NANOPARTICLES FOR NON-VIRAL GENE DELIVERY

3.1 INTRODUCTION

Nano-structured ceramic particles, particularly, nano-particles of calcium phosphate (CaP) remain an attractive option among the various types of non-viral gene delivery vectors studied because of their safety, biocompatibility, biodegradability, and ease of handling as well as their adsorptive capacity for DNA. However, they are still not accepted as the ideal choice for gene delivery because of the known difficulties associated with endosomal escape, and the partial protection of DNA from nuclease degradation that automatically results in lower levels of gene expression [132]. The inherent propensity of CaP particles to aggregate rapidly with time in dispersing media is also another determining factor for achieving efficient gene delivery [133]. Rejman et al. have reported that particles <100 nm are readily endocytosed by cells[94]. The expected uncontrolled growth and aggregation of CaP particles however, expectedly results in lower levels of gene expression. Therefore, this chapter examines the influence of ionic substitution to overcome the limitations stated above to enhance the transfection efficiency of NanoCaPs.

Motivation for ionic substitution of NanoCaPs further arises from the fact that the natural bone mineral is composed of not only calcium and phosphate moieties, but also carbonate,

sodium, magnesium, potassium, zinc, barium, copper, aluminum, iron, fluoride, chloride, and silicon ions[108, 134]. Recent work in the literature has also shown that incorporation of silicon into hydroxyapatite (HA) results in changes to the properties of HA such as the lattice parameter, morphology, crystallinity, surface chemistry, kinetics of dissolution, etc. [134-137]. Despite the fact that silicon substituted HA is considered to be a bioactive bone substitute due to its enhanced solubility [135, 136], no attempt to date, to the best of our knowledge, has been made to evaluate the potential of silicon substituted CaPs (NanoSiCaPs) as a gene delivery vector. This therefore sets the stage for an ideal opportunity to explore silicon substituted CaPs as a potential gene delivery vector and explore further whether these properties of modified HA would prove beneficial particularly, for non-viral gene delivery.

In a previous study, our group has already reported a novel simple synthesis approach that generates nanocrystalline HA particles (NanoCaPs) approximately 50-100 nm in size under physiological conditions that were efficient at both binding and condensing the pDNA [67]. Furthermore, the results of transfection indicate their superior response compared to other commercially available non-viral transfection agents [69]. The current work therefore aims to demonstrate further improvement resulting in dramatic enhancement of the transgene expression by the inclusion of a critical concentration of silicate species into the NanoCaPs system to generate silicate substituted NanoCaPs that is aptly termed as NanoSiCaPs (Figure 3.1).

The focus of the current work presented here is therefore to exploit the aforementioned properties of silicate substituted HA (SiHA) to improve the gene delivery prowess, by incorporating different levels of silicate anions into the nanostructured CaPs (NanoCaP) to accordingly form the NanoSiCaPs system. Different analytical techniques were further utilized to understand the role of silicate substitution on the structure, morphology, dissolution properties

and phase change of the substituted HA phase. The impact of silicate substitution on the transfection efficiency of NanoCaPs complexes was further assessed using flow cytometry while also assessing the binding capability of NanoSiCaPs compared to un-substituted NanoCaPs. Results of all these studies are presented and discussed in this chapter.

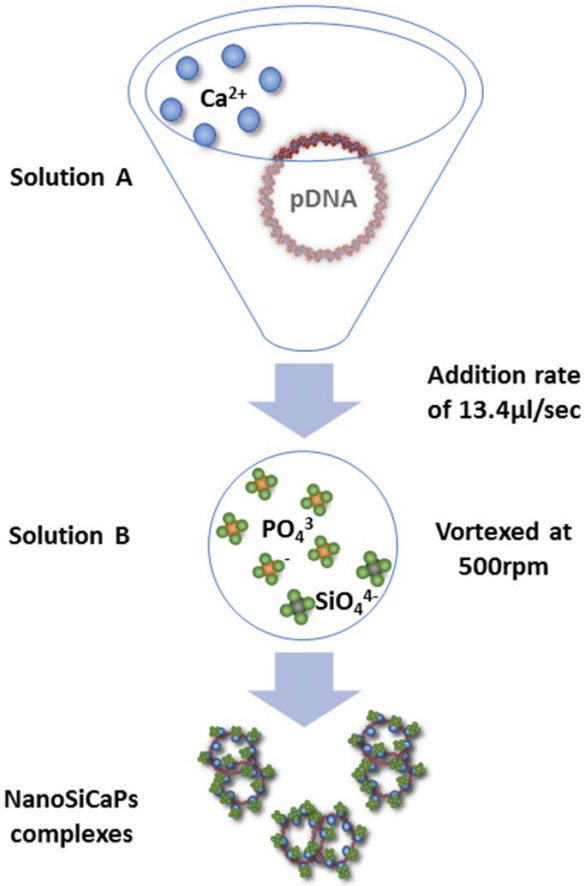

Figure 3.1. Schematic representation of synthesis of NanoSiCaPs complexes.

3.2 MATERIALS AND METHODS

3.2.1 Materials

Calcium chloride ($CaCl_2 \cdot 2H_2O$), tri-sodium phosphate do-decahydrate ($Na_3PO_4 \cdot 12H_2O$), sodium chloride (NaCl), Bis-Tris, and dextrose were purchased from Fisher Scientific (Pittsburgh, PA). Potassium chloride (KCl) was purchased from Sigma Aldrich (St. Louis, MO). Sodium hydroxide (NaOH) was purchased from Mallinckrodt Baker Inc. (Phillipsburg, NJ). Sodium metasilicate ($Na_2SiO_3 \cdot 5H_2O$) was purchased from Alfa Aesar (Ward Hill, MA). HEPES and ethidium bromide (EtBr) were obtained from EMD Chemicals (Gibbstown, NJ). Reporter plasmid, gWiz™ GFP (Green Fluorescent Protein), were purchased from Aldevron LLC (Fargo, ND). All of the reagents were used as received without further modification or purification.

3.2.2 Synthesis of as-prepared bulk HA and SiHA

The precursors used for synthesizing as-prepared HA were $CaCl_2 \cdot 2H_2O$, $Na_3PO_4 \cdot 12H_2O$, and NaOH, based on the following chemical reaction which has also been reported by us earlier [138]:

$$10CaCl_2 + 6Na_3PO_4 + 2NaOH \rightarrow Ca_{10}(PO_4)_6(OH)_2 + 20NaCl \quad \text{(Equation 3-1)}$$

The molar ratio of Ca/P was fixed at 1.67, and correspondingly, stoichiometric amounts of OH were added to maintain the HA phase and composition. To summarize the synthesis, 5.8 g of $CaCl_2 \cdot 2H_2O$ was dissolved in 100 ml of double-distilled water (ddH_2O) with a conductivity of 18.2 Ω/cm to form solution A. 9.12 g of $Na_3PO_4 \cdot 12H_2O$ and 0.36 g of NaOH were dissolved in

another 100 ml of ddH_2O to form solution B. Solution A was then added into solution B drop by drop under constant stirring at room temperature. The solution mixture quickly turns turbid, and the formation of a white precipitate is instantly observed. The white precipitate was collected using a Beckman J2-MC centrifuge (Beckman Coulter Inc, Fullerton, CA) at 2000 rpm and the supernatant was accordingly discarded. The white precipitate was then re-suspended into ddH_2O to rinse away the NaCl salt, obtained as a byproduct. The washing and centrifugation steps were repeated at least 3 times to ensure the complete removal of NaCl. The white precipitate obtained was then air dried in an oven (Isotemp, Fisher Scientific, Pittsburgh, PA) at 70°C for 72 hours and ground to a fine powder before conducting any further materials characterization.

Silicate substituted HA, or SiHA referred henceforth, was also synthesized in a similar fashion. Various amounts of silicate (Si) were substituted into HA based on the molar ratio of Ca/ (P+Si) (SiHA). The precursors used for synthesizing SiHA were once again, $CaCl_2 \cdot 2H_2O$, $Na_3PO_4 \cdot 12H_2O$, NaOH, while $Na_2SiO_3 \cdot 5H_2O$ served as the Si precursor for generating SiHA. The ratios of Ca/ (P+Si) were fixed at 1.67, and correspondingly, stoichiometric amounts of OH^- were also added to maintain the HA composition. The proposed chemical reactions for SiHA is:

$$10\ CaCl_2 + (6\text{-}x)\ Na_3PO_4 + x\ Na_2SiO_3 + (2\text{-}x)\ NaOH + x/2O_2 \rightarrow Ca_{10}(PO_4)_{6\text{-}x}(SiO_4)_x(OH)_{2\text{-}x} + (20\text{-}2x)\ NaCl + xCl_2 \quad \text{(Equation 3-2)}$$

Where, x = number of moles of substituted silicate and the percentage of molar substitution is determined by the site substitution of PO_4^{3-} (% mol substitution =x/6*100). Note that all the reactions followed for synthesizing SiHA only considered the physical site substitution of SiO_4^{4-} ions into any of the available PO_4^{3-} or OH^- sites, while any potential charge imbalances that may arise due to the substitutions of anions with the different ionic charges of

trivalent or pentavalent P and tetravalent Si were disregarded throughout this study. Table 1 summarizes the amount (mol.) and weight (wt.) of Ca, P and Si precursors used for generating each of the SiHA powder prepared with x equal to 0, 0.5, 1, 2, 3, 4, or 5 hereafter designated HA, 8.3SiHA, 16.6SiHA, 33.3SiHA, 50SiHA, 66.6SiHA and 83.3SiHA, respectively. Herein, we follow the convention for representing the silicate substitution in mol %, and not on a weight percent (wt.%) basis.

Table 1: Precursor composition of calcium, phosphorus and silicon for synthesis of HA and SiHA.

Substitution	x= 0	x=0.5	x=1	x=2	x=3	x=4	x=5
% mol	0	8.3	16.6	33.3	50	66.6	83.3
% weight	0	1.4	2.8	5.8	8.7	11.6	14.6
$CaCl_2 \cdot 2H_2O$ (mol)	0.4	0.4	0.4	0.4	0.4	0.4	0.4
$Na_3PO_4 \cdot 12H_2O$ (mol)	0.240	0.220	0.200	0.160	0.120	0.080	0.040
$Na_2SiO_3 \cdot 5H_2O$ (mol)	0	0.019	0.039	0.079	0.12	0.159	0.199
NaOH (mol)	0.09	0.09	0.09	0.09	0.09	0.09	0.09
Ca/(P+Si)	1.66	1.66	1.66	1.66	1.66	1.66	1.66
Ca/P	1.66	1.81	2	2.5	3.33	5	10

3.2.3 Synthesis of pDNA loaded NanoCaPs and Si-substituted NanoCaPs

The synthesis of the pDNA loaded NanoCaPs and Si- substituted NanoCaPs (NanoSiCaPs) is very much dependent on the Ca/P ratios of the corresponding Ca and P precursors. To maintain the nano-scale size range of the substituted and un-substituted calcium phosphate (CaP) particles, the ratios of Ca/P and Ca/(P+Si) were set at 130 instead of the 1.67 ratio normally used for

synthesizing HA in the bulk. The ratio of 130 was selected based on the Ca/P ratio that resulted in formation of nanostructured HA, while also displaying the most optimal transfection levels from our previously published report [139]. Herein, the reported nanostructured HA particles are designated as NanoCaPs complexes (containing pDNA) for un substituted samples and correspondingly, following the nomenclature mentioned above, NanoSiCaPs complexes for silicate substituted samples with different amounts of silicate substitution being 8.3, 16.6, 33.3, 50, 66.6 and 83.3 NanoSiCaPs (% mol) as shown in Table 1. The synthesis of un-substituted NanoCaPs complexes and NanoSiCaPs complexes were adapted from the synthesis of HA and SiHA described above. Briefly, 15.53 µl of 2M $CaCl_2$ and 6.35 µl of plasmid DNA (1mg/ml, gWiz GFP) were diluted in 103.2 µl of ddH_2O to form the solution A (125µl total). An equal volume (125µl) of solution B containing HEPES-buffered solution (280 mM NaCl, 10 mM KCl, 12 mM dextrose, and 50 mMHEPES) and 1.5 mM Na_3PO_4 was also prepared. The HEPES-buffered solution was intended to maintain the pH of the precursors at 7.5. The precursors of NanoSiCaPs contained the same solution A, and the solution B used for NanoSiCaPs also contained the HEPES-buffered solution and a mixture of 1.5 mM of (Na_3PO_4 + Na_2SiO_3) for silicate, respectively with the appropriate adjustments needed for the addition of the silicate ion. The molar ratios of *Ca/P and Ca/(P+Si)* as mentioned above, was also maintained at 130 for all the samples synthesized. The un-substituted NanoCaPs complexes and NanoSiCaPs complexes were then synthesized using a Harvard Apparatus PHD 2000 Infuse/Withdraw syringe pump (Holliston, MA) to introduce and mix the two solutions in a controlled drop wise fashion to generate the desired homogeneous dispersion of the NanoCaPs and NanoSiCaPs in solution similar to our published reports. Hence, solution A was added drop by drop into solution B at an addition rate of 13.4µl/s while solution B was vortexed at 500 rpm (Figure 3.1). The addition rate

was also selected following our previously published report [139]. Accordingly, the as-synthesized NanoCaPs complexes and NanoSiCaPs complexes in suspension were used for in-vitro transfection, particle size characterization and pDNA binding experiments.

3.2.4 Materials characterization

X-ray Diffraction (XRD) patterns for both the as-prepared bulk HA and SiHA powders (8.3, 16.6, 33.3, 50, 66.6 and 83.3SiHA) were collected using a Philips X'Pert PRO X-ray diffraction system (PAN Analytical, Westborough, MA) with CuKα radiation (λ = 1.5418Å). The diffractometer was operated at 45 kV and 40 mA and scanned over the 2θ range of 20-60°. The step size was 0.03 and the time per step was 50.17 s for each X-ray run. The XRD patterns were generated using the Philips X'PertData Collector and analyzed using the Philips X'PertHighscore Plus software. All the XRD patterns were verified and compared to existing library of references from the Joint Committee on Powder Diffraction Standards (JCPDS). Fourier-transform Infrared Spectroscopy (FTIR) was used to identify the various functional groups present in the as-prepared HA and different SiHA powders. FTIR spectra of the as-prepared HA and silicate substituted SiHA samples were collected using the Nicolet 6700 spectrophotometer (Thermo Electron Corporation) using a diamond ATR (Smart Orbit) Scanning electron microscopy (SEM) was used to observe the morphology of both, the as-prepared HA and SiHA samples. Powdered samples of as-prepared HA and 8.3SiHA, 50SiHA and 83.3SiHA were accordingly mounted onto double-sided carbon tapes and sputter coated with palladium using a Cressington sputter coater 108A (Cressington Scientific Instruments, Ltd, Watford, UK). The SEM images were taken on a Philips XL30 field emission gun SEM (Philips-XL30 FEG, Philips) and Energy Dispersive X-ray Analysis (EDAX) results were obtained using the built-in

EDAX system (EDX Genesis, EDAX Inc.). To measure the dissolution properties of HA and SiHA samples, ion release test was performed in Bis-Tris buffer at pH 7.2, pH 6.5 and pH 5.8, respectively. Bulk synthesized samples were used for the dissolution study, wherein 100mg of as-prepared HA, 8.3 SiHA, 50 SiHA and 83.3 SiHA was dispersed in 150ml of buffer at different pH and incubated at 37^{o}C for 24 hours. 10ml of the Bis-Tris Buffer was taken for elemental analysis to be used for estimating the calcium ion concentration (n=3). Immediately after taking each aliquot, the samples were centrifuged at 7000rpm for 20 minutes to ensure separation of any residual solids. After centrifugation, the supernatant was carefully aspirated and stored at 4°C until elemental analysis was conducted. Spectroscopic elemental analysis was performed through inductively coupled plasma optical emission spectroscopy (ICP-OES, iCAP duo 6500 Thermo Fisher). The calcium ion concentrations were correspondingly measured for different samples using 0.2, 0.5, 1, 5, 10, 50 and 100 ppm standards.

3.2.5 In-vitro experiments

All cells were cultured in 75 cm^2 flasks in a humidified incubator at 37^{o}C in 5% CO_2. NIH3T3 cells were cultured with DMEM supplemented with 10% FBS and 1% P/S; and MDA-MB-231 cells were cultured with EMEM supplemented with 10% FBS, 1% sodium pyruvate and 1% P/S. Cells were maintained to a sub-confluence state and were passaged at least twice a week. For the transient transfection experiments, the cells were seeded in 12-well plates at cell-density of about 1.0 x 10^5 cells per well. The gWiz GFP was complexed with either NanoCaPs or silicate substituted NanoCaPs, i.e. NanoSiCaPs as described above in Section 2.2, and immediately transferred drop by drop into each well (n=3). The volume of the NanoCaPs-pDNA complexes or NanoSiCaPs-pDNA complexes added into each well was maintained at 81.5µl. The amount of

total pDNA complexed with each sample was 6.35µg, equivalent to 2.11µg per well. The NanoCaPs were incubated with the cells for 24 hours after which transfection efficiency was measured by counting the GFP positive cells using the Accuri C6 Flow Cytometer. Cells were allowed to incubate with NanoCaPs and NanoSiCaPs for 24 hours after which they were extracted from the well plates using 0.5% trypsin-EDTA solution. The cells were re-suspended in 400 µl PBS (pH of 7.4) and transferred to 15 mm tubes for flow cytometry. On the Accuri C6 (Accuri Cytometers, Ann Arbor, MI) flow cytometer, the FLA-1 filter set corresponds to the GFP wavelengths. The cells were selected using a forward v/s side scatter plot from a sample of GFP negative cells serving as the control by using accordingly, cells transfected with void NanoCaPs (without plasmid DNA). This also gave us a filter for correcting the auto fluorescence. After filtering out the auto fluorescence, the ratio of GFP-positive to total number of cells was then obtained for each well (total of 5000 cells were counted for each sample). This ratio was subsequently used as a measure for calculating the transfection efficiency for the respective transfection agent.

3.2.6 Plasmid DNA binding assay

The extent of pDNA binding for particles synthesized was determined via Nanodrop 2000 spectrophotometer (Thermo Fisher). 250 µl solutions of un-substituted NanoCaPs and NanoSiCaPs, loaded with pDNA as well as void, were prepared for each sample (n=3). Once synthesized, all the solutions were then centrifuged at 4°C for 10 minutes at 12,000g using a Mikro 200R ultracentrifuge (Andreas Hettich GmbH & Co.KG, Tuttlingen, Germany). Following centrifugation, the amount of unbound, non-precipitated DNA remaining in the supernatant of each solution was then quantified by measuring the optical density (OD) at 260

nm using the NanoCaPs without pDNA as a blank. It was also verified that none of the supernatants absorbed at 320nm, since this would indicate that either not all of the precipitate was removed by centrifugation or that further precipitation occurred after centrifugation. The binding efficiencies were then determined using the following equation:

$$E\% = ([pDNA]_o - [pDNA]_f)/[pDNA]_o \, x \, 100 \quad \text{(Equation 3-3)}$$

Where, $[pDNA]_o$ represented the concentration of pDNA added to the reaction mixture and $[pDNA]_f$ represented the concentration of the non-precipitated pDNA remaining in the supernatant.

3.2.7 Transmission electron microscopy (TEM) of the synthesized NanoCaPs and NanoSiCaPs complexes

The NanoCaPs complexes were prepared according to the aforementioned synthesis protocol (Section 2.2). One drop, approximately 5µl, of un-substituted NanoCaPs, 8.3, 50 and 83.3 NanoSiCaPs complexes was then immediately added onto a carbon coated copper grid (Electron Microscopy Sciences, Hatfield, PA) and allowed to equilibrate for 3 min. The grids were then stained with 2% ACS grade uranyl acetate (Sigma Aldrich, St. Louis, MO), rinsed in 95% ethanol and allowed to air dry. Images were subsequently taken using a JEOL 1011 transmission electron microscope (TEM) (Tokyo, Japan) set to an accelerating voltage of 200 kV.

3.2.8 Statistical analysis

Statistical calculations were performed using the IBM SPSS Statistics 20 statistical analysis program. The data was analyzed to test for significant ($p<0.05$) mean differences on dissolution

properties, pDNA binding values and in vitro transfection efficiencies for both NIH3T3 and MDA-MB-231 cells across the various substituted nanoparticles using the one-way analyses of variance (ANOVA). Post hoc tests for pair-wise differences and identification of homogeneous subgroups were also all performed using the Tukey HSD procedures and discussed in the results section for the relevant groups.

3.3 RESULTS

3.3.1 Materials characterization

XRD analysis of samples prepared in the bulk was performed to identify the crystalline phases present and to verify whether the substituted silicate species were incorporated into the HA lattice structure preserving the single-phase HA structure or phase separate out as a distinct and detached phase. The XRD patterns of HA, 8.3SiHA and 16.6SiHA contained peaks that matched with the standard diffraction pattern of HA (JCPDS 01-074-0565), with major peaks centered at $2\theta = 26.0^{\circ}$ (hkl = 002 plane), 32.1° (112), 33.1° (300), and 34° (202) (Figure 3.2). XRD pattern of the as-prepared HA and the different silicate containing HA are shown in Figure 3.2b. No other phase was detected for all these samples although samples exhibit broad diffraction lines, which indicates low crystallinity and nano-crystalline state of the synthesized materials. With further increase in substitution to 33.3mol%, the XRD pattern becomes completely amorphous with no characteristic peaks of HA. The pattern for 50 SiHA, 66.6SiHA and 83.3SiHA however, in addition to the semi-amorphous phase, displayed characteristics of calcium silicate hydrate phases (Figure 3.3). Although the crystalline XRD peaks for 66.6SiHA and 83.3SiHA matches

with the 1.4-nm crystallite size of the tobermorite phase ($Ca_5Si_6O_{16}(OH)_2.8H_2O$) of calcium silicate hydrate [140], no further attempts were however, made in this study to characterize the compositions and structures of the tobermorite and the amorphous phases. The XRD patterns thus indicate that for the amount of silicon, Si mol. % < 33.3 (or 0<x<1), the crystalline phase of the precipitates is HA and silicon can be incorporated into the apatite structure or amorphous phase or in both likely in the form of silicate species.

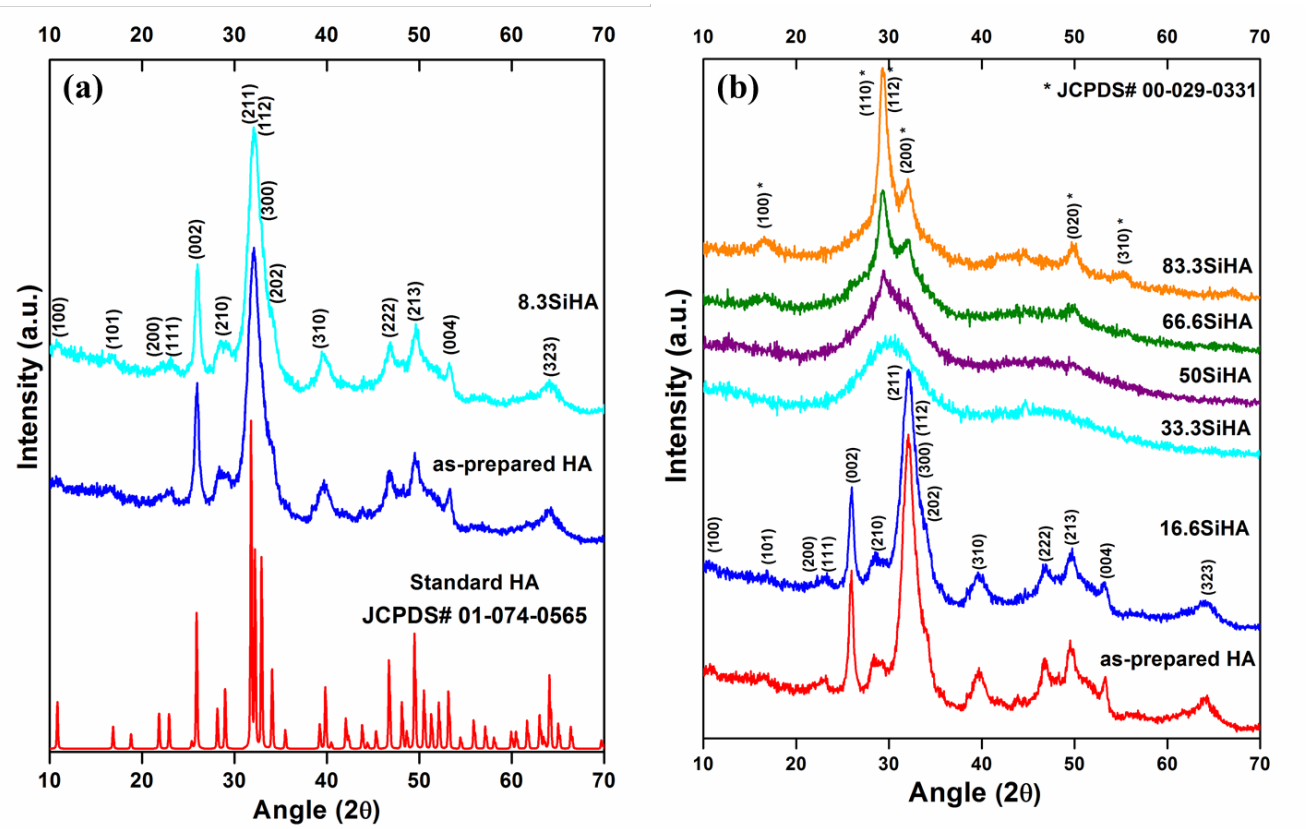

Figure 3.2. X-ray diffraction patterns of as-prepared samples.

(a) XRD patterns of standard HA, as-prepared HA and 8.3SiHA. Peaks were indexed based on the JCPDS #01-074-0565. (b) XRD patterns of as-prepared HA and SiHA with different silicon concentrations. XRD peaks of 16.6SiHA and 83.3SiHA were indexed based on JCPDS # 01-74-0565 and JCPDS # 00-029-0331, respectively.

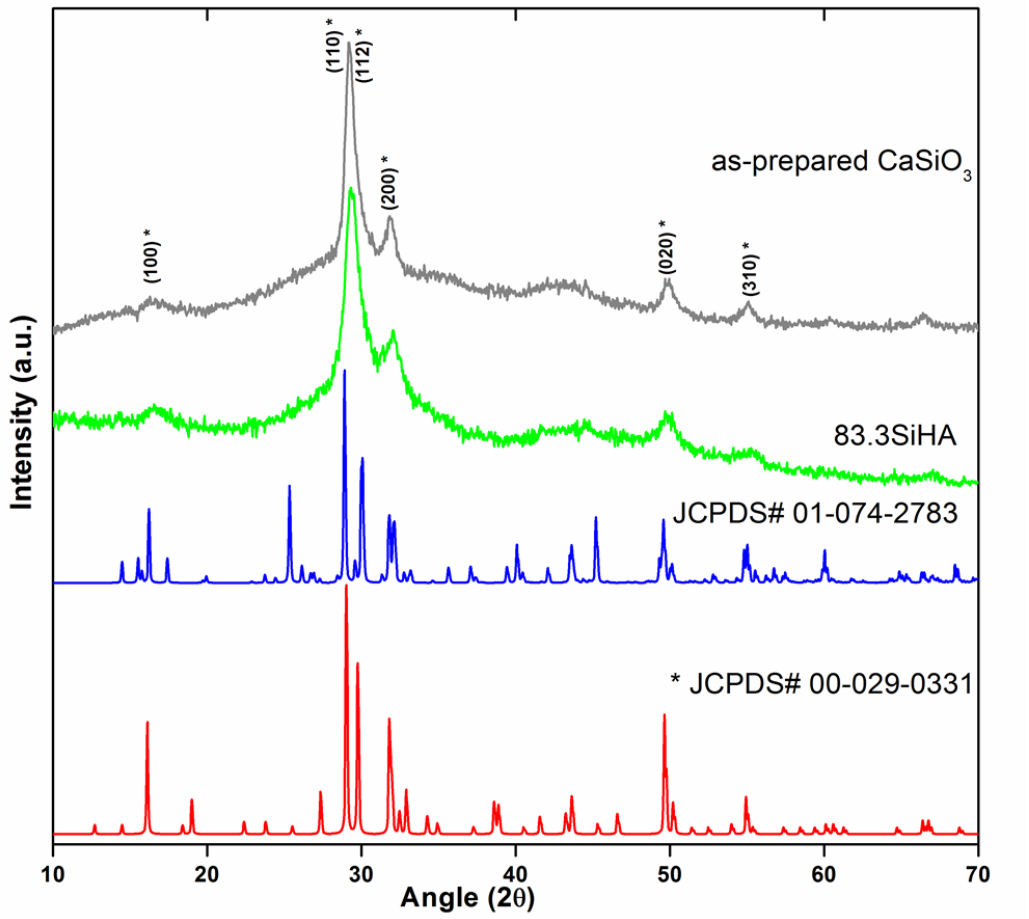

Figure 3.3. X-ray diffraction patterns of as-prepared 83.3SiHA and calcium silicate.

XRD patterns showing comparison of 83.3SiHA with as-prepared CaSiO3 with standard hydrated calcium silicates.

FTIR was therefore performed to identify the molecular groups present in the samples, which in conjunction with XRD, can be used to identify the crystalline and amorphous phases present in the samples. Figure 3.4a show the FTIR spectra for pure HA, as-prepared HA and 8.3SiHA. The FTIR spectrum of the as-prepared HA and 8.3SiHA exhibited bands characteristic of pure HA, including $\nu_4(PO_4)$ bands at 559 cm^{-1} and 599 cm^{-1}, $\nu_3(PO_4)$ bands at 1017 $cm^{-1}$and 1089 cm^{-1}, $\nu_1(PO_4)$ band at 962 cm^{-1}, OH^- stretching band at 3571 cm^{-1} and OH^- bending band at 631 cm^{-1} [108, 138]. Other bands corresponding to HA were also observed, including bands for absorbed

water at 1639 cm^{-1} and 3385 cm^{-1}, and ν_3 bands for carbonate CO_3^{2-} at 1421 cm^{-1} and 1459 cm^{-1}, and $\nu_2$bands for CO_3^{2-} at 875 cm^{-1} that could be attributed to the incorporation of atmospheric CO_2 into the sample. The presence of both absorbed water and CO_3^{2-} has also been previously reported [136, 138, 141]. Few small additional bands not apparent in samples below 33.3 mol% substitution, were observed for 50SiHA, 66.6SiHA and 83.3SiHA (Figure 3.4b) at ~980 cm^{-1} which are attributed to Si-O stretching vibrations and group of bands near 500cm^{-1} that become apparent with increasing silicate concentration are an indication of calcium silicate hydrate phases[142], present as an amorphous phase as indicated by XRD results discussed above. Detection of these molecular vibrations via FTIR irrespective of the amorphous or crystalline state is a clear indicator that all of the silicates for low levels of substitution exhibited the HA phase.

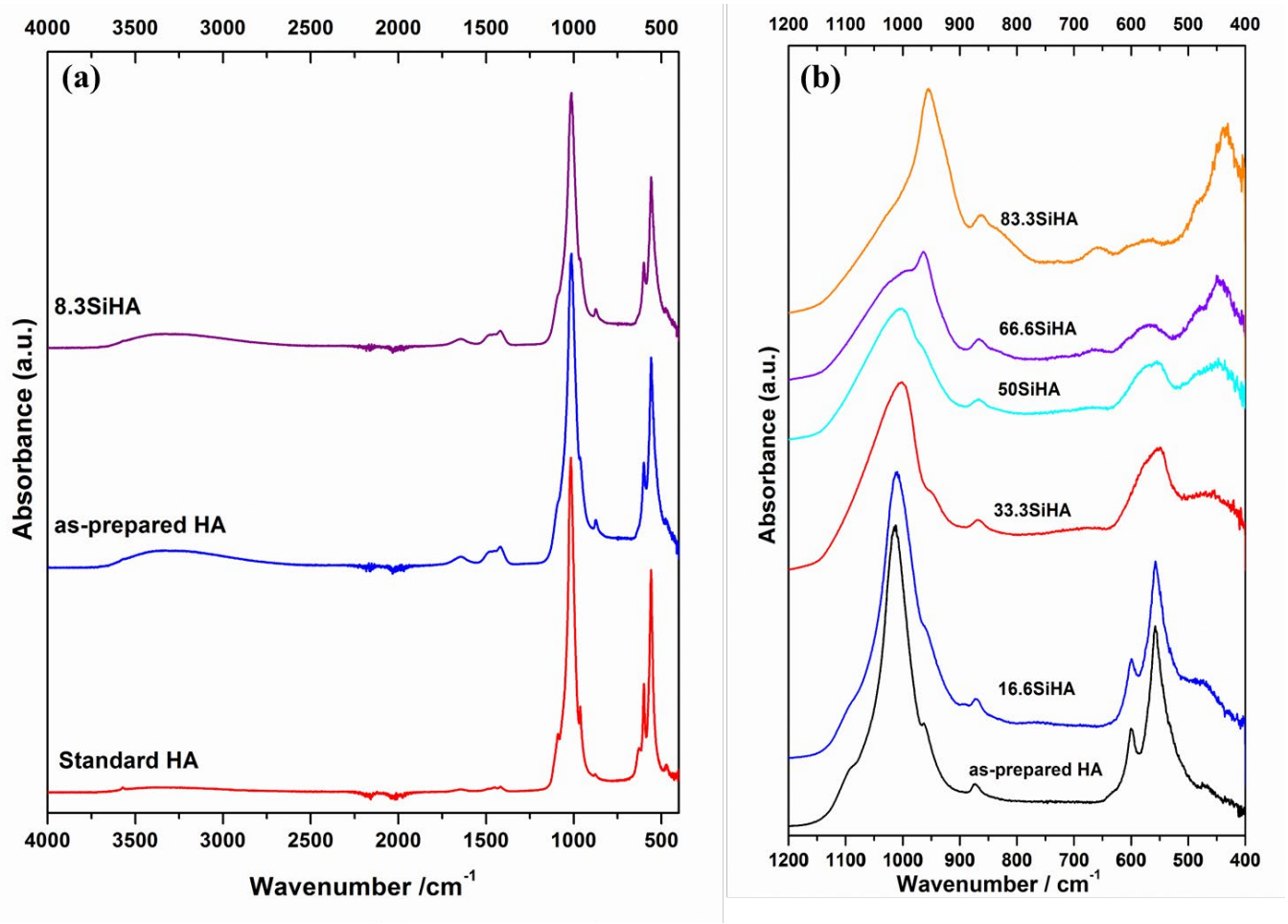

Figure 3.4. FTIR spectra of as-prepared samples.

(a) FTIR spectra of standard HA, as-preapred HA and 8.3SiHA. (b) FTIR spectra of standard HA and SiHA with different silicon concentrations.

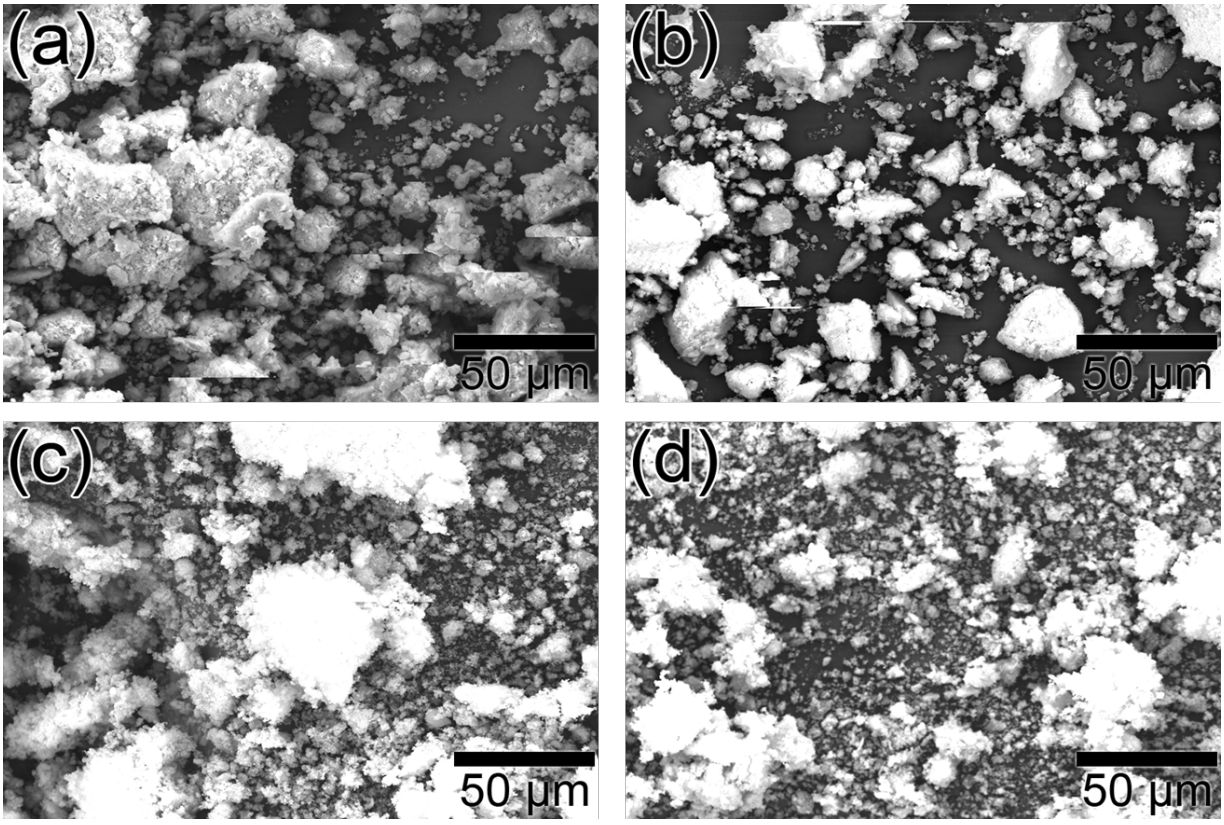

Figure 3.5. SEM of as-prepared HA and SiHA samples.

(a) as-prepared HA, (b) 8.3SiHA, (c) 50SiHA and (d) 83.3SiHA

SEM was then used to observe the morphology of the as-prepared HA and SiHA powders. Due to the semi-amorphous nature of the as-prepared samples, most of the samples appeared to comprise hard aggregates (Figure 3.5) showing no preferred or characteristic features of facets or platelet formation typical of the apatite structures. Hence, it was difficult to detect or distinguish any particular morphology of the particles. Visually, therefore there was also no secondary phase clearly observed in the SiHA samples.

EDAX spectra collected on the samples considered for SEM analysis were used to verify the elemental composition of the samples. The EDAX spectrum obtained for the as-prepared HA powders showed peaks belonging to calcium (Ca) and phosphorus (P) indicating presence of

both elements, as well as small peaks for oxygen (O) (Figure 3.6). The presence of Ca, P, and O confirmed that the sample contained calcium phosphate. Figure 6 depicts the EDAX spectra for 8.3SiHA, 50SiHA and 83.3SiHA, respectively. In addition to Ca, P, O peaks, a silicon (Si) peak was also detected in each of these samples. As anticipated, the 8.3SiHA sample exhibited a larger P peak than Si peak, while the 83.3SiHA sample showed the opposite, reflecting the initial amounts of P and Si in the precursor. The Ca/P molar ratio (1.57) of the as prepared HA powder was lower than the expected value of 1.67 based on the concentration of the starting precursors. Moreover, the ratio of Ca/(P+Si) decreases with increase in silicate substitution most likely due the formation of structural defects, substitution of other cations and anions, and the formation of secondary phases that have been observed in the XRD and FTIR discussed above.

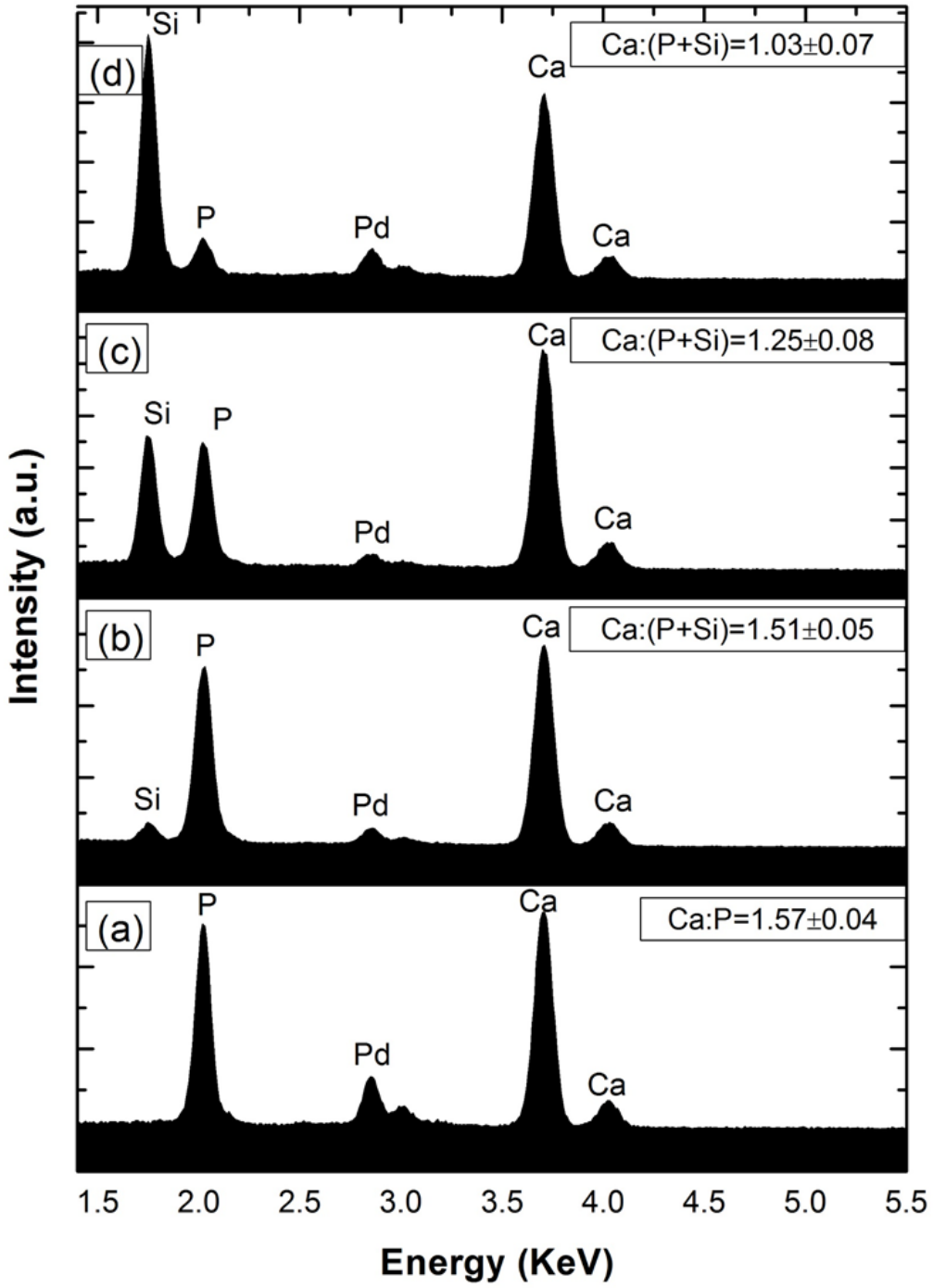

Figure 3.6. EDAX spectra of as-prepared HA and SiHA samples.

(a) as-prepared HA, (b) 8.3SiHA, (c) 50SiHA and (d) 83.3 SiHA

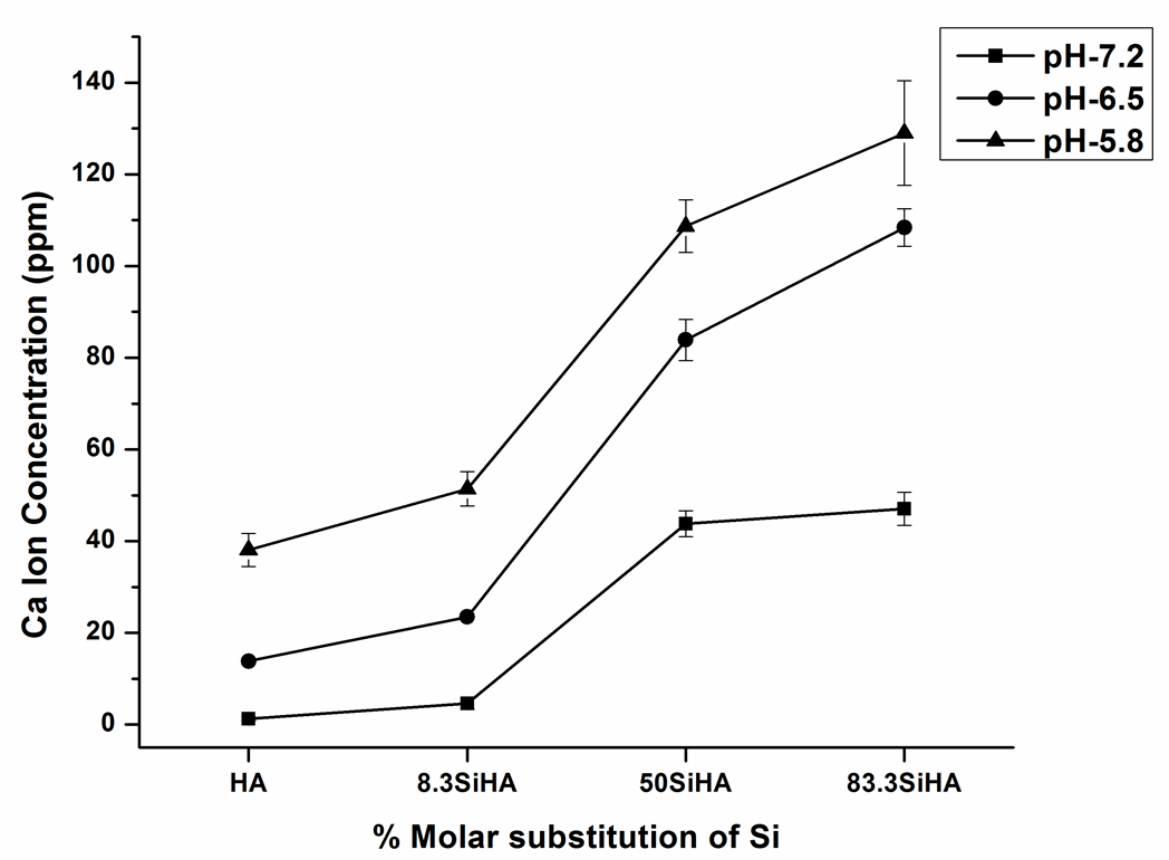

Figure 3.7. Dissolution kinetics of as-prepared HA and SiHA samples.

ICP dissolution study of as-prepared HA and SiHA in BisTris buffer showing released ion concentration of calcium. The data were reported as mean ± SD (n=3).

Dissolution characteristics of the as-prepared samples were evaluated in order to understand the effect of silicate substitution on HA dissolution at different pH. Accordingly, the as-prepared HA and SiHA samples were dispersed in Bis-Tris buffer and aliquots were taken at 24-hour time points. ICP-OES was then used to determine the calcium ion concentrations in the buffers at pH 7.2, 6.5 and 5.8, respectively. ICP-OES measurements show that the silicate substituted samples released much higher levels of calcium than the as-prepared HA, and the dissolution profile of samples increased with higher amounts of silicate (Figure 3.7). It should also be noted that the dissolution increases with decreasing pH, as all the samples released higher amounts of calcium

ion in the increasing order of pH 5.8 > 6.5 > 7.2 ($p<0.05$). This dissolution profile for the various silicate substitutions is clearly an important factor that will contribute to the *in vitro* transfection of these silicate substituted compositions that will be discussed in the following.

3.3.2 In-vitro transfection results

The flow cytometry results of GFP transfected MDA-MB-231 and NIH3T3 cells by NanoCaPs complexes and NanoSiCaPs complexes are shown in Figure 3.8. GFP Fluorescent results at 24 hours post-transfection showed that both cell lines transfected with NanoCaPs, 8.3 NanoSiCaPs, and 16.6 NanoSiCaPs complexes exhibited the highest number of green-fluorescing cells. On the other hand, decrease in GFP expression with 66.6 NanoSiCaPs and 83.3 NanoSiCaPs complexes are observed indicating that very poor transfection is observed for these large silicate substitutions. For NIH-3T3cells (Figure 3.8) in particular, the transfection levels displayed a volcano trend as the anion substitution increased from 0 mol% (un-substituted NanoCaPs) up to 83.3 mol% (83.3 NanoSiCaPs) with increased transfection levels observed for NanoCaPs corresponding to 8.3, 16.6, 33.3 and 50 Si (mol%) substitutions. The transfection results for both the cell lines showed a considerable increase in transfection levels for 8.3, 16.6 and 33.3 NanoSiCaPs compared to the un-substituted NanoCaPs ($p<0.05$). For samples with 66.6 and 83.3 Si (mol%) substitutions, the transfection levels however, began to drop by nearly 10-fold, to the point that the transfection levels practically became insignificant with more than 50% silicate substitution indicating the strong influence of incorporation of silicate ions into the HA structure on pDNA transfection.

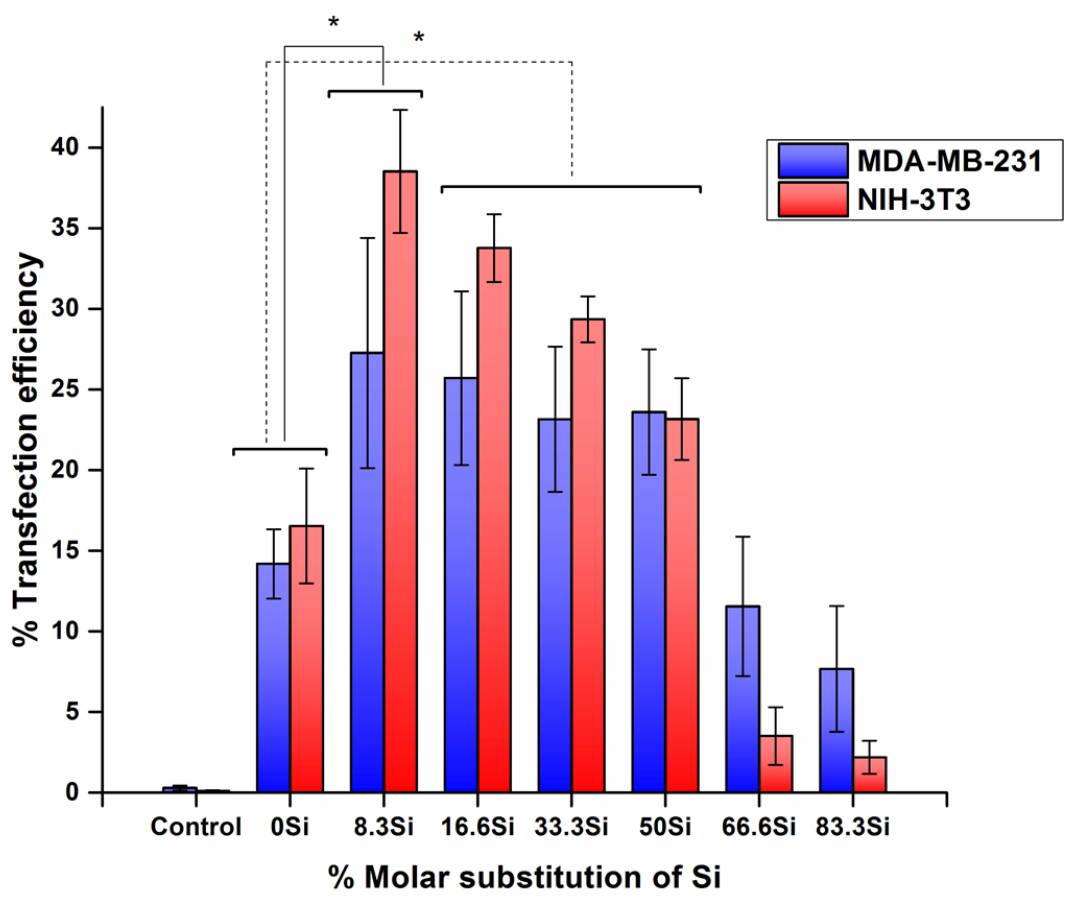

Figure 3.8. Transfection efficiency of NanoCaPs and NanoSiCaPs complexes.

Flow cytometry analysis (at 24hours) of GFP transfected MDA-MB-231 and NIH-3T3 cells by NanoCaPs and NanoSiCaPs complexes with different silicon concentrations. The control used for the flow analysis included GFP negative cells using cells transfected with void NanoCaPs (without pDNA). Transfection experiments were run in duplicates for each sample and repeated three times, n=6 ($p<0.05$). The data were reported as mean ± SD. Post hoc analysis of the transfection profile of NanoSiCaPs with NanoCaPs showed statistical significance ($p<0.05$), indicated by the asterisk (*).

3.3.3 Plasmid DNA binding analysis

DNA loading efficiencies of NanoCaPs and NanoSiCaPs are shown in Figure 3.9. 8.3 NanoSiCaPs were found to be capable of packaging 81% of total pDNA, similar to the control sample of un-substituted NanoCaPs (~82% of total pDNA), statistically not significant. However, as the amount of silicate substitution increased, the corresponding loading efficiency was observed to decline. In fact, for 66.6 and 83.3 NanoSiCaPs, only as much as 10-30% of pDNA was observed to be loaded onto the particles while most of the initial pDNA was observed to remain in the supernatant. This drastic decline in the pDNA loading efficiency in these samples therefore likely contributed to the poor transfection levels since the majority of the initial pDNA was unable to be bound to the NanoSiCaPs gene delivery carriers due to the likely presence of multiple phases as discussed above as well as the probable instability of these phases in the solid state causing the pDNA to remain largely in solution.

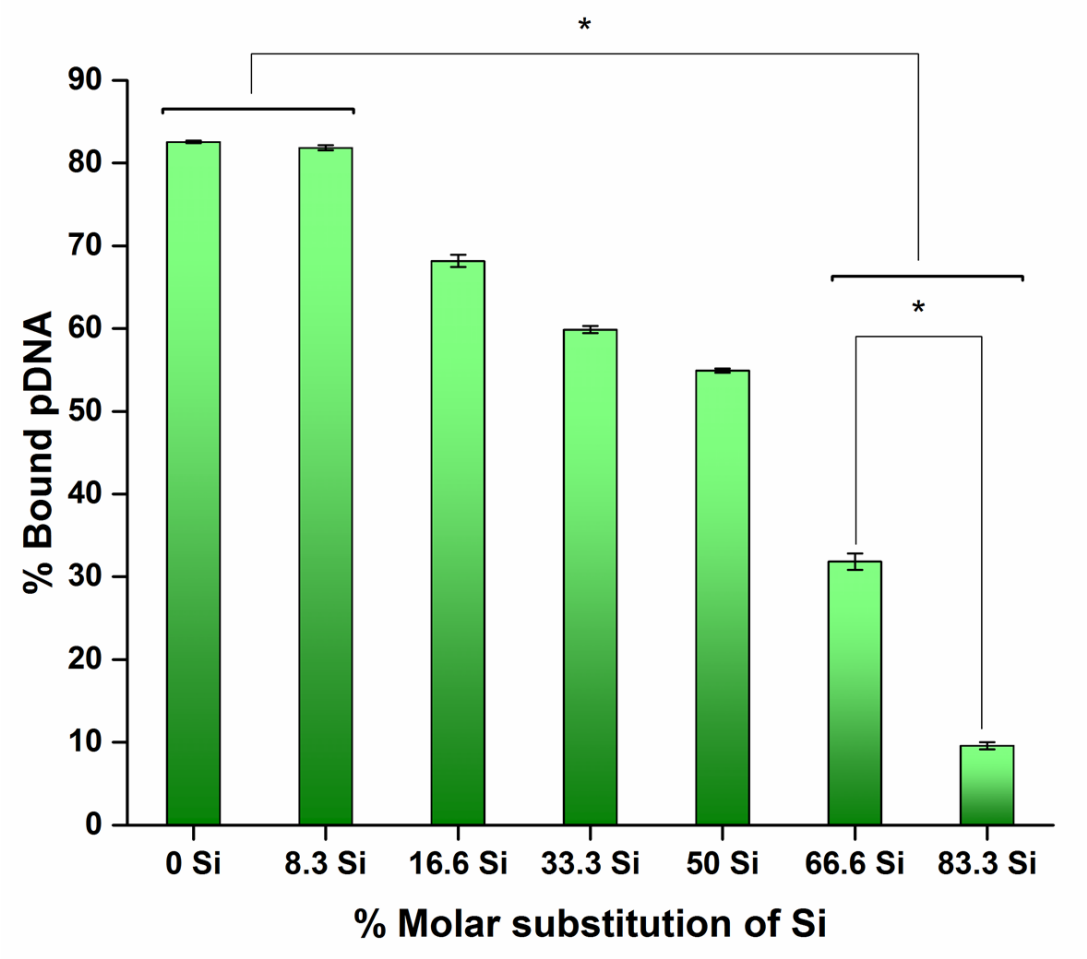

Figure 3.9. pDNA binding efficiency of NanoCaPs and NanoSiCaPs complexes.

Samples were analysed in duplicates and repeated three times, n=6 ($p<0.05$). The data were reported as mean ± SD. Post hoc analysis of pDNA binding efficiency of NanoCaPs, 8.3 NanoSiCaPs with 66.6 and 83.3 NanoSiCaPs were statistically significant ($p<0.05$), indicated by asterisk (*).

3.3.4 Transmission electron microscopy analysis of NanoCaPs and NanoSiCaPs complexes

TEM was used to qualitatively assess the particle size and morphology of the un-substituted NanoCaPs and NanoSiCaPs complexes (8.3, 50 and 83.3 mol% Si substitutions). As shown in Figure 3.10, un-substituted NanoCaPs and NanoSiCaPs complexes appear to be spherical in nature. However, for the un-substituted NanoCaPs, all the particles observed appear agglomerated and with the increase in substitution, the particles appear to be smaller and less agglomerated demonstrating the influence of Si substitution. The particle size estimate for un-substituted NanoCaPs complexes is in the range of 80-100nm where as for the NanoSiCaP complexes, the particle size is in the smaller size range of 50-100nm size.

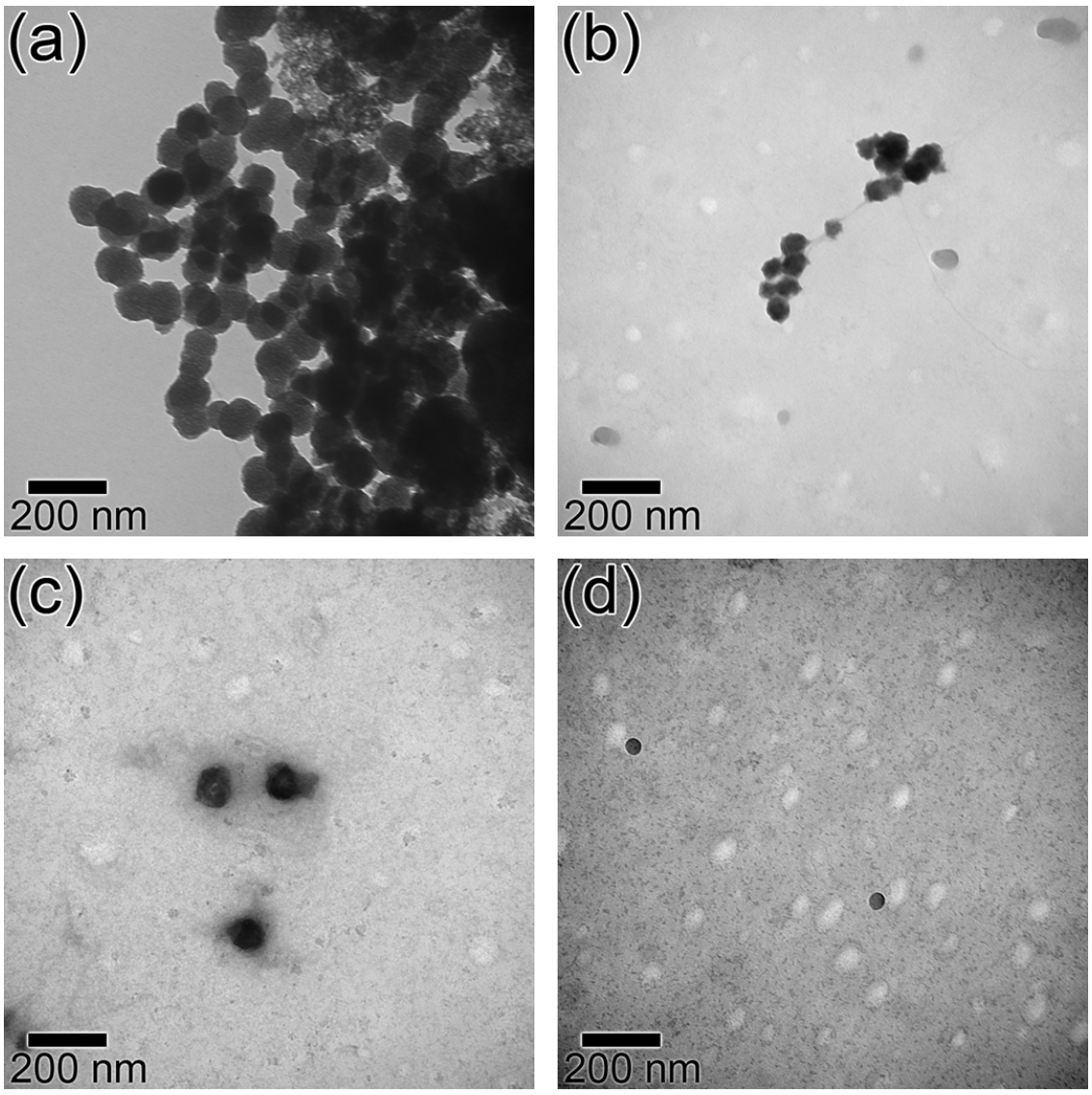

Figure 3.10. TEM images of NanoCaPs and NanoSiCaPs complexes.

(a) un-substituted NanoCaPs complexes, (b) 8.3 NanoSiCaPs complexes, (c) 50 NanoSiCaPs complexes and (d) 83.3 NanoSiCaPs complexes.

3.4 DISCUSSION

There are many potential implications for substituting metallic or non-metallic ionic species into HA, since the substitutions are likely to cause complex structural changes at the unit-cell level [143]. Possible consequences of such ionic substitutions include changes in the physical and chemical properties of HA such as lattice parameter, particle morphology, crystallinity, thermal stability, surface chemistry, overall phase solubility, as well as kinetics of dissolution [106, 107, 135, 144]. Silicon has been reported to be incorporated as a substituent into HA, tri-calcium phosphate (TCP) [145] and bone cements [146], even though HA continues to remain the most popular choice for generating substituted apatites. It has also been demonstrated that the substitution of silicon into HA increases the *in vivo* bioactivity of HA by enhancing its dissolution and that the dissolution rate is enhanced by the presence of site deficiencies and crystallographic imperfections within the HA structure created by the different ionic substitutions [137, 147, 148]. The fact however, still remains that silicon substitution into HA creates a vast range of improvements over pure HA in the field of bioactive bone substitutes. This proven conclusion indicates that it is also possible to achieve similar effects by incorporating silicon into the already published and demonstrated efficacy of NanoCaPs as gene delivery vectors. Therefore, the aim of the current study was to investigate the critical concentration of silicate ions that could be incorporated into the HA lattice without inducing a phase change and consequently, evaluate the gene delivery potential of the silicate substituted HA which is aptly termed as NanoSiCaPs.

Unlike conventional methods involving hydrothermal treatments to force the incorporation of ionic substituents into the HA lattice at extreme temperatures, this study focused on a simple aqueous precipitation approach at room temperature, under ambient pressure and

more importantly, physiological conditions. From the XRD and FTIR data it is clear that the as-prepared HA and SiHA are indeed semi-amorphous, and nanocrystalline in nature, but nevertheless, display the presence of the HA phase only at low concentrations of silicate. With increase in silicate substitution, the XRD patterns become completely amorphous for 33.3SiHA, and upon further increase in the silicate concentration in addition to the semi amorphous phase, there is also the presence of a secondary phase of calcium silicate hydrate having a structure of 1.4 nm crystallite size phase of tobermorite (Figure 3.3).

Based on the published literatures the exact amount of silicate ion incorporation is not well established. However, some recent literature clearly suggests that low levels of silicon, in the range of 0<Si wt. %< 3.51, substitution is possible into the HA lattice [135]. Although the synthesis conditions used in our study is very different from the work reported earlier, the agreement nevertheless is a validation of the solubility of low silicate concentrations into the HA lattice with varying starting precursors, and the formation of single-phase HA structure with no evidence of any crystalline secondary phase.

In addition, FTIR data reveals that other than very slight wavenumber shifts in some of the band positions (Figure 3.4), the 8.3SiHA spectrum very closely matches that of the un-substituted HA. It is also evident that as the Si substitution increased beyond 33.3 mol %, the intensities of the PO_4 bands become less prominent, which correspond to decreasing phosphate and increasing silicate incorporation into the SiHA. In addition to the changes in the PO_4 bands intensities, the OH bands at 3571 (stretching) cm^{-1} and 631cm^{-1}(bending) also decreased in intensity for the 8.3SiHA sample and disappeared altogether for samples with 33.3 (mol%) Si substitution and beyond. This may be due to two possible phenomena occurring. First, increasing the Si substitution could lead to the OH^- groups being substituted by the SiO_4^{4-}, or second, loss of

OH^- groups in order to maintain the overall charge balance [149, 150]. Moreover, the FTIR spectra of the as-dried samples present the characteristic pattern of partially carbonated hydrated hydroxyapatites, as extensively discussed elsewhere [151]. It is also clear that all of the silicates for low levels (≤16.6 mol % or ≤2.8 wt. %) of substitution exhibited the partially hydrated carbonated HA phase. The incorporation of atmospheric CO_2 into the HA structure during the synthesis is also well known which results in the formation of carbonated substituted hydroxyapatite or dahllite [138]. According to literature, the presence of carbonate ion within the as-precipitated apatite phase is also known to inhibit the conversion of the amorphous precipitate to the crystalline phase [152, 153], thus being responsible for the low crystallinity of the as-precipitated samples as evidenced by the XRD results. The influence of time-temperature history on the as-prepared powders were however, not included in this study as the main focus was primarily on the synthesis of silicate-substituted nanoparticles for in-vitro gene transfection under ambient conditions.

Due to the semi amorphous nature of the as-prepared samples it was difficult to detect or distinguish any preferential morphology of the particles. As the particles were agglomerated, presence of any distinct secondary phase morphology for 50SiHA and 83.3SiHA was not unequivocally visible (Figure 3.5). However, EDAX spectra collected from the SEM images revealed the elemental composition of the samples (Figure 3.6). As anticipated, the 8.3SiHA sample exhibited a larger P peak than Si peak, while the 83.3SiHA sample showed the opposite, corresponding to the initial nominal precursor amount of P and Si.

It should also be noted that the obtained ratio of Ca/P of 1.57 by EDAX in the as prepared HA is very similar to the value reported earlier by our group using ICP-OES [154]. The non-stoichiometry of the as prepared HA powder by simple precipitation is very common and is

known to mostly depend on the influence of various process parameters[154, 155] and also due to the formation of defects such as vacancies in the crystal lattice[156, 157], and also the substitution of diverse ions such as carbonate, sodium and chloride in the lattice structure[158]. Therefore, the slight decrease in (Ca/P+Si) ratio for 8.3SiHA (Figure 3.6) is not surprising and most likely due the formation of vacancies or defects and other ion substitutions into the HA structure. However, a large decrease in (Ca/P+Si) ratio for the 50SiHA and 83.3SiHA is most likely due the presence of a secondary phase in addition to the vacancies or substitution of by other ions in the HA structure. The XRD and FTIR results (Figure 3.2, Figure 3.3 and Figure 3.4) have confirmed the formation secondary phases of 1.4-nm crystallite sized tobermorite phase ($Ca_5Si_6O_{16}(OH)_2$). $8H_2O$) and other amorphous calcium silicate hydrate phase. The Ca/Si ratio in tobermorite is 0.83 and therefore, it expected that the formation of tobermorite will reduce the overall (Ca/P+Si) ratio. This also implies that some part of the calcium salt remained unreacted in the solution and did not precipitate due to the lack of critical concentration of anions necessary for reaching the required solubility product to initiate the precipitation of the compound.

The in vitro gene delivery potential of NanoCaPs and NanoSiCaPs was evaluated using pDNA encoding GFP on a hard to transfect [159], NIH-3T3 fibroblast cell line and MDA-MB-231, a breast cancer cell line (Figure 3.8). At higher levels of silicate substitution, the chemical composition of the nanoparticles appeared to have a major impact on the gene delivery results. As evidenced from the XRD and FTIR results, formation of different phases at high levels of silicate substitution and their varying ability to bind pDNA together could be attributed for the decline in the observed gene delivery transfection results for these samples. The drastic decline in DNA loading efficiency in these samples therefore resulted in the poor transfection levels since the majority of the initial DNA was unable to be bound to the NanoSiCaPs gene delivery

carriers (Figure 3.9) due to the likely presence of multiple phases with poor pDNA binding affinity as discussed above. Further, the differences in the negative charge caused by the incorporation of higher amounts of silicate could have led to increased repulsion between the silicate and the negatively-charged DNA, as well as the increase in the site defects and vacancies within the structure of NanoSiCaPs caused by higher silicate substitution. All of these aspects could contribute to the decreased capacity for the NanoSiCaPs of higher silicate content to efficiently bind DNA. Due to these reasons, increasing the silicate substitutions to a large degree primarily contributed to causing a reduction in the observed transfection efficiency. Additionally, we assessed transfection efficiency of NanoSiCaPs (8.3 mol% Si) with commercially available transfection reagents (see Section A.3 for results and discussion).

On the other hand, 8.3 NanoSiCaPs that maintained the HA structure indicated a two-fold increase in the transfection efficiency for NIH-3T3 cells (Figure 3.8). Previous studies have indicated that incorporation of silicate ions into the HA lattice would distort and destabilize the structure, therefore making it energetically favorable for substituted HA to dissolve faster than the as prepared HA phase [136]. This higher solubility and unstable characteristic of Si substituted HA could play a crucial role in the rapid dissolution of the endocytosed nanoparticles and thus facilitate escape of the lysosomal degradation, preserving the DNA in its pathway to the nucleus. The faster dissolution will lead to rapid release of ions in the endosomes and these ions will in turn increase the osmotic pressure thereby rupturing the endosome membrane enabling release of their contents in the cytosol.

In order to validate this reasoning, dissolution characteristics for other anion and cation substituted calcium phosphate gene delivery systems have been investigated [104, 106, 107]. Dissolution of the as prepared HA and SiHA samples in Bis-Tris buffer (Figure 3.7) clearly

showed that the silicate substituted samples underwent more dissolution as compared to HA. ICP data also clearly indicated that higher amounts of calcium ions are released from the SiHA samples in the buffer system having a physiological pH-7.2, early endosome pH-6.5 and late endosome pH-5.8 (Figure 3.7). ICP analysis of 50SiHA and 83.3SiHA at pH-7.2 also shows that at higher concentrations of silicate, the prepared SiHA samples are unstable at physiological pH and undergo rapid dissolution, thereby further explaining the low transfection and pDNA binding capabilities of these samples. This result also clearly indicates that Si gets incorporated into the HA lattice at low levels of substitution, which thereby influences the dissolution characteristics of the as prepared samples. The presence of Si in the as prepared samples is also extensively explained by Hayakawa et al, wherein the authors have shown that as prepared SiHA consists mainly of partially amorphous hydrated and carbonated calcium phosphate incorporating polymeric silicate specie [136]. It is indeed the presence of Si in the system that leads to accelerated degradation of apatite particles in line with our observations reported here. TEM analysis of the complexes also revealed that the particles tend to agglomerate less with silicate substitution (Figure 3.10). However, the primary particle size of NanoCaPs-pDNA and NanoSiCaPs-pDNA seem to be in the same range of 50-100nm, although the NanoSiCaPs complexes consist of smaller aggregates. This trend was also observed at multiple locations on the TEM grid for NanoCaPs and 8.3 NanoSiCaPs. On the other hand, 50 and 83.3 NanoSiCaPs-pDNA complexes had nearly no aggregate formation to an extent that it was difficult to image any complexes for 83.3 NanoSiCaPs-pDNA. This can also be attributed to the poor stability of these samples under physiological pH as evidenced in the dissolution study (Figure 3.7), which can explain the presence of fewer particles for these samples in the TEM analysis. These results are in accordance with previous reports describing cationic substitution of magnesium and

anionic substitution of fluoride ions, wherein substitution of ions in trace amounts resulted in enhanced transfection owing to faster dissolution and reduced particle aggregation of CaP based vectors [104, 105]. Therefore, combination of rapid dissolution and smaller agglomerate formation of the NanoSiCaPs-pDNA complexes combined with the maintenance of the HA structure result in efficient pDNA binding and condensation. In summary, these aspects altogether thus render 8.3 mol% Si substituted NanoSiCaPs a superior gene delivery vector compared to pure and unsubstituted NanoCaPs.

3.5 CONCLUSIONS

In this study different silicate substituted nano-particulates of calcium phosphates were prepared and characterized using XRD, FTIR, SEM and TEM. Silicate substitution below a certain concentration ($x \leq 16.6$ mol %) retains the single phase of partially hydrated and carbonated hydroxyapatite structure. Upon increasing the silicate incorporation (16.6 mol % $\leq x \leq$ 33.3 mol %), the nanoparticles of hydroxyapatite phase of calcium phosphate changes to an amorphous form and upon further increase in substitution ($x \geq 33.3$ mol %) leads to formation of nanoparticles containing hydrated calcium silicate phases. pDNA transfection results indicate that 20-50 % increase in transfection was observed for 8.3-50 mol % silicate containing samples compared to NanoCaPs. However, further silicate substitution (>60 mol %) resulted in considerable reduction in transfections. Instability of the silicate substituted NanoCaPs and the optimal concentration of Si responsible for maximal binding of pDNA result in the 8.3 mol% Si substituted NanoSiCaPs demonstrating optimal transfection. From these results it can thus be concluded that suitable concentration of substitution of phosphates by silicates in nanostructured

calcium phosphates forming NanoSiCaPs thus significantly improve the *in-vitro* pDNA transfection suggesting NanoSiCaPs to be promising gene delivery systems.

3.6 ACKNOWLEDGEMENTS

The work presented in this chapter was partially supported by NSF (CBET-0933153) and has been published in the Materials Science and Engineering C journal [160]. We would also like to acknowledge the Edward R. Weidlein Chair Professorship Funds and the Center for Complex Engineered Multifunctional Materials (CCEMM), Swanson School of Engineering, and the University of Pittsburgh for providing partial support in the form of support for student, reagents, equipment and other accessories much needed for conducting this research. Specifically, we would like to thank Dr. Ipsita Banerjee, Department of Chemical Engineering, University of Pittsburgh, for the use of flow cytometry.

4.0 FABRICATION OF POLYELECTROLYTE NANOSICAPS ASSEMBELIES ON TITANIUM SUBSTRATES FOR SURFACE MEDIATED GENE DELIVERY

4.1 INTRODUCTION

Surface properties of biomaterials play a crucial role in determining the initial host tissue response, which in turn plays a significant role in determining the long-term success of the implants [161, 162]. Surface mediated gene delivery from implants is an attractive approach to stimulate specific cellular response at the molecular level [163]. Currently, layer by layer (LbL) assembly [164] and biomineralization [39] are two common approaches for surface modification of orthopedic implants to incorporate substantial amounts of plasmid DNA (pDNA) on the implants. However, these methods involve prolonged incubation (>48 hours) of substrates in supersaturated calcium phosphate solution [165, 166], or multistep procedures comprising alternate dipping cycles in polycationic and polyanionic solutions [167]. Therefore, herein we focused on the development of a novel surface modification technique that: 1) involves a quick and easily adaptable methodology applicable to materials used for dental and bone repair, with different geometries and composition; 2) provides an easily accessible medium promoting cell attachment and proliferation; and 3) acts as a gene-activating material [163].

Commercially available pure Ti is by far one of the most widely used material for dental and bone repair due to its superior mechanical properties and biocompatibility [168, 169].

However, despite its beneficial properties numerous physical and chemical methods are employed for surface modification of Ti surfaces to promote osseointegration [168, 170]. Therefore, gene delivery through the Ti surface makes it an ideal choice of substrate for the current study. Chapter 3 described the development of NanoSiCaPs, a modified version of our previously reported work on nanostructured calcium phosphate particles (NanoCaPs), with 8.3 mol% or 1.4 weight% of silicate substituted in lieu of the phosphate [160]. This substitution resulted in two-fold increase in gene transfection capability of NanoSiCaPs, due to its superior solubility and ensuing materials properties [160]. As outlined in Figure 4.1, our goal is to incorporate NanoSiCaPs (complexed with pDNA) on Ti substrates, where NanoSiCaPs mediate the delivery of plasmid DNA (pDNA) to MC3T3-E1, a murine pre-osteoblasts cell line, seeded on top of the Ti surface.

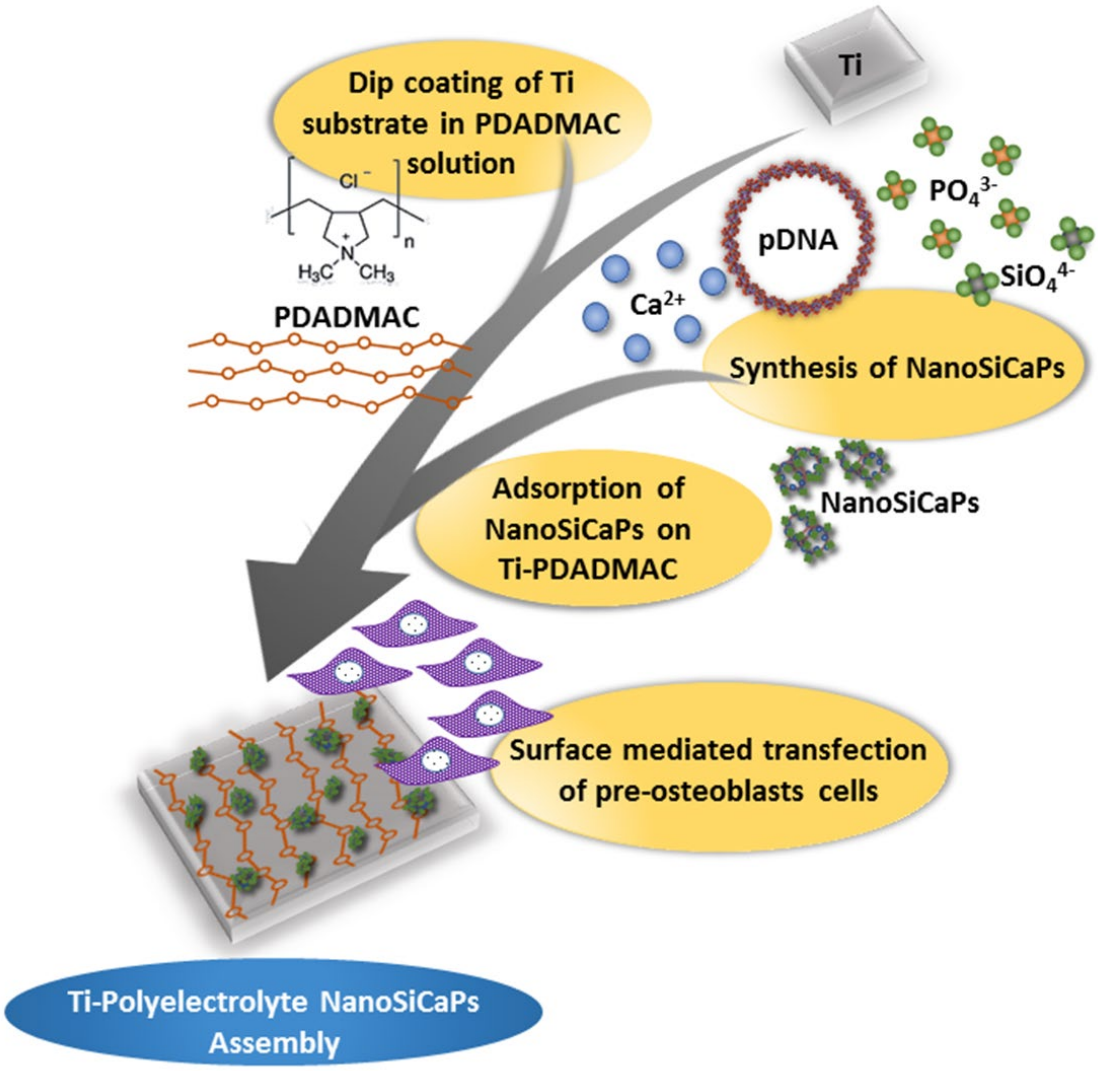

Figure 4.1. Schematic representation of fabrication of Ti-polyelectrolyte NanoSiCaPs assembly (PNA).

4.2 MATERIALS AND METHODS

4.2.1 Materials

Calcium chloride ($CaCl_2 \cdot 2H_2O$, 99% purity), trisodium phosphate ($Na_3PO_4 \cdot 12H_2O$), sodium chloride (NaCl), dextrose, AlamarBlue Cell Viability Assay were purchased from Fisher Scientific (Pittsburgh, PA). Poly-(diallyl-dimethyl-ammonium chloride) medium molecular weight (Mw 100-200kDa, 20wt% in water), Potassium chloride (KCl, 99+%), Paraformaldehyde, and Phalloidin-Tetramethylrhodamine B isothiocyanate (phalloidin-TRITC) was purchased from Sigma Aldrich (St. Louis, MO). 4',6-Diamidino-2-phenylindole (DAPI) was purchased from PacReacAppliChem (Maryland Heights, MO). Sodium hydroxide (NaOH) was purchased from Mallinckrodt Baker Inc. (Phillipsburg, NJ). Sodium metasilicate ($Na_2SiO_3 \cdot 5H_2O$) and Titanium (Ti) (99.7%, metal basis), 0.89mm thick, was purchased from Alfa Aesar (Ward Hill, MA). HEPES (99%) and were obtained from EMD Chemicals (Gibbstown, NJ). Reporter plasmid, gWiz^{TM} GFP (Green Fluorescent Protein) was purchased from Aldevron LLC (Fargo, ND). All the reagents were used as received without further modification or purification.

4.2.2 Synthesis and fabrication of Ti-PNA

4.2.2.1 Substrate preparation

Titanium substrates were cut into squares of 1 cm x 1 cm x 0.89mm and cleaned using acid etching and repeated washing with acetone. The substrates were then polished with 320, 600 and 1200 grit SiC paper and cleaned under ultrasonication using acetone.

4.2.2.2 Fabrication of Ti-PDADMAC

Cleaned Ti-substrates were immersed in PDADMAC solution (5 mg/mL), in phosphate buffer (pH-7.5) at room temperature (RT). After 15 minutes the substrates were then drawn at a constant speed of 200 μm s^{-1} using a dip coater (Desktop Dip Coater, MTI Corporation, USA, Model No EQ-HWTL-01-A). Substrates were subsequently washed in deionized (DI) water for 1 minute and dried at RT.

4.2.2.3 Synthesis of NanoSiCaPs complexes

NanoSiCaPs were synthesized according to a protocol previously described (see Section 3.2.3). Briefly, 62 μl of 2M $CaCl_2$ and 25.6 μl of plasmid DNA (1mg/ml, gWiz GFP) were diluted in 412.4 μl of ddH_2O to form solution A (500μl total). An equal volume (500μl) of solution B containing HEPES-buffered solution (280 mM NaCl, 10 mM KCl, 12 mM dextrose, and 50 mMHEPES) with 1.37 mM of Na_3PO_4 and 0.13 mM of Na_2SiO_3 [160]. The HEPES-buffered solution was intended to maintain the pH of the precursors at 7.5. The molar ratios of *Ca/(P+Si)* maintained at 130. NanoSiCaPs were then synthesized using a Harvard Apparatus PHD 2000 Infuse/Withdraw syringe pump (Holliston, MA) to introduce and mix the two solutions in a controlled drop wise fashion to generate a homogeneous dispersion of the NanoSiCaPs in solution. Hence, solution A was added drop by drop into solution B at an addition rate of 13.4μl/s while solution B was vortexed at 500 rpm (Figure 3.1). The addition rate and molar ratio of *Ca/(P+Si)* was also selected following our previously published report [171].

4.2.2.4 Fabrication of polyelectrolyte NanoSiCaPs assemblies (PNA)

Ti-PDADMAC substrates were gently placed in a 24-well plate. 1 mL of freshly synthesized NanoSiCaPs was added for each substrate and incubated for 10 minutes at room temperature

(RT) in the cell culture hood. After 10 minutes of incubation, substrates were carefully withdrawn manually with help of tweezers and allowed to dry at RT for 5 minutes. Substrates were subsequently washed by dipping in DI water for 1 minute. Coated substrates were then either used for cell culture studies or stored in desiccator for surface characterization studies (Figure 4.1). For some studies, where specified, Ti-PDADMAC-pDNA substrates were also made, by immersing Ti-PDADMAC substrates in equal volume of pDNA solution (25.6 μg in 1ml DI water).

4.2.3 Surface characterization techniques

PDADMAC polymer solution, bare Ti and Ti-PDADMAC were analyzed using attenuated total reflectance Fourier transform infrared spectroscopy (FTIR; Nicolet 6700 Thermo Scientific). The spectra were collected in the range of 4000–500 cm^{-1}. The surface morphology of Ti-PNA was studied using scanning electron microscopy (SEM) with a Philips-XL30 FEG operating at 10.0 kV. All the samples used for SEM analysis were coated with Pd using a sputter coater system. The surface topography and roughness of the bare Ti, Ti-PDADMAC and Ti-PNA were characterized by non-contact atomic force microscopy (AFM) using MFP-3D AFM (Asylum Research) and Igor Pro (Wavemetrics) analysis software as previously described [172]. Topography images of 80 by 80 microns were taken with a silicon nitride conical tip ($k = 40Nm^{-1}$, Mikromasch, Ltd) at a scan rate of 1Hz and 512 by 512-pixel resolution. Root mean square (RMS) surface roughness quantification was performed at n = 3 random 20 by 20-micron regions within the images. Water contact angle was determined using a Theta Lite Optical Tensiometer (Attension, Biolin Scientific) equipped with image analysis software (Theta Lite). By applying the sessile drop method, drop of 200 pixels were created at the tip of the syringe and carefully

placed on top surface of the substrate. Measurements were conducted immediately after placing the drop at RT. The contact angle was calculated using the Young-Laplace fit equation.

4.2.4 In-vitro experiments

Murine osteoblast cell line MC3T3-E1 was obtained from ATCC (Manassas, VA). Cells were cultured in humidified incubator at 37 °C and 5% CO_2, in minimum essential medium alpha (MEM α; Gibco, Grand Island, NY) supplemented with 10% fetal bovine serum (FBS) and 1 % penicillin/streptomycin (P/S). Cells at third to seventh passage were used in these experiments. For *in-vitro* transfection, cells were plated at a density of 4.0 x 10^4 cells on tissue culture polystyrene (TCPS) as control, Ti-PDADMAC-pDNA and Ti-PNA substrates placed in a 24-well plate. Level of GFP-expression was qualitatively assessed using fluorescence microscope (Olympus, CKX41). For quantitative analysis of GFP expression, flow cytometry was performed on day 3. Growth media was aspirated out from each well and phosphate buffered saline (PBS, pH-7.4) was added (500 µl each) to wash off the FBS, which can inhibit trypsin action. After about 30 s, the PBS was aspirated and 200 µl of 0.5% trypsin-EDTA solution was added to each well. The cells were incubated in trypsin for ~3 minutes at 37 °C followed by addition of 800 µl of growth media containing FBS. After some agitation to ensure removal of all the cells from the well surface, the suspension was aspirated into epi-tubes and centrifuged at 500 rpm for 5 minutes. The supernatant was aspirated; the cells were re-suspended in 400 µl PBS (pH-7.4) and transferred to 15 mm tubes for flow cytometry. On the Accuri C6 (Accuri Cytometers, Ann Arbor, MI) flow cytometer, the FL1-A filter set corresponds to the GFP wavelengths. The cells were selected using a forward v/s side scatter plot from a sample of GFP negative cells as control (cells plated on TCPS). This also gave us a filter for auto fluorescence.

After negating the auto fluorescence, the ratio of GFP-positive to total number of cells was obtained for each well (total of 5000 cells were counted for each sample, n=3). This ratio was used as a measure for calculating the % transfection efficiency. In vitro viability of MC3T3-E1 cells at different time points (n=3) was performed using AlamarBlue Cell Viability Assay according to manufacturer's protocol. Media containing 1/10 volume of Alamarblue was freshly prepared and incubated at 37°C for 3 hours to measure cell activity. Media was transferred to 96-well plates and then measured the fluorescence at 560nm/585nm (excitation/emission) using microplate reader (Biotek, Synerge2). Qualitative assessment of pDNA coverage on coated substrates was performed using DAPI staining. DAPI staining solution was diluted in PBS at 300nM and then added to bare Ti, Ti-PDADMAC-pDNA and Ti-PNA substrates. Substrates were incubated for 15 minutes, washed in PBS then imaged using fluorescence microscope (Olympus, CKX41). Cytoskeletal staining of filamentous actin (F-actin) was visualized using Phalloidin-Tetramethylrhodamine B isothiocyanate (phalloidin-TRITC). Cells attached to substrates (bare Ti, Ti-PDADMAC and Ti-PNA) were fixed using 4% Paraformaldehyde for 10 minutes then incubated 0.1% tritonX 100 to facilitate permeabilization. After blocking in 1% BSA, cells were incubated with phalloidin-TRITC for 40 minutes at room temperature washed with PBST then imaged with fluorescence microscope (Olympus, CKX41). DAPI was used as a counter stain.

4.2.5 Statistical analysis

Statistical calculations were performed using GraphPad Prism software. The data was analyzed to test for mean differences on contact angle, RMS values, *in vitro* cell viability results for different samples using one-way analyses of variance (ANOVA) and p-value of <0.05 was

considered statistically significant. Each ANOVA on these response variables was significant at $p<0.05$, n=3. Post hoc tests for pair-wise differences and identification of homogeneous subgroups were performed using the Tukey HSD procedures for contact angle and RMS measurements. For *in-vitro* transfection analysis using flow cytometry, paired t-test was performed with a $p<0.05$.

4.3 RESULTS

4.3.1 Surface characterization

FT-IR was used to confirm the presence of PDADMAC on Ti substrates. The FT-IR spectrum of Ti substrate coated with PDADMAC matched the spectrum of pure PDADMAC with IR absorption peaks at 1470cm^{-1} (C-H_2 stretching) and 1409cm^{-1} (symmetric bending mode of the $^{+}$N-CH_3 group) [173, 174] indicating the presence of PDADMAC on the Ti substrates (Figure 4.2).

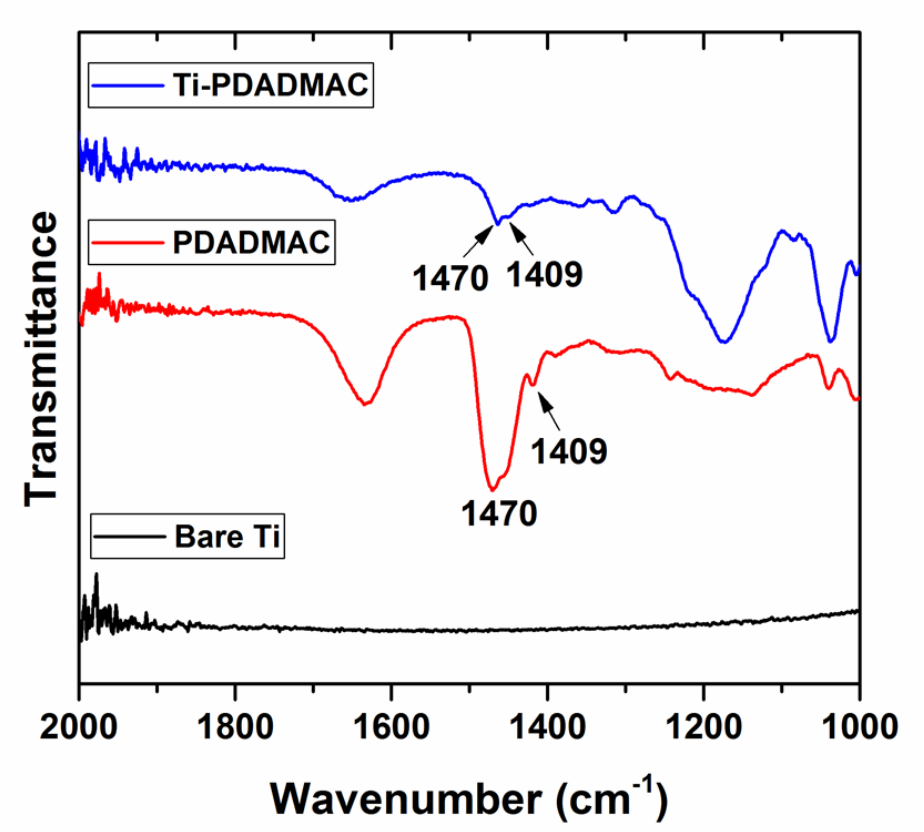

Figure 4.2. FTIR spectrum of coated substrates.

The surface morphology of the coated substrates was investigated using scanning electron microscopy (SEM) and atomic force microscoy (AFM). SEM images of the Ti-PNA are shown in Figure 4.3, which suggests that NanoSiCaPs were uniformly coated on the entire Ti substrate (Figure 4.3a). Moreover, the primary particle size of the NanoSiCaPs are in the range of 50-100nm as reported in our earlier work [160] (Figure 4.3).

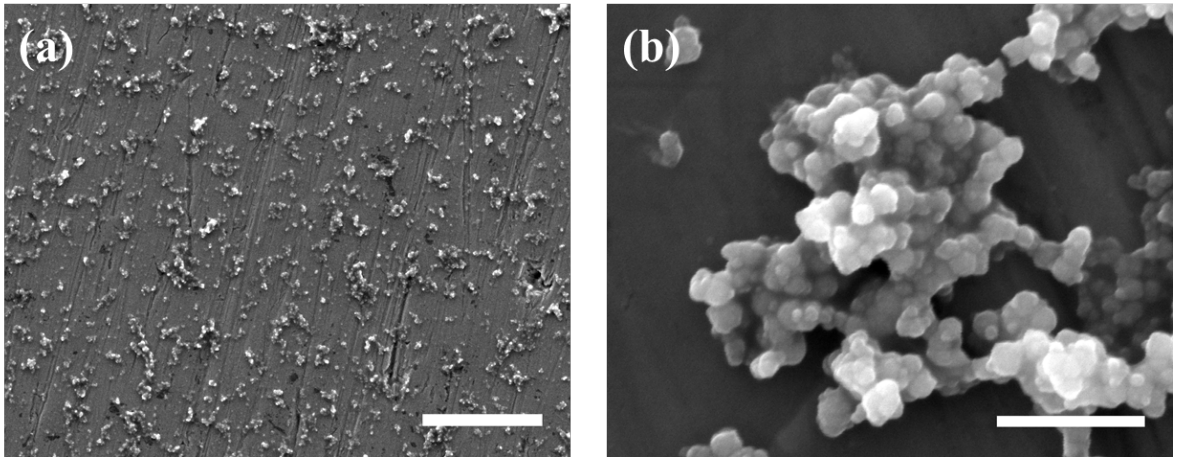

Figure 4.3. SEM micrograph of Ti-PNA.

(a) scale 20µm and (b) scale 1µm.

AFM images of Ti-PNA films are generated using non-contact mode shown in Figure 4.4a, Figure 4.4c and Figure 4.4e. Root mean square (RMS) surface roughness quantification was performed at (n = 3) random 20 by 20-micron regions within the images. The surface morphology of the coated substrates changes from a smooth surface for bare Ti, RMS~80nm and Ti-PDADMAC films, RMS~45nm (Figure 4.5), to a rougher surface covered by the complexed particles after NanoSiCaPs adsorption, RMS~145nm. To further illustrate these differences, 3D-image reconstructions for the Ti-PNA films is presented in Figure 4.4b, Figure 4.4d and Figure 4.4f. SEM and AFM analysis proved the change in surface morphology upon fabrication of PNA on Ti-surfaces.

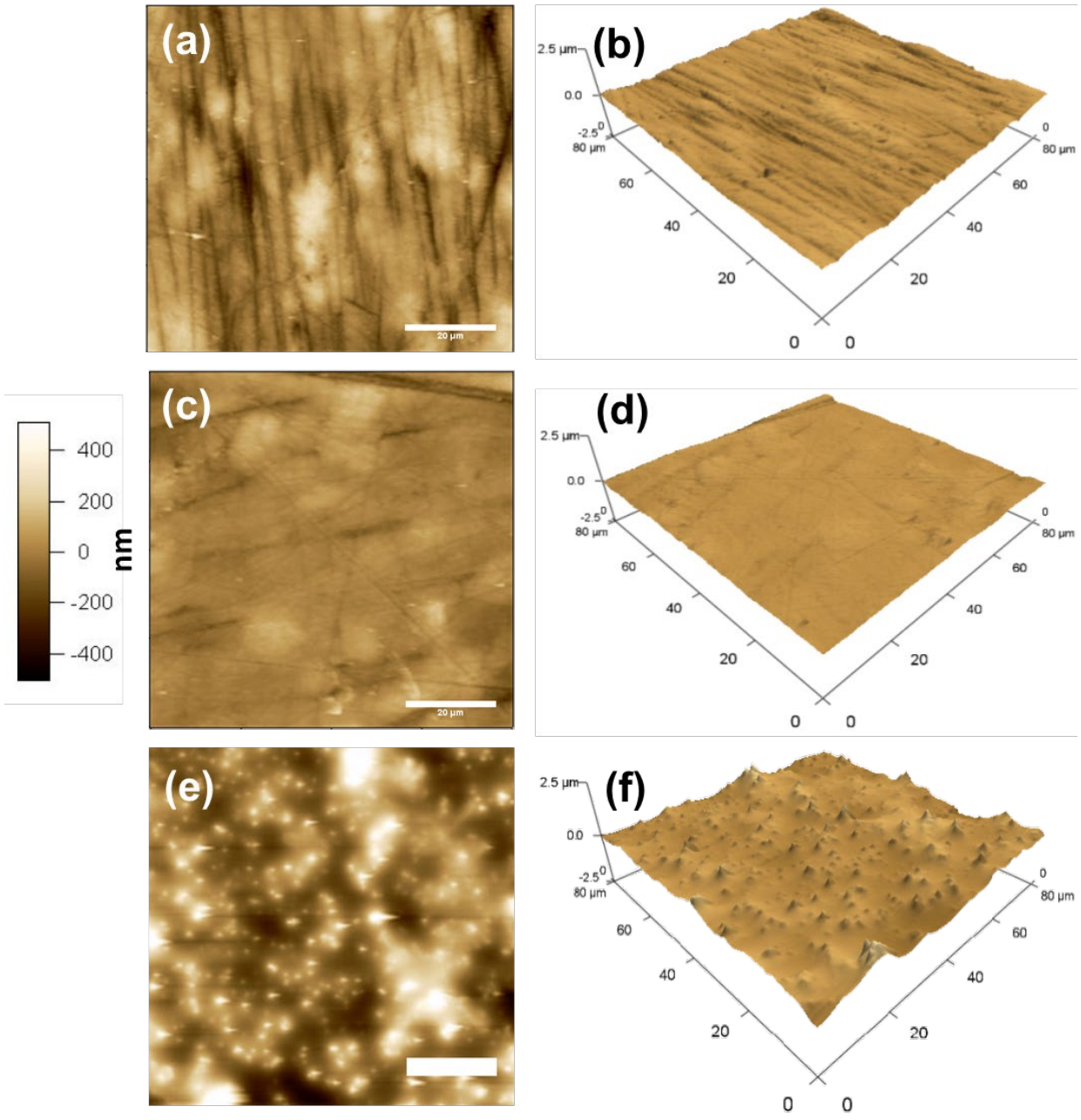

Figure 4.4. AFM analysis of coated substrates.

AFM height images of (a) bare Ti, (c) Ti-PDADMAC and (e) Ti-PNA (scale 20µm). 3-D image reconstruction of AFM height images showing the morphology of: (b) bare Ti, (d) Ti-PDADMAC and (f) Ti-PNA.

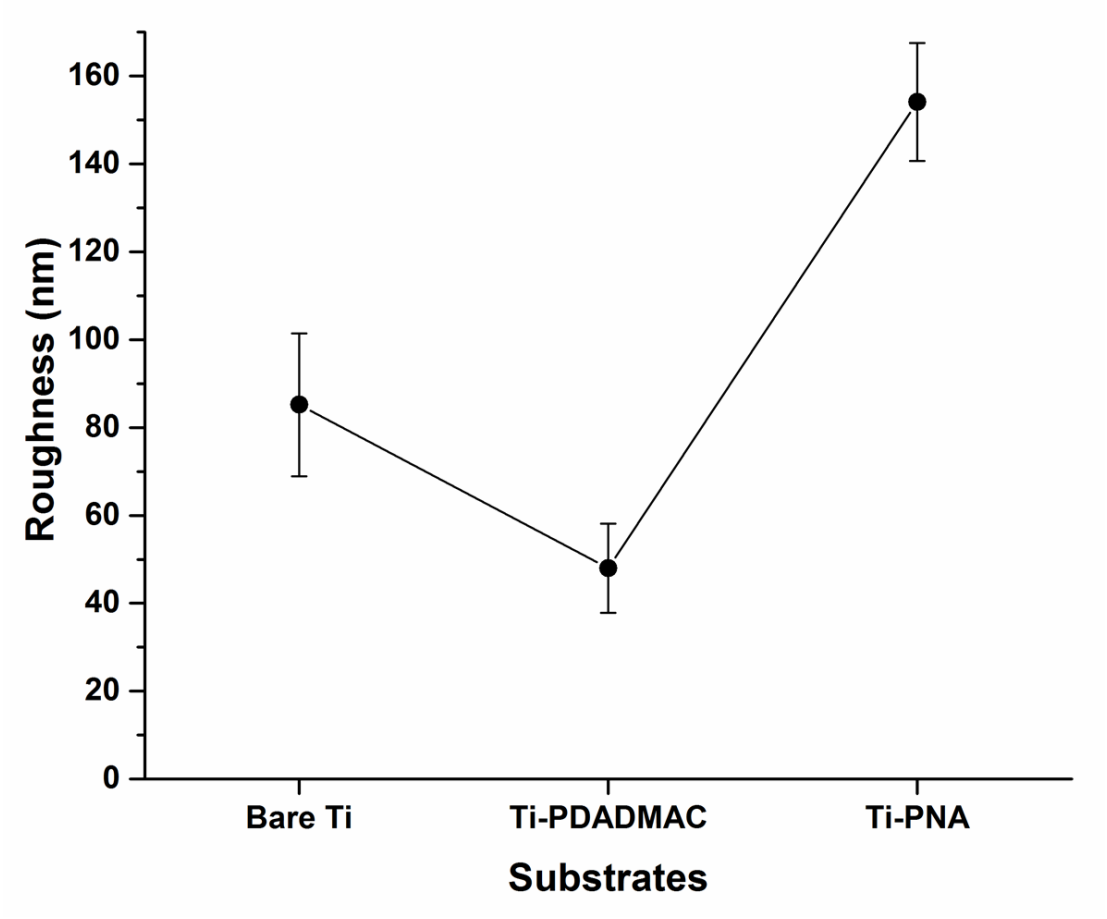

Figure 4.5. Surface roughness quantification of coated substrates.

Root mean square (RMS) roughness quantification using AFM ($p<0.05$). The data were reported ± SD, n=3.

Additionally, surface wetting properties was also investigated by measuring the water contact angle at three separate locations on the coated substrates. It was determined that the contact angle of bare Ti (61.5±2.1°) was similar to Ti-PDADMAC (63±3.5°), as shown in Figure 4.6. However, the contact angle decreased to 29±1.4° ($p<0.05$), with accompanying NanoSiCaPs adsorption on the substrates, which suggests that the adsorption of NanoSiCaps renders the surface more hydrophilic.

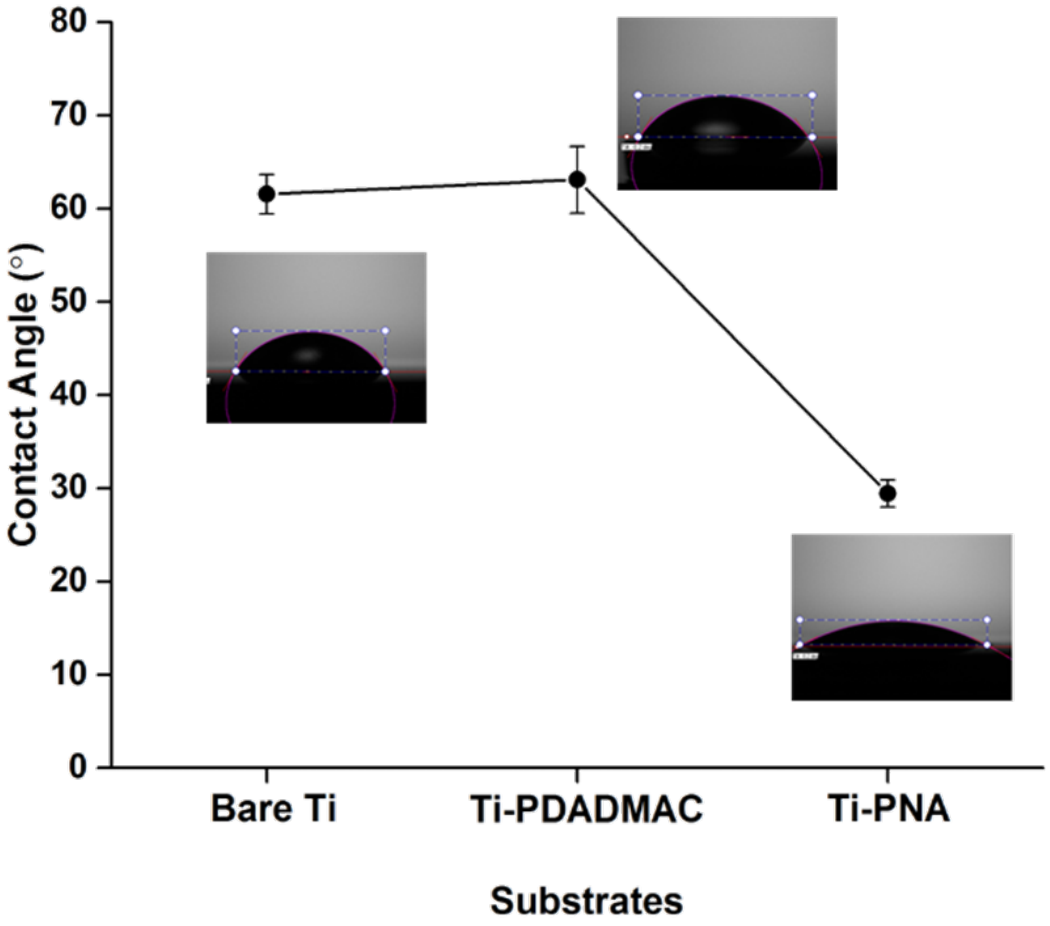

Figure 4.6. Contact angle measurements.

Water contact angle measurements on bare Ti, Ti-PDADMAC and Ti-PNA ($P < 0.05$). The data were reported ± SD, n=3.

Presence of pDNA on the Ti-PNA films was detected by DAPI staining of the substrates (Figure 4.7). Overall, surface characterization results demonstrate that PNA coating strategy is successful in obtaining a nanoceramic coating on Ti substrates and has a direct influence on the surface properties of the substrates.

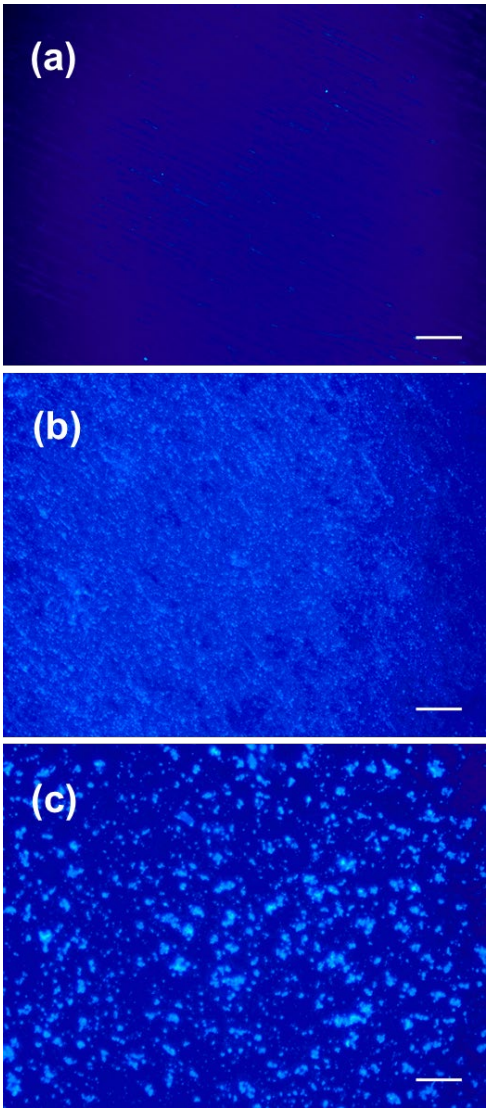

Figure 4.7. DAPI staining of coated substrates.

DAPI staining of substrates showing presence of pDNA in the coatings. (a) bare Ti, (b) Ti-PDADMAC-pDNA and (c) Ti-PNA (scale 200µm).

4.3.2 In-vitro transfection

In-vitro transfection potential of Ti-PNA was evaluated using pre-osteoblast (MC3T3-E1) cells. Subject to the same conditions, a control group received equal amounts of pDNA on Ti-PDADMAC substrates, but without NanoSiCaPs. Substrates were prepared on the day of cell seeding. GFP expression of the transfected cells was monitored using a fluorescent microscope. Transfected cells were observed as early as day 1 and the GFP expression peaked at day 3 (Figure 4.8) for Ti-PNA, while the substrates lacking NanoSiCaPs (only pDNA) showed little to no GFP expression, Figure 4.8d, Figure 4.8e and Figure 4.8f. GFP expression of MC3T3-E1 cells was also quantified using flow cytometry at day 3, Figure 4.8g. The Ti-PNA coated substrates exhibited transfection in ~13% of cells, whereas the substrates lacking NanoSiCaPs showed no transfection in agreement with fluorescence microscopy results ($p<0.05$). These results thus indicate that Ti-PNA serves as a gene-activating material and highlights the importance of incorporating a pDNA vector in the coating to achieve successful delivery of pDNA to cells.

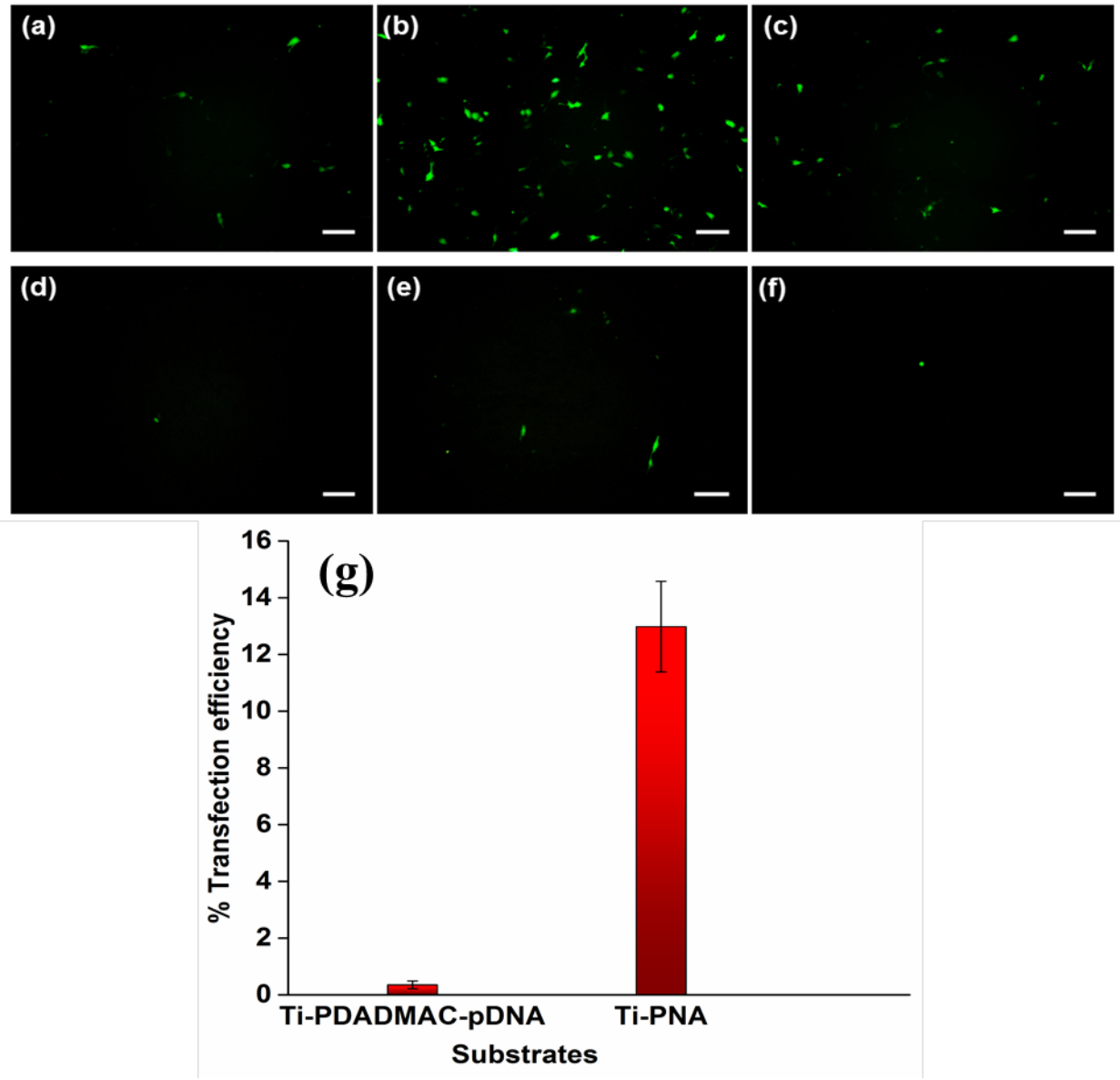

Figure 4.8. Surface mediated in-vitro transfection of MC3T3-E1 cells.

Fluorescence microscopy images of MC3T3-E1 cells on: Ti-PNA on (a) day 1, (b) day 3 and (c) day 7 (scale 200µm); Ti-PDADMAC-pDNA on (d) day 1, (e) day 3 and (f) day 7 (scale 200µm). Flow cytometry analysis measuring GFP expression in MC3T3-E1 cells at day 3. The data were reported ± SD, n=3 ($p<0.05$).

4.3.3 Cell attachment and viability

Finally, we determined the cell viability of MC3T3-E1 cells seeded on the coated substrates using alamar blue assay™. Tissue culture polystyrene (TCPS) and bare Ti were used as control groups. Cell viability of the coated substrates was no different than the positive control (bare Ti) or the negative control (TCPS) with no statistically significant difference at each time point (Figure 4.9).

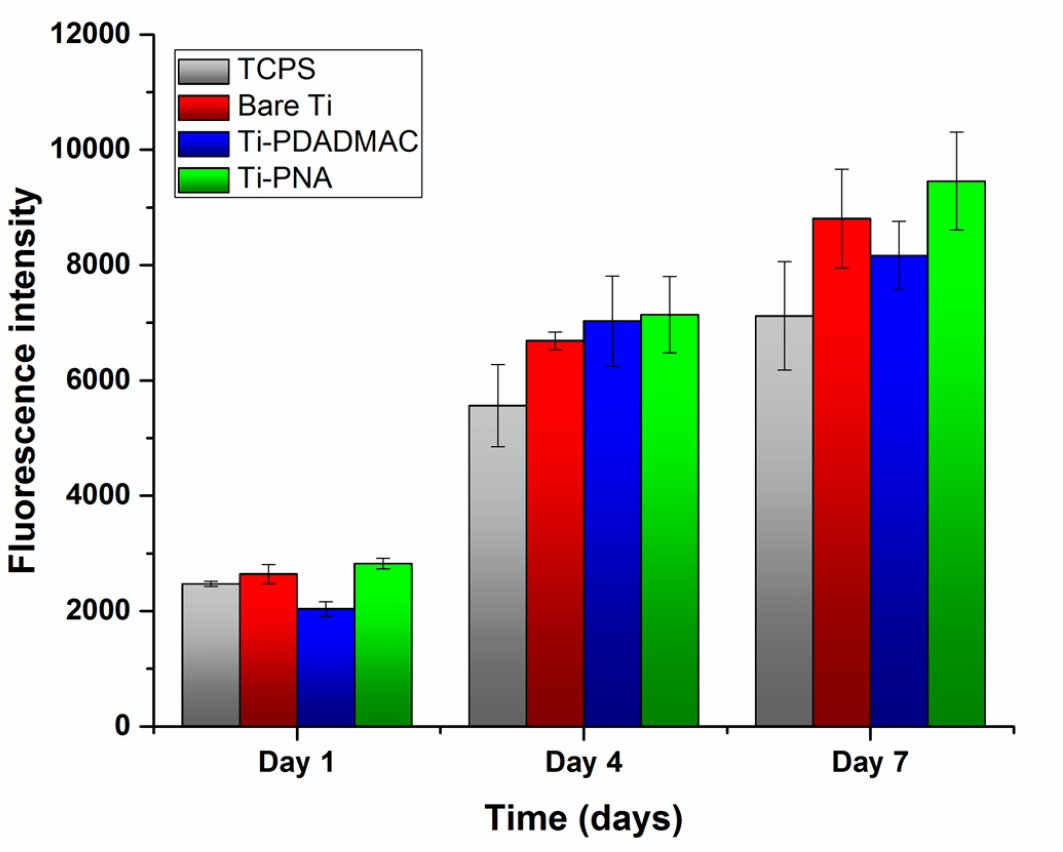

Figure 4.9. Cell viability assay of coated substrates.

Cell viability measured using MTT assay at different time points ($p<0.05$). No statistical significance between groups ($p>0.05$). The data were reported ± SD, n=3.

The cell morphology was also observed to evaluate cell attachment and spreading on the substrates as cytoplasmic extensions are crucial for cell adhesion, migration and formation of cell-cell junctions [83, 175], which are also key factors dictating tissue integration of the implants [119]. MC3T3-E1 cells attached on the substrates were stained for F-actin (filamentous-actin), a cytoskeletal element (in red) and nucleus (in blue), on day 3. Figure 4.10a-f demonstrates that bare Ti, Ti-PDADMAC, and Ti-PNA favorably supported attachment and proliferation of the pre-osteoblast cells. These results thus indicate that Ti-PNA enables attachment, spreading and proliferation of pre-osteoblast cells.

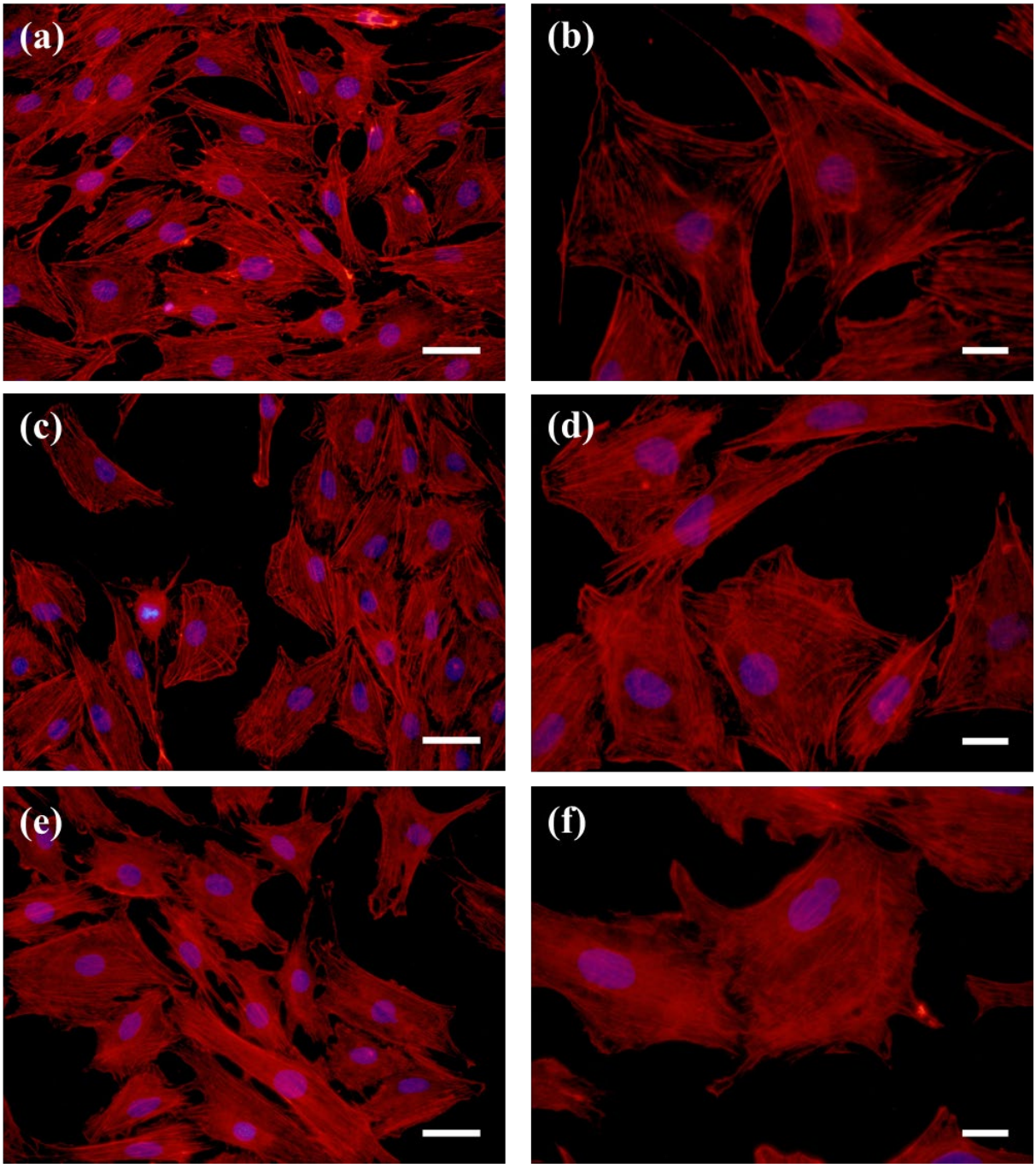

Figure 4.10. Cytoskeletal staining of MC3T3-E1 cells.

Cytoskeletal staining showing F-actin (red) and nucleus (blue) for (a) bare Ti, (c) Ti-PDADMAC and (d) Ti-PNA (scale 50µm). (b) bare Ti, (d) Ti-PDADMAC and (e) Ti-PNA (scale 20µm).

4.4 DISCUSSION

Gene delivery from the surfaces of implants is a unique strategy to facilitate tissue regeneration and integration. However, it has been challenging, because of the difficulty to incorporate and deliver sufficient amounts of plasmid DNA (pDNA) to cells from the implant surface allowing efficient gene expression. This study shows enhanced and optimized non-viral transfection of MC3T3-E1 cells, murine pre-osteoblasts cells mediated via NanoSiCaPs complexes. Additionally, we describe a novel and simple coating approach using NanoSiCaPs that preferentially adsorb onto titanium (Ti) substrates coated with poly (diallyldimethylammonium chloride) (PDADMAC) (Figure 4.1). The Ti-polyelectrolyte NanoSiCaPs assemblies aptly called PNA deliver pDNA to MC3T3-E1 cells and induce protein production, without eliciting cytotoxicity, while simultaneously encouraging cell attachment on the substrate.

There were four reasons that suggested that the PNA assembly was fabricated onto the Ti surface. First, the presence of polyelectrolyte PDADMAC was confirmed by FTIR which particularly is a useful analytical technique for identification of molecular groups present, validating the formation of the coating (Figure 4.2). Second, the particle diameters observed via scanning electron microscopy (SEM) images (Figure 4.3a and Figure 4.3b) were consistent with the size of NanoSiCaPs complexes displayed in the TEM as reported in Section 3.2.7. The results also demonstrated that NanoSiCaPs complexes covered the Ti-PDADMAC coating with primary particle size of 100nm (Figure 4.3b). Third, AFM measurements displayed change in surface morphology of the Ti surface from rough to smooth surface upon PDADMAC adsorption, and to even rougher surface following NanoSiCaPs adsorption (Figure 4.4a-f and Figure 4.5). Fourth, the alternate fluctuation of contact angles of the surface indicated that the layer of PDADMAC and NanoSiCaPs was assembled on to the surface (Figure 4.6).

The polyelectrolyte used in the current study, PDADMAC, is a typical representative of a water-soluble polycation with quaternary amines with a surface charge ~ 70mV [176]. PDADMAC is known for its role in separation of biomolecules [177], protein immobilization [178], and flocculation of silica and latex particles [179]. Zhao et al demonstrated use of PDADMAC and poly (acrylate sodium) (PAS, as polyanion) for synthesis of hybrid CaP particles for delivery of anticancer drug, which demonstrated good dispersibility and colloidal stability in water [174]. Due to its high surface charge, it was hypothesized that the use of positively charged, PDADMAC as a surface coating would enable higher adsorption of negatively charged NanoSiCaPs complexes [67] (zeta potential ~ -20mV) through electrostatic interactions. Although, the amount of NanoSiCaPs complexes adsorbed on the Ti-surface was not calculated in the current study, qualitative assessment of the Ti surfaces using SEM, AFM and DAPI staining clearly showed that the NanoSiCaPs complexes was indeed present on the Ti-PDADMAC coatings. The practical significance of this fabrication technique is that it takes less than 30 minutes for adsorption of both the layers, in contrast to existing surface mediated gene delivery techniques using CaP based methodologies that require more than 48 hours of incubation in super saturated calcium phosphate solutions [122-124]. Thus, the approach described herein may be particularly translated to medical device applications where degradable scaffolds are utilized, such as Mg-based alloys, thereby avoiding any potential degradation of the bulk material with prolonged incubation in aqueous conditions. In addition, this methodology can be utilized for creation of off-the-shelf coated implants for their use in bone tissue engineering applications.

The cytocompatibility and transfection ability of the fabricated coating was assessed using in-vitro experiments with MC3T3-E1 cells. F-actin and DAPI staining of cells revealed

that the cell morphology was not affected by the presence of either the polymer or NanoSiCaPs coating (Figure 4.10a-f). Cell viability assay of MC3T3-E1 cells on different coatings indicated that the coatings with or without NanoSiCaPs complexes did not induce any significant cytotoxicity compared with tissue culture plastic or bare Ti (Figure 4.9). The in-vitro transfection results of Ti-PNA showed that GFP expression peaked at day 3 and then decreased by day 7 (Figure 4.8a-c and Figure 4.8g), which was probably due to degradation of pDNA and cell proliferation. On the other hand, Ti-PDADMAC-pDNA samples showed very little transfection at all-time points (Figure 4.8d-f and Figure 4.8g). These results indicated the importance of including a transfection agent in achieving successful surface mediated gene delivery. Other commercially available cationic polymer-based transfection vector was not incorporated in the current study for comparison since the fabrication technique relied on electrostatic interaction between the positively charged polymer, PDADMAC and negatively charged complexes, either pDNA alone or NanoSiCaPs (with pDNA).

Although, direct comparison of transfection results observed in this study with surface mediated results reported by others is not possible at large, some generalizations can be made based on studies incorporating same cell-line and reporter gene (GFP) for estimating transfection efficiency. Notably, Liu et al reported assembly of multilayers of cationic lipid/pDNA (LDc) and hyaluronic acid (HA) on Ti surfaces by LBL technique [180]. The authors estimated transfection efficiency of MC3T3-E1 cells by measuring the GFP expression of transfected cells. The authors observed highest transfection efficiency at day 1 with 21.25% GFP positive cells, which decreased to 7.37% GFP positive cells by day 3 [180]. In contrast, the Ti-PNA displayed 13% GFP positive cells by day 3. It is also important to note that the high transfection efficiency reported by the Liu et al on day 1 was for the Ti-samples coated with 8 bi-layers of HA/LDc

[180], whereas the current study only incorporated one layer of NanoSiCaPs on the Ti surface. Decline in transfection efficiency by day 3 for the reported work was attributed to the fact of potential cytotoxicity of cationic lipids incorporated in the bi-layers [180], which was consistent with a previous study [181]. This further proves the cytocompatibility and efficiency of NanoSiCaPs vectors in comparison to reported lipid and cationic polymer based non-viral vector systems. In light of this knowledge, the polyelectrolyte NanoSiCaPs assembly (PNA) studied here may offer great opportunities for achieving enhanced surface mediated non-viral gene delivery for localized gene delivery applications for functional bone tissue repair and regeneration.

4.5 CONCLUSIONS

We have developed a novel two-step, and a user-friendly coating strategy on Ti surfaces using electrostatic interaction between a polycation, PDADMAC and negatively charged NanoSiCaPs. Interestingly, the coated Ti-PNA substrates enable rapid cell attachment, spreading and proliferation of the pre-osteoblast cells. Most notably, the entire PNA fabrication process requires only 30 minutes to obtain a nanoceramic complexed coating, and this methodology can be easily used to coat various substrates of different composition and geometries due to its simplicity. The *in-vitro* transfection results indicate that Ti-PNA is an excellent platform for surface mediated gene delivery, offering the potential to generate and herald a new class of surface functionalized gene-stimulating biomaterials for clinical application. Future studies will involve testing these biomaterials in animal experiments to further validate the bioactivity of the coated PNA architectures.

4.6 ACKNOWLEDGEMENTS

The work presented in this chapter was partially supported by the NSF (CBET-0933153) and NSF-ERC (Grant#EEC-0812348) and has been published in the Materials Today Communications journal [182]. We would also like to acknowledge the Edward R. Weidlein Chair Professorship Funds and the Center for Complex Engineered Multifunctional Materials (CCEMM), Swanson School of Engineering, and the University of Pittsburgh for providing partial support in the form of support for graduate student, reagents, equipment and other accessories much needed for conducting and completing this research. Specifically, we would like to thank Dr. Ipsita Banerjee, Department of Chemical Engineering, University of Pittsburgh, for the use of flow cytometry, and Dr. Yadong Wang, Department of Bioengineering, University of Pittsburgh for the use of tensiometer.

5.0 FORMULATION AND SYNTHESIS OF 3-D GENE DELIVERY SYSTEM USING FIBRIN HYDROGELS TO ENCAPSULATE NANOSICAPS

5.1 INTRODUCTION

Incorporation of therapeutic genes into 3-D biomaterials is a promising strategy for enhancing tissue regeneration. Even though it was demonstrated in the previous chapter that NanoSiCaPs complexes can be immobilized on top of Ti substrates to achieve surface mediated gene delivery, there is still, a need for 3-D gene delivery system (GDS that can provide sustained release of NanoSiCaPs from the bulk of the scaffold. Additionally, precise control over the amount of NanoSiCaPs incorporated in the scaffold would be beneficial, which was lacking in the surface modification technique. Therefore, work described in this chapter focuses on the development of 3-D scaffolds than can provide precise control over the amount of NanoSiCaPs incorporated in the scaffold for achieving sustained gene expression.

Nucleic acids have been incorporated into and delivered from a variety of materials including natural, synthetic, ceramic as well as composite materials [183]. Among these materials, naturally derived polymers are favorable because they are biocompatible, biodegradable and further, they possess a natural affinity for growth factors [15]. As a result, they are attractive candidates for tissue engineering purposes including protein-based polymers, such as collagen, gelatin, alginate, fibrin, etc, as well as polysaccharide-based polymers such as

chitosan, alginate and hyaluron [15]. For the current application fibrin has been selected as the carrier matrix for the nanoparticles because of the following reasons: 1) Fibrin is the only agent approved as a hemostat, sealant, and tissue adhesive by the Food and Drug Administration (FDA); 2) Fibrin plays a leading role in hemostasis and wound healing; 3) Its ability to support cell adhesion, spreading, proliferation, and angiogenesis; 4) Ease of manipulation of material properties of resulting fibrin hydrogels [184-186]. Although, fibrin hydrogels have been employed for bone tissue engineering applications for delivery of growth factors [187, 188], cells [189, 190], mRNA [191], and plasmid DNA delivery via viral particles [192, 193] or lipoplexes [194-196], there are no reports to date however, on use of fibrin gels encapsulating CaP based vectors for pDNA delivery. Therefore, in this aim we explore the use of fibrin hydrogels to incorporate NanoSiCaPs complexes for scaffold mediated gene delivery.

In addition to developing a 3-D scaffold for NanoSiCaPs delivery, it is also crucial to develop a technique that allows long-term storage of NanoSiCaPs complexes under ambient conditions. This would allow the transport of pre-made NanoSiCaPs complexes and eliminate the need for freshly preparing the complexes prior to synthesis of Fibrin-NanoSiCaPs hydrogels, thereby making them feasible to use under a clinical setting. For this purpose, we assessed the ability of sucrose to preserve both the nanoparticle size as well as the transfection efficiency of the NanoSiCaPs complexes. The use of disaccharides as an effective lyoprotectant is well established [115, 116, 197-199]. It is believed that disaccharides stabilize the nanoparticles during the free-drying steps via the “water replacement” and the “vitrification” processes [111]. However, the main objective of the current study was to evaluate the effect of sucrose as a stabilizing agent for lyophilization of NanoSiCaPs complexes and maintain their transfection efficiency.

The long-term objective of this work is to develop a gel form of the Fibrin-NanoSiCaPs scaffold that can be used either alone or to infiltrate scaffolds commonly employed in bone tissue engineering. Therefore, this aim focuses on the development of a gene delivery system using fibrin as the degradable matrix incorporating freshly prepared and lyophilized NanoSiCaPs complexes over a 3-D volume, which promotes cell attachment, infiltration, proliferation and subsequent gene transfection. The present study is the first step towards this goal and describes a method to incorporate lyophilized NanoSiCaPs complexes in fibrin gel under physiological conditions (Figure 5.1). The present study characterizes the gel micro structure, in-vitro cytocompatibility, transfection efficiency of lyophilized NanoSiCaPs and Fibrin-NanoSiCaPs formulations.

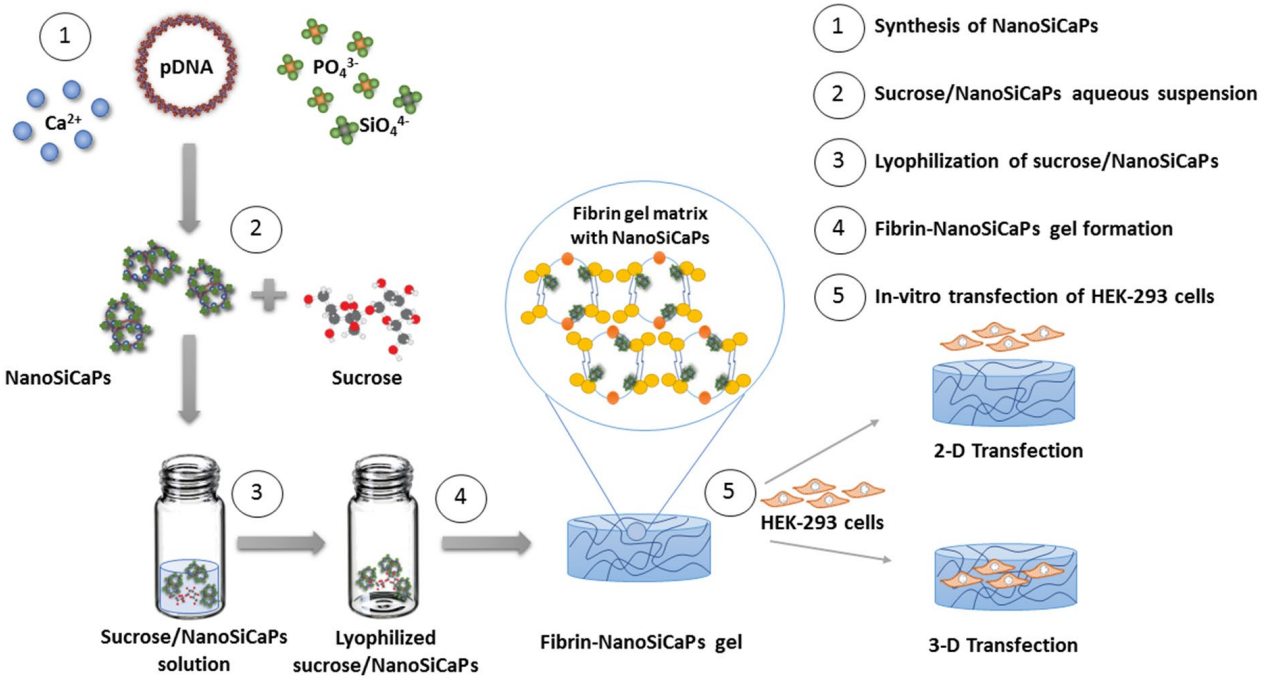

Figure 5.1. Schematic representation of Fibrin-NanoSiCaPs gel formulation.

5.2 MATERIALS AND METHODS

5.2.1 Materials

Calcium chloride ($CaCl_2 \cdot 2H_2O$), tri-sodium phosphate do-decahydrate ($Na_3PO_4 \cdot 12H_2O$), sodium chloride (NaCl), Bis-Tris, and dextrose were purchased from Fisher Scientific (Pittsburgh, PA). Potassium chloride (KCl) was purchased from Sigma Aldrich (St. Louis, MO). Sodium hydroxide (NaOH) was purchased from Mallinckrodt Baker Inc. (Phillipsburg, NJ). Sodium metasilicate ($Na_2SiO_3 \cdot 5H_2O$) was purchased from Alfa Aesar (Ward Hill, MA). HEPES obtained from EMD Chemicals (Gibbstown, NJ). Reporter plasmid, gWiz GFP (Green Fluorescent Protein), were purchased from Aldevron LLC (Fargo, ND) , Reporter gene expression plasmid with secreted embryonic alkaline phosphatase (SEAP) pSELECT-zeo-SEAP plasmid, Recombinant SEAP protein and QUANTI-Blue detection system were purchased from InivoGen (San Diego, CA), polyethylene glycol (PEG)-8000 from Fisher Scientific (Pittsburgh, PA), SigmaUltra grade potassium chloride (99.0%) from Sigma Aldrich (St. Louis, MO), ACS reagent grade sodium citrate tribasic dehydrate (>99.0%) from Sigma Aldrich (St. Louis, MO), Human Fibrinogen (Plasminogen Depleted) and Human alpha Thrombin from Enzyme Research Laboratories (South Bend, IN), Aprotinin (from bovine lung) purchased from Sigma Aldrich (St. Louis, MO), Dulbecco's minimum essential medium (DMEM) and penicillin/streptomycin (P/S) from Invitrogen (Carlsbad, California) and characterized fetal bovine serum (FBS) from Hyclone (Logan, UT). HEK-293 cells were obtained from Stratagene (La Jolla, CA). This cell line was selected for use because they are easily transfected. All of the reagents were used as received without further modification or purification.

5.2.2 Lyophilization experiments

5.2.2.1 Synthesis of NanoSiCaPs complexes

Nanoparticles of silicate substituted calcium phosphate complexes with pDNA were synthesized as previously described (see Section 3.2.3). Briefly, 125.0µl of a calcium precursor solution, comprised of 6.25µl (1µg/µl) of pDNA (pSEAP), 15.53µl of 2M $CaCl_2$ and 103.2µl of de-ionized water was added to an equal volume of (125µl) of a HEPES Buffered Saline Solution (HBS), at pH 7.5. 8.3 mol% of Si-HBS was used for all experiments since this is the silicate concentration that yielded enhanced transfection as outlined in Chapter 3. The calcium precursor was added to the phosphate solution at an addition rate of 13.4µl/sec simultaneously as the phosphate precursor was vortexed at 500rpm using VWR digital mini vortexer (West Chester, PA). The addition rate and Ca/P ratio was optimized previously by our group and reported [67].

5.2.2.2 Stability of NanoSiCaPs complexes

For determining the influence of sucrose on stability of NanoSiCaPs complexes, 250µl of NanoSiCaPs dispersions were diluted with 250µl of 10%, 20% and 40% sucrose (w/v) solution to yield a final volume of 500µl of sucrose/NanoSiCaPs solution containing 5%, 10% and 20% sucrose (1:1 v/v). Samples without sucrose (0% sucrose) were prepared as per the protocol without any dilution with de-ionized water. Freshly prepared samples were used for in-vitro transfection and cell viability studies.

5.2.2.3 Lyophilization of NanoSiCaPs complexes

Transfection solutions lyophilized with sucrose were prepared by first diluting 250µl of NanoSiCaPs dispersions with 250ul of 20% sucrose (w/v) solution to yield a final 500µl of

sucrose/NanoSiCaPs solution of 10% (1:1 v/v). Samples lyophilized without sucrose were freeze-dried as-prepared without further dilution in de-ionized water (250ul). Additional sample of freshly prepared sample was allowed to age on bench-top at room temperature without any treatment. All the relevant samples were freeze-dried using the following protocol. First, the samples (either 250µl or 500µl) were placed in 2ml Serum Vials, Type I clear glass (Wheaton, Millville, NJ), covered with aluminum foil and were frozen at -80°C for 60 minutes. Approximately 5-6 holes were made in the aluminum foil to facilitate the sublimation of water during the lyophilization process. These holes were created using a 22G 1 1/2 needle (BD, Franklin Lakes, NJ). Second, the samples were lyophilized for 24 hours using a Labconco freeze-dryer (Model 4.5, Kansas City, MO). Third, following lyophilization, the aluminum foil covering the tubes was removed. The tubes were then capped and sealed under a glove bag purged with argon gas under sterile conditions.

5.2.2.4 Long-term stability

For stability testing, sealed lyophilized samples were stored either at 4°C or room temperature (approximately 25°C) for up to 3 weeks.

5.2.2.5 In-vitro experiments

Human embryonic kidney 293 cells (HEK-293) were cultured in Dulbecco's Modified Eagle Medium (DMEM) supplemented with 1% (v/v) Antibiotic–Antimycotic and 10% (v/v) fetal bovine serum (FBS), at 37 ºC with 10% CO_2. Cells were maintained at sub confluency and passaged every 2-3 days. A day prior to transfection, cells were seeded in 12-well plates at a concentration of $1.63x10^5$ cells/well. To study the influence of sucrose on transfection efficiency of NanoSiCaPs complexes, sucrose was mixed with aqueous suspension of freshly prepared

samples and 166.6µl of sucrose/NanoSiCaPs complexes were added per well. For samples, receiving no sucrose, 83.3µl of NanoSiCaPs were added per well. For transfection studies of the lyophilized NanoSiCaPs complexes, freeze-dried samples were taken at respective time points and reconstituted with 500µl of de-ionized water for samples lyophilized with sucrose and 250µl of de-ionized water for samples lyophilized without sucrose. Twenty-four hours post transfection, the gene expression was quantified using SEAP assay by mixing 20µl of growth media with 180µl of QUANTI-Blue solution in a 96-well plate for detection of the secreted embryonic alkaline phosphatase (SEAP) by transfected cells. Plate were incubated at 37ºC for 1 hour and optical density (OD) was measured at 620-655nm using a microplate reader (Biotek, Synerge2). SEAP expression was normalized to total cell number using CyQuant cell proliferation assay kit (ThermoFisher) and represent as SEAP (nanograms) /10^4 cells. Cell viability was determined by MTT assay. 100 ml of MTT (5 mg/ml) was added to each well and incubated at 37 C for 4 hours. MTT containing medium was removed and 0.5 ml dimethyl sulfoxide (DMSO) was added to dissolve formazan crystals. The optical density of the solution was measured at 490 nm.

5.2.2.6 Transmission electron microscopy of freshly prepared and lyophilized NanoSiCaPs

Lyophilized samples were taken from storage at week 0, 1, 2 and 3, reconstituted with 500µl of de-ionized water. Two-three drops, approximately 15µl of freshly prepared and reconstituted NanoSiCaPs complexes were then added onto a carbon coated copper grid (Electron Microscopy Sciences, Hatfield, PA) and allowed to equilibrate for 3 min. The grids were then stained with UranyLess EM stain (Electron Microscopy Sciences, Hatfield, PA), rinsed in de-ionized water and allowed to air dry. Images were subsequently taken using a Hitachi 9500 transmission electron microscope (TEM) (Tokyo, Japan) set to an accelerating voltage of 100 kV.

5.2.3 Synthesis and assessment of fibrin gene delivery system

5.2.3.1 Synthesis of Fibrin/NanoSiCaPs gels

In-vitro transfection studies assessing the influence of fibrinogen concentration, pDNA dose and aprotinin employed use of 96-well plate. For these experiments, 50µl or 70µl of fibrin gel were synthesized per well depending on the amount of NanoSiCaPs complexes (i.e. pDNA amount) incorporated in the gel. Fibrinogen and aprotinin were diluted in 20mM sodium citrate-HCl buffer (pH-7.4) to obtain the required concentrations (5, 10 and 20 mg/ml fibrinogen, and 10µg/ml aprontinin) and thrombin (10U/ml) was accordingly diluted in a buffer comprising of 50mM sodium citrate, 0.2M NaCl and 0.1% PEG-8000. For gel formation, fibrinogen was either used alone or mixed with aprotinin solution and added to the well of 96-well plate. NanoSiCaPs complexes were then freshly prepared as per the protocol (see Section 5.2.2.1) and subsequently mixed with thrombin. For gels containing 0.5µg pDNA (SEAP) per well, 20µl of NanoSiCaPs were used, and gels containing 1µg pDNA (SEAP) per well, 40µl of NanoSiCaPs complexes were used, such that the total reaction volume for both gels were 60µl per well. Throughout the text, the concentrations of fibrinogen, thrombin, aprotinin and pDNA are given as the final concentration in the resultant gel after mixing and polymerization. NanoSiCaPs complexes/thrombin suspension was then added to well containing fibrinogen (with or without aprotinin) for fibrin gel formation for 30mins at room temperature. Control groups incorporated the gels synthesized with equal volume of the calcium precursor solution required for synthesis of 60µl gels, but without the pDNA or phosphate buffer (to prevent NanoSiCaPs formation).

5.2.3.2 In-vitro experiments

For in-vitro studies, $5.1x10^3$ HEK-293 cells/per well were seeded on the gels with 100µl of growth media per well. To determine the transfection efficiency of the synthesized Fibrin-NanoSiCaPs gels, the cells were plated on top of the gels and the amount of SEAP secreted by the transfected cells into medium was measured on day 2, day 4 and day 6. At the respective time points, 100µl of medium was replaced with fresh medium, and immediately frozen at 80 ºC until further analysis. To measure levels of SEAP, frozen media was thawed at 37 ºC and 20µl of media was mixed with 180µl of QUANTI-Blue solution in a 96-well plate for detection of SEAP by transfected cells. The plates were incubated at 37 ºC for 1 hour and optical density (OD) was measured at 620-655nm using a microplate reader (Biotek, Synerge2). SEAP expression was normalized to total cell number using CyQUANT cell proliferation assay and represented as SEAP (nanograms) /10^4 cells.

5.2.3.3 Fibrin-NanoSiCaPs formulation for 2-D and 3-D transfection

For this part of the study, 300µl of gels were synthesized with 10mg/ml fibrinogen, 10U/ml thrombin and 10µg/ml of aprotinin containing 200µl of freshly prepared or lyophilized NanoSiCaPs (reconstituted prior to gel formation) (stored for up to 1 week). The volume of NanoSiCaPs complexes contained 5µg of pDNA-SEAP and pDNA-GFP. Two techniques of transfection were investigated in this study, namely 2-D and 3-D method of transfection (Figure 5.1). For 2-D transfection, the gels were synthesized as described in previous section by mixing fibrinogen/ aprotinin solution with NanoSiCaPs/thrombin solution. $5x10^4$ HEK-293 cells were plated on top of the gel. For 3-D method, $5x10^4$ HEK-293 cells were suspended in NanoSiCaPs/thrombin solution and immediately mixed with fibrinogen/aprotinin solution for gel formation. After 30minutes of polymerization, growth media was added to the gels. Assessment

of transfection efficiency was carried out by quantifying the SEAP levels by transfected cell in the media as described in the previous section (see Section 5.2.3.2) and expressed as SEAP (nanograms)/10^4 cells. Qualitative assessment of transfection efficiency was carried out by visualizing GFP expression at specific time points using an inverted microscope with a fluorescence illuminator (CKX41, Olympus, Olympus America Inc.) and imaged with a digital camera (Olympus DP25 Microscope Camera, Olympus, Olympus America Inc.). Cell viability of 2-D and 3-D transfection methods was determined by MTT assay. 100 ml of MTT (5 mg/ml) was added to each well and incubated at 37 ºC for 4 hours. MTT containing medium was removed and 0.5 ml dimethyl sulfoxide (DMSO) was added to dissolve formazan crystals. The optical density of the solution was measured at 490 nm.

5.2.3.4 SEM imaging of Fibrin-NanoSiCaPs

For this experiment, 300µl of fibrin gels were synthesized with freshly prepared and lyophilized NanoSiCaPs complexes. Following gel formation, the gels were dehydrated in the following graded series of alcohol solutions for 15minutes each: 30%, 50%, 70%, 90% and 100 % ethanol (3 times). The samples were then critically point dried from CO_2 using a CPD 750 Emscope (Ashford, England). Once dried, the samples were sputter coated with palladium and were then imaged using a FEI-Apreo scanning electron microscope (ThermoFisher Scientific, Hillsboro, OR).

5.2.4 Statistical analysis

Statistical calculations were performed using GraphPad Prism software. The data was analyzed to test for significant ($p<0.05$) mean differences on in-vitro transfection efficiency, cell viability

and proliferation for different samples utilized in lyophilization and fibrin gel experiments using one-way analyses of variance (ANOVA). Experiments were run in duplicates and repeated three times with n=6. Each ANOVA on these response variables was significant at $p<0.05$. Post hoc tests for pair-wise differences and identification of homogeneous subgroups were also all performed using the Tukey HSD procedures and discussed in the results section for the relevant groups.

5.3 RESULTS

5.3.1 Influence of sucrose on NanoSiCaPs stability

Since the mass ratio stabilizer/nanoparticle is important, the effect of different concentrations of sucrose on transfection ability of freshly prepared NanoSiCaPs was evaluated. NanoSiCaPs were freshly prepared on the day of transfection resulting in final volume of 5%, 10% and 20% sucrose (% w/v) in NanoSiCaPs suspension. SEAP expression 24-hour post transfection revealed that 10% sucrose resulted in the highest transfection of HEK-293 cells, 62±2.8 SEAP ng/10^4 cells (Figure 5.2). Interestingly, the transfection efficiency of 10% sucrose containing NanoSiCaPs suspension was higher than the NanoSiCaPs suspension without any sucrose (49.5±2.3 SEAP ng/10^4 cells). This indicated the possibility of sucrose stabilizing the nanoparticles and inhibiting particle aggregation. However, at 20% sucrose concentration SEAP expression decreased in comparison to NanoSiCaPs suspension without sucrose, 39.3±2.6 SEAP ng/10^4 cells (Figure 5.2). MTT assay was performed to investigate the influence of sucrose concentration on cell metabolic activity. Cell viability was not significantly influenced by the

presence of sucrose in the NanoSiCaPs suspension, other than 20% sucrose sample that resulted in decrease in cell metabolic activity, ~80% viable cells (Figure 5.3). Decline in transfection efficiency for the 20% sucrose/NanoSiCaPs was attributed to the decrease in cell metabolic activity for these samples.

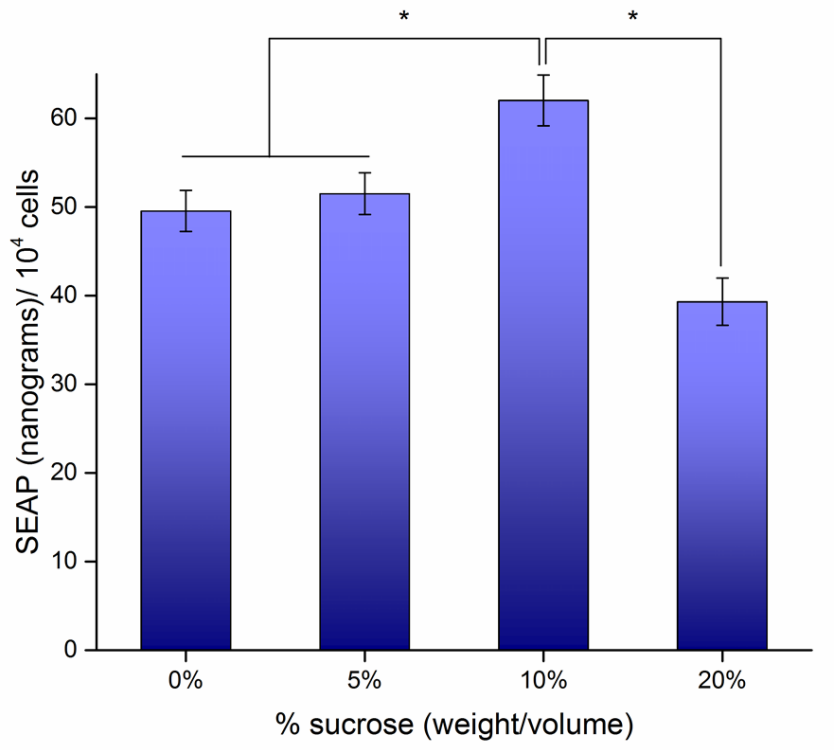

Figure 5.2. Influence of sucrose on transfection efficiency of NanoSiCaPs complexes.

In-vitro transfection of HEK-293 cells by NanoSiCaPs complexes with different concentrations of sucrose at 24h. SEAP expression is normalized to cell number, n=6. The data were reported ± SD, n=6 ($p<0.05$). Post hoc analysis of the transfection profile showed statistical significance between groups, indicated by the asterisk (*)

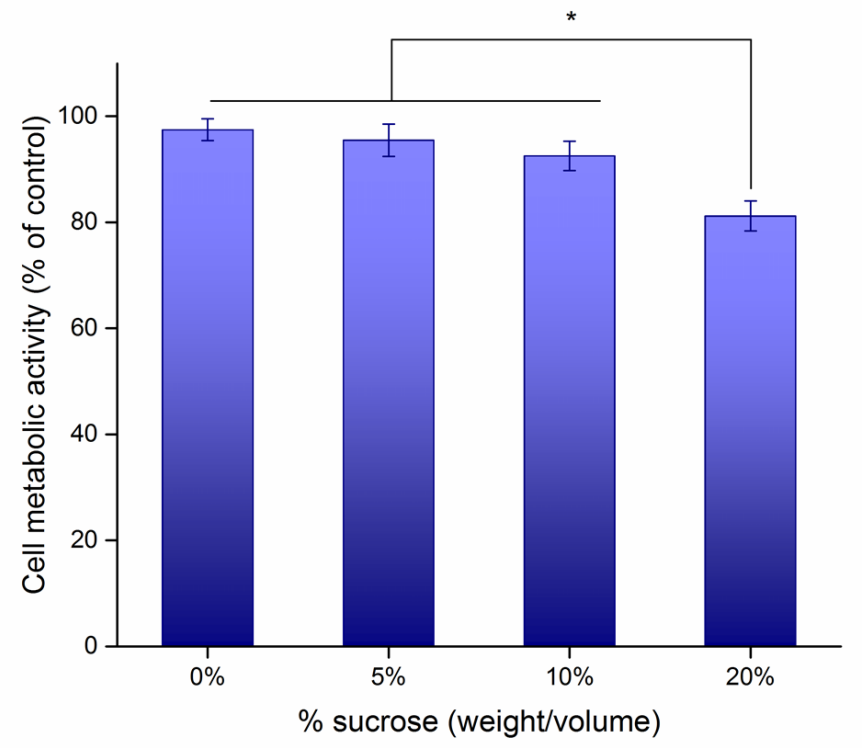

Figure 5.3. Influence of sucrose/NanoSiCaPs complexes on cell metabolic activity.

MTT assay measuring in-vitro cell metabolic activity of HEK-293 cells by NanoSiCaPs complexes with different concentrations of sucrose at 24h. Data is normalized to control group that received no treatment, n=6. The data were reported ± SD, n=6 ($p<0.05$). Post hoc analysis of the cell metabolic activity showed statistical significance between groups, indicated by the asterisk (*)

5.3.2 Influence of lyophilization and storage on transfection efficiency of sucrose/NanoSiCaPs complexes

The 10% sucrose/NanoSiCaPs complexes were lyophilized using a benchtop freeze-dryer. To ensure complete freezing, the samples were frozen to -80 ºC prior to freeze drying for 24-hours. Lyophilized samples, except the sample without any sucrose showed good cake appearance and

instantly dissolved in water. After reconstitution few large, undissolved particles were observed for the lyophilized samples without sucrose. This effect was more evident for NanoSiCaPs that were subjected to no lyophilization and stored at bench-top for 24-hours. Next, the influence of the lyophilization process on transfection efficiency of NanoSiCaPs was evaluated. SEAP expression of lyophilized 10% sucrose/NanoSiCaPs complexes, 44.11±3.4 SEAP ng/10^4 cells, was comparable to the SEAP expression observed for freshly prepared samples, 49.5±2.3 SEAP ng/10^4 cells (statistically not significant) (Figure 5.4). However, freeze-drying of NanoSiCaPs in the absence of sucrose had a detrimental effect on the reported gene expression resulting in a ~ 40-fold reduction in SEAP expression, 1.2±1.4 SEAP ng/10^4 cells (Figure 5.4). This was also the case for NanoSiCaPs complexes that were subjected to aging for 24-hours (without lyophilization), 2.1±1.5 SEAP ng/10^4 cells (Figure 5.4). These results clearly indicated that the process of lyophilization in presence of sucrose does help in preserving the transfection ability of the NanoSiCaPs complexes.

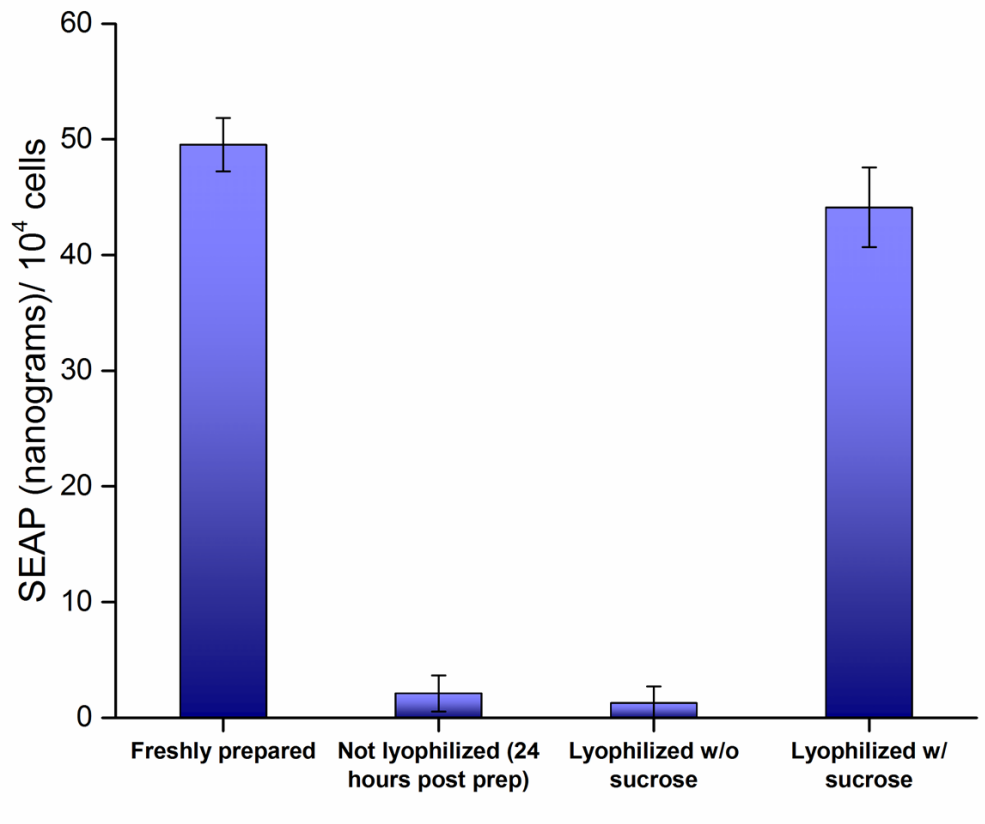

Figure 5.4. Effect of lyophilization on transfection efficiency of NanoSiCaPs complexes. In-vitro transfection of HEK-293 cells by NanoSiCaPs complexes at 24h. The nanoparticles were freshly prepared (no sucrose), prepared and stored at bench top for 24h (without sucrose), lyophilized (without sucrose) and lyophilized (with 10% sucrose). SEAP expression is normalized to cell number, n=6 ($p < 0.05$). The data were reported as mean ± SD.

In order to evaluate the long-term stability and storage conditions, the sealed lyophilized formulations were stored at 4ºC and room temperature (R.T.) for up to 3 weeks. After reconstitution, the samples were analyzed for transfection efficiency. In-vitro transfection of HEK-293 cells with lyophilized formulations was not significantly changed by the storage temperature at all the time points, Figure 5.5 (statistically not significant). This indicated that NanoSiCaPs complexes lyophilized in with 10% sucrose can be stored under ambient conditions. However, decrease in transfection efficiency was observed for lyophilized samples stored at both

temperatures with prolonged storage. The stability of the lyophilized particles with prolonged storage is known to affect the transfection potential of the lyophilized non-viral vectors due to particle aggregation [117].

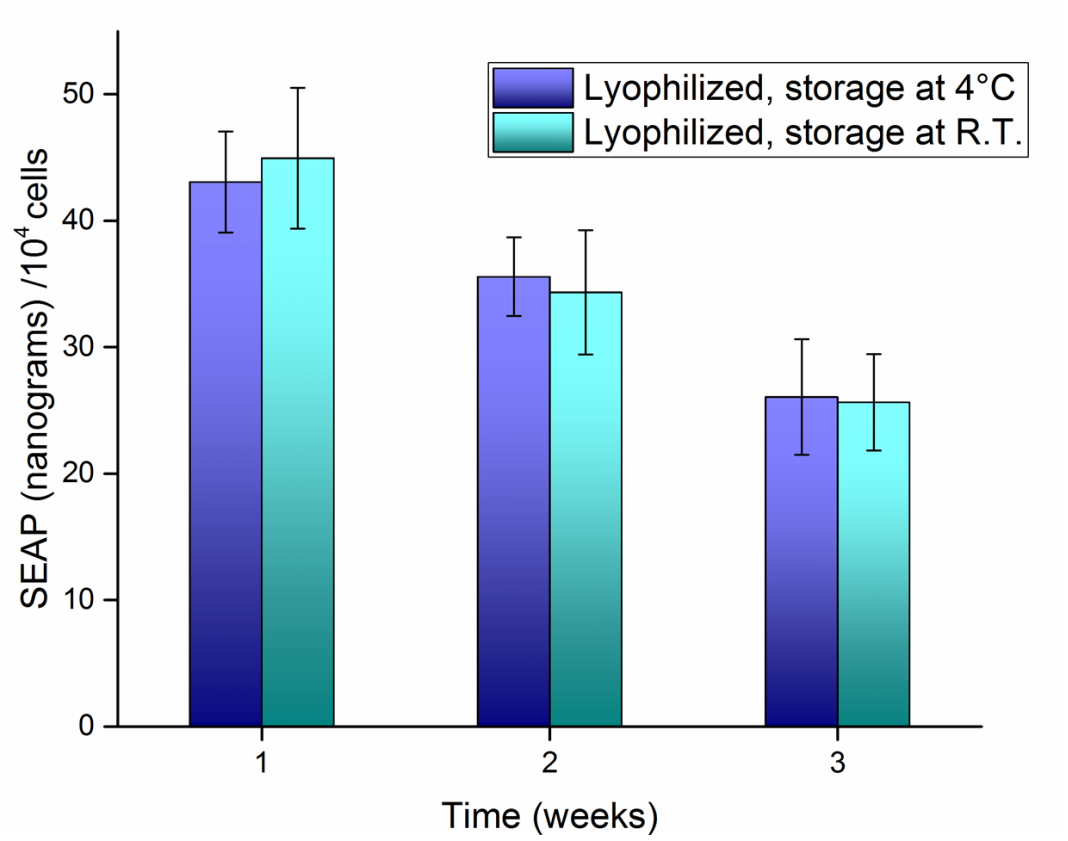

Figure 5.5. Effect of storage on transfection efficiency of lyophilized NanoSiCaPs complexes. NanoSiCaPs complexes were lyophilized with 10% sucrose, sealed and stored at 4ºC or room temperature (R.T.) for week 1, 2 and 3. In-vitro transfection of HEK-293 cells showing SEAP expression 24h post transfection by reconstituted NanoSiCaPs complexes. SEAP expression is normalized to cell number. The data were reported ± SD, n=6 ($p<0.05$).

5.3.3 TEM analysis of lyophilized NanoSiCaPs complexes

TEM was used to qualitatively assess the particle size and extent of aggregation of sucrose/NanoSiCaPs with long-term storage at R.T. As shown in Figure 5.6a, Figure 5.6b and Figure 5.7a, sucrose/NanoSiCaPs complexes appeared to be spherical in nature with primary particle size ~100nm as seen earlier in Section 3.3.4 (Figure 3.10). However, the reconstituted samples at week 2 and week 3 displayed larger clumps of sucrose/NanoSiCaPs complexes demonstrating the effect of storage conditions on the stability of NanoSiCaPs (Figure 5.8a and Figure 5.8b).

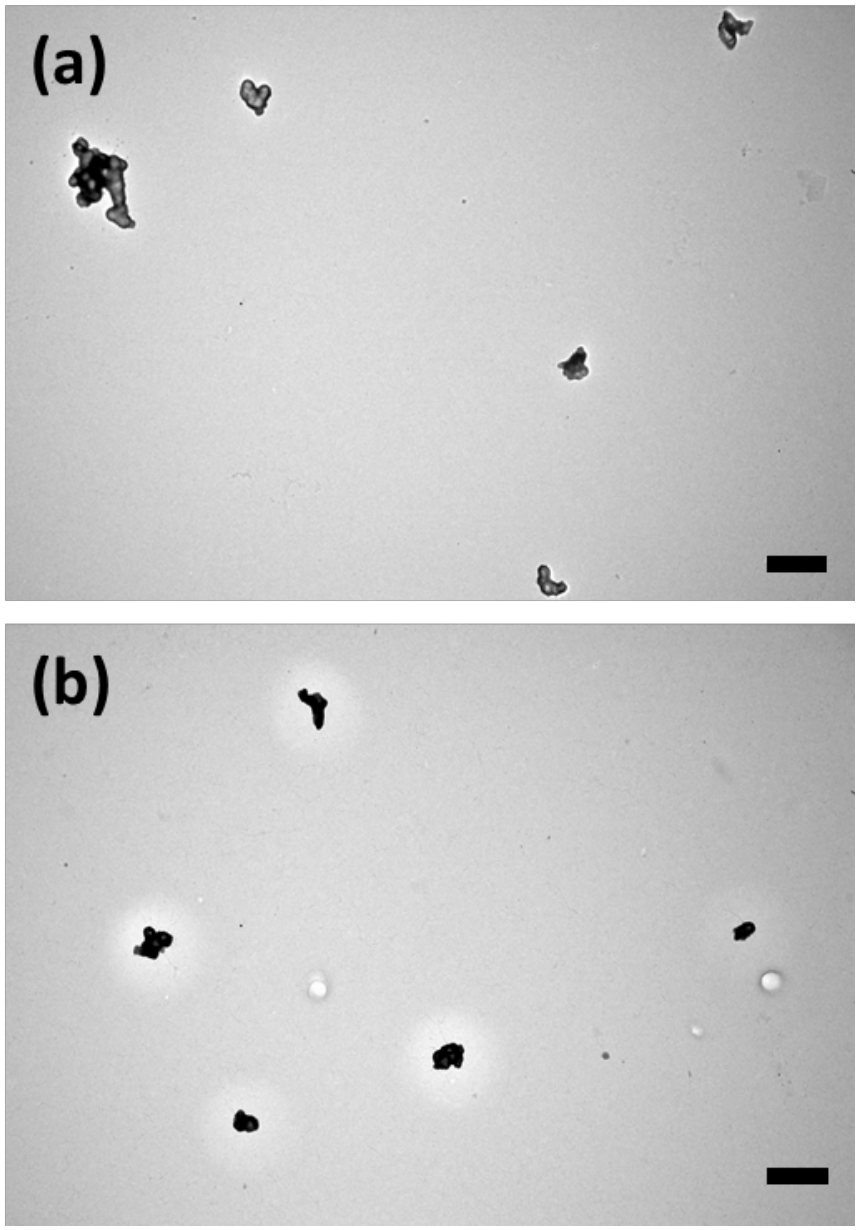

Figure 5.6. TEM analysis of freshly prepared NanoSiCaPs complexes.

(a) freshly prepared NanoSiCaPs without sucrose and (b) freshly prepared NanoSiCaPs with 10% sucrose (scale 500nm).

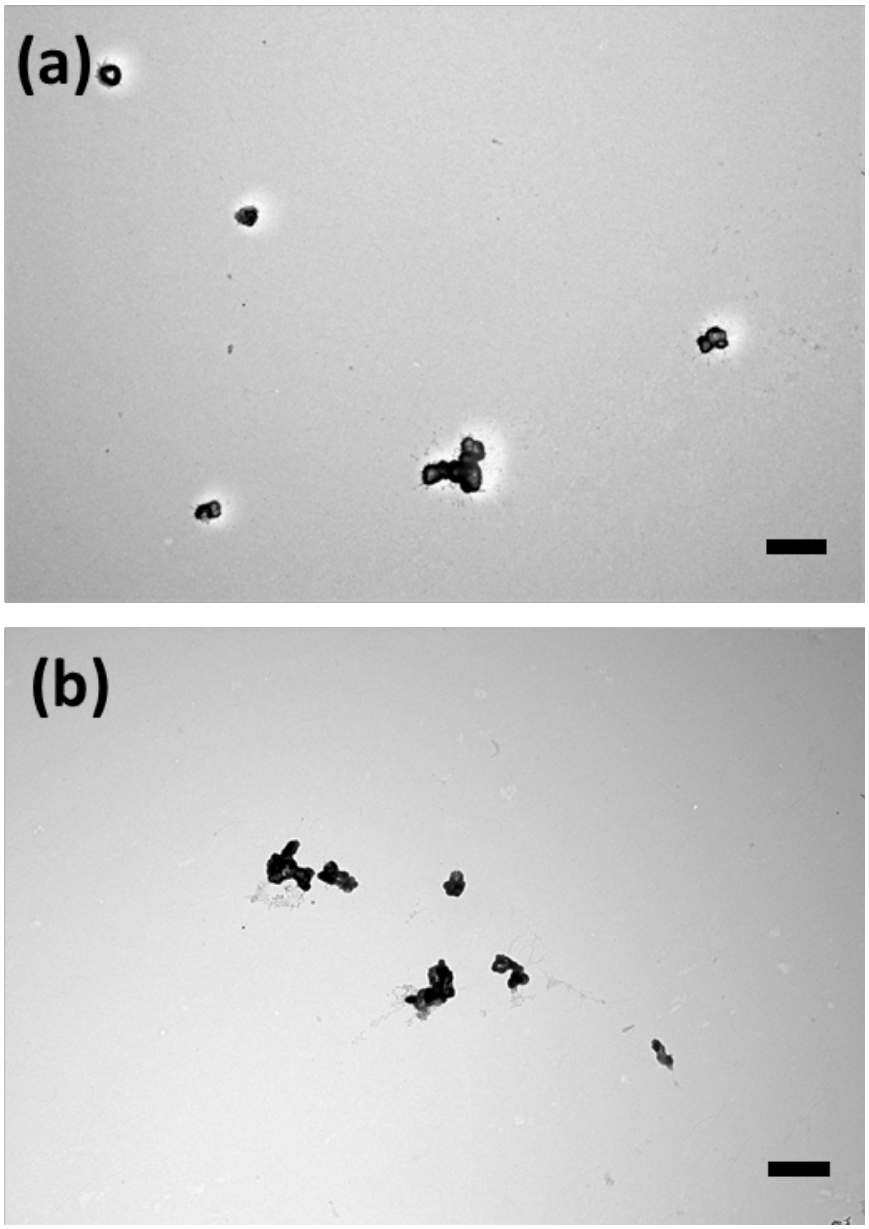

Figure 5.7. TEM analysis of lyophilized NanoSiCaPs complexes.

(a) reconstituted after freeze-drying for 24h (no storage) and (b) reconstituted after 1-week storage at R.T. (scale 500nm).

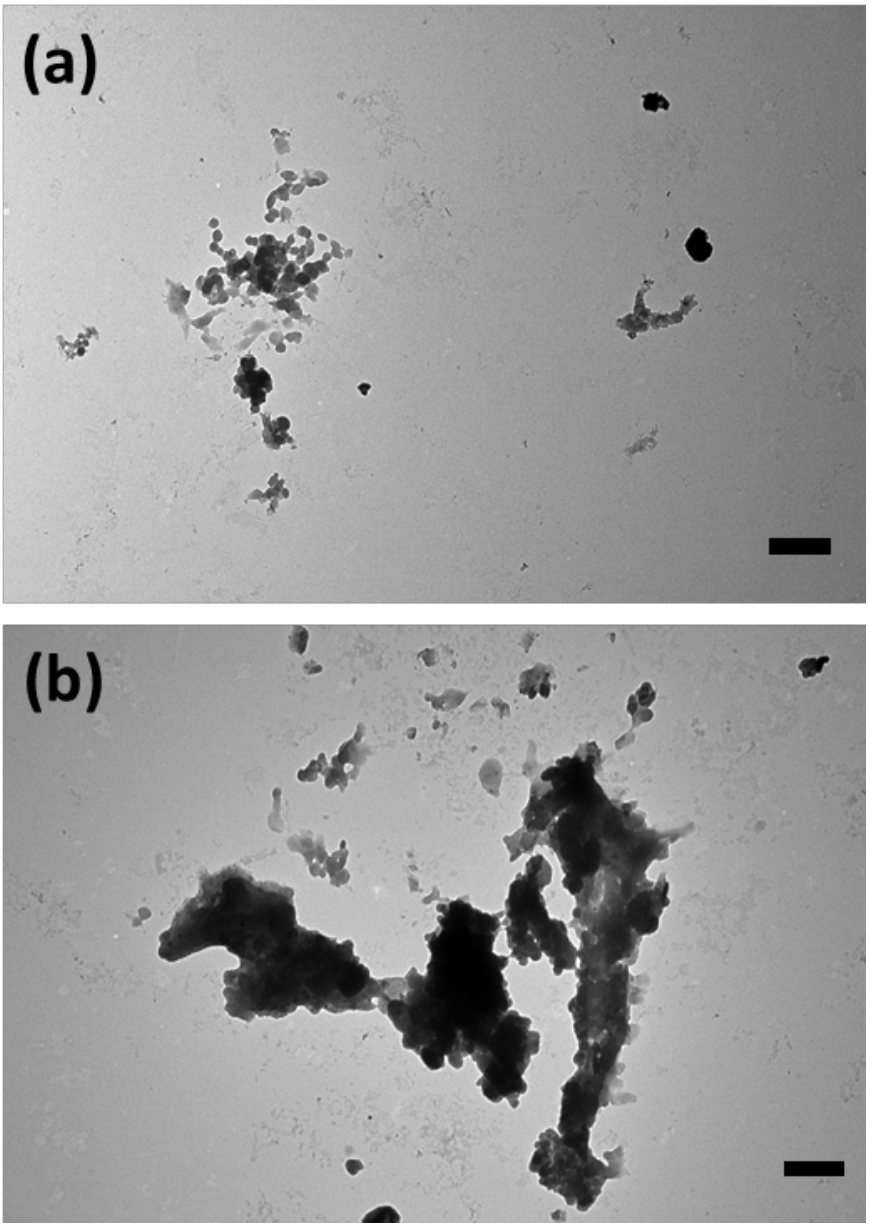

Figure 5.8. TEM analysis of lyophilized NanoSiCaPs complexes (extended storage).

(a) reconstituted after 2-weeks storage at R.T and (b) reconstituted after 3-weeks storage at R.T.

(scale 500nm).

5.3.4 In-vitro transfection studies using Fibrin-NanoSiCaPs formualtion

Transfection studies initially employed HEK-293 cells and 2-D transfection systems where cells were seeded on top of the synthesized Fibrin-NanoSiCaPs gels. We investigated the effect of different concentrations of fibrinogen on the gene transfer ability of various Fibrin-NanoSiCaPs formulations. Hydrogels were formed by mixing NanoSiCaPs with thrombin subsequently mixing it with fibrinogen solution (5, 10 or 20mg/ml fibrinogen). Gene expression for all the gel formulation was significantly low at day 2 but increased by day 4. In general, gene expression decreased with increase in fibrinogen concentration (Figure 5.9). Fibrinogen concentration of 5mg/ml displayed peak expression at day 4, 19.8±1.1 SEAP ng/10^4 cells (Figure 5.9) but had completely degraded by day 6. The increased gene expression for gels synthesized with fibrinogen concentration of 10mg/ml at day 6, 24.18±1.8 SEAP ng/10^4 cells (Figure 5.9) reflects the balance between gel stability and cell proliferation. Since Fibrin-NanoSiCaPs gels synthesized with 10mg/ml fibrinogen displayed the highest gene expression for the duration of cell culture of 6 days, and retained their integrity for the cell culture period, all the subsequent studies were performed under this condition.

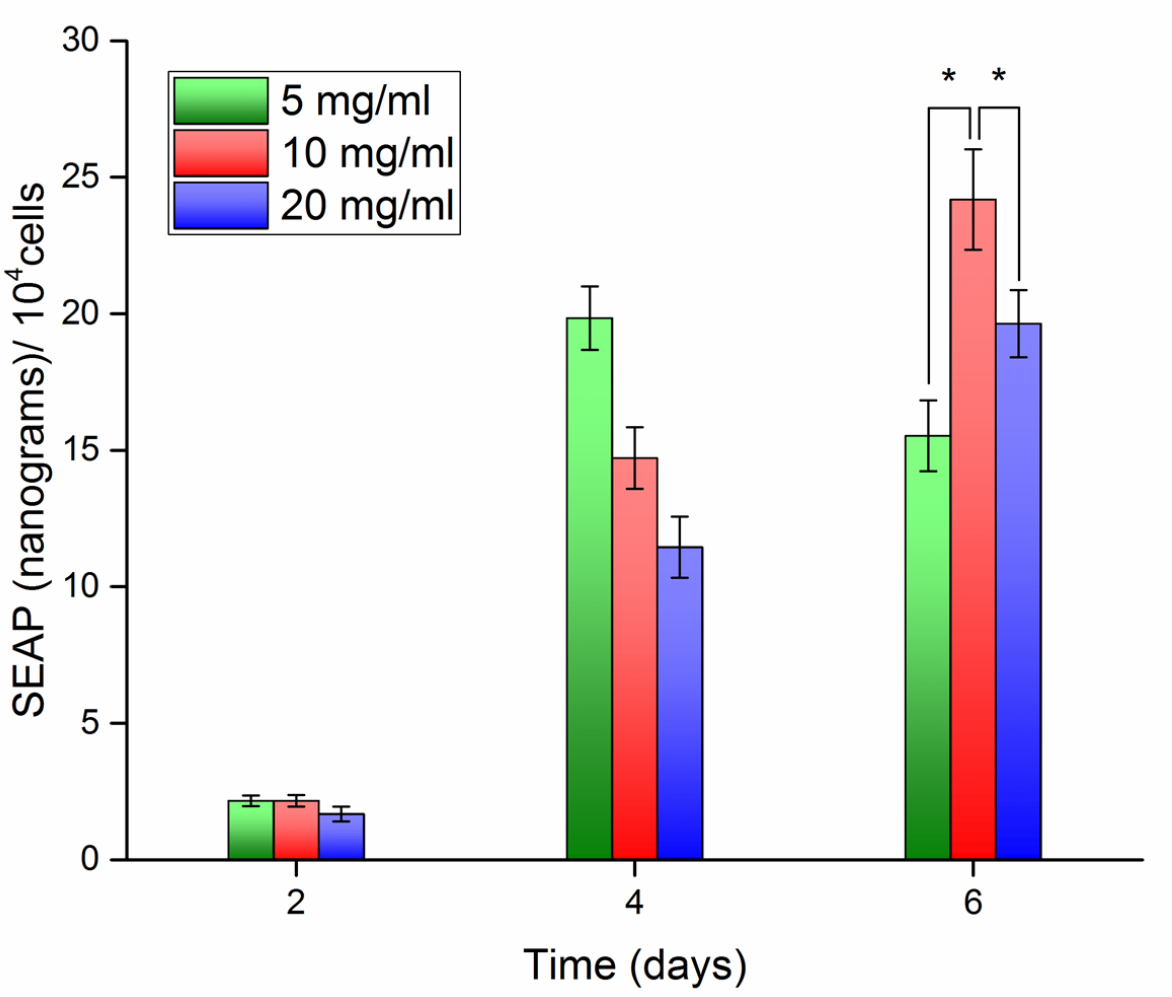

Figure 5.9. Effect of fibrinogen concentration on transfection efficiency.

In-vitro transfection efficiency of HEK-293 cells showing SEAP expression at day 2, 4 and 6 by fibrin-NanoSiCaPs hydrogels synthesized using different concentrations of fibrinogen, 5mg/ml, 10mg/ml and 20mg/ml. SEAP expression is normalized to cell number. Control group included gels synthesized with 10mg/ml fibrinogen (without pDNA or NanoSiCaPs complexes). The data were reported ± SD, n=6 ($p<0.05$). Post hoc analysis of statistically significant groups indicated by asterisk (*).

Next, we determined the amount of NanoSiCaPs (also refers to the amount of pDNA, see 5.2.3.1) that resulted in the highest level of gene expression. Two different dosages of pDNA, 0.5µg and 1µg of pDNA per well were tested. There was no difference in gene expression

between gels synthesized with two different dosages of pDNA, Figure 5.10 (statistically not significant). This was attributed to the rapid degradation and bulk release of NanoSiCaPs complexes from the fibrin network from both gels.

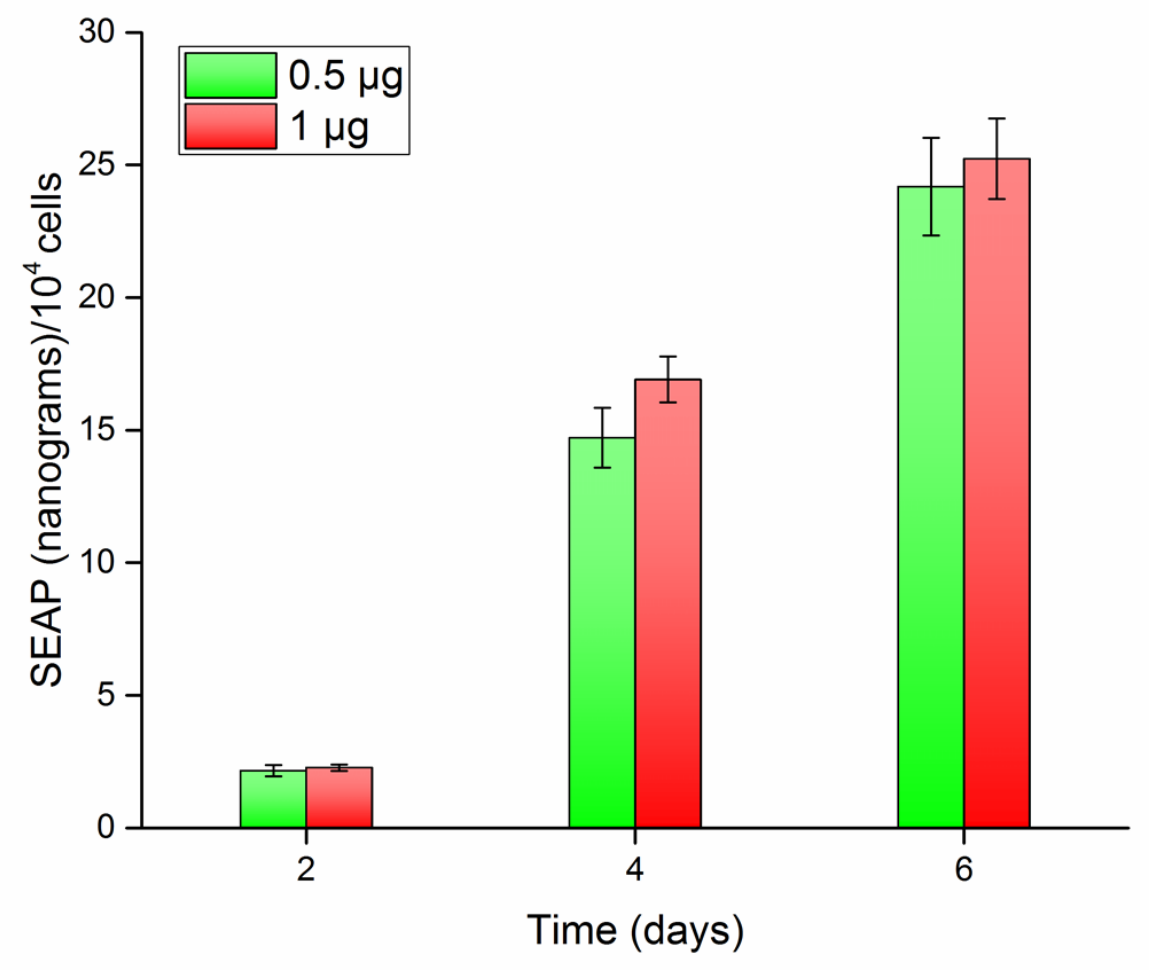

Figure 5.10. Effect of pDNA doese on transfection efficiency.

In-vitro transfection efficiency of HEK-293 cells showing SEAP expression at day 2, 4 and 6 by fibrin-NanoSiCaPs hydrogels synthesized using two amounts of pDNA corresponding to different amounts of NanoSiCaPs. SEAP expression is normalized to cell number. Control group included gels synthesized with 10mg/ml fibrinogen (without pDNA and NanoSiCaPs). The data were reported ± SD, n=6 ($p<0.05$).

Subsequently we investigated if fibrin degradation can be controlled by incorporating a fibrinolytic inhibitor in Fibrin-NanoSiCaPs formulation and its influence on gene transfection abilities of synthesized gels. Aprotinin, a bovine pancreatic trypsin inhibitor was incorporated in the Fibrin-NanoSiCaPs formulation with both pDNA amounts of 0.5μg and 1μg. Addition of aprotinin at 10μg/ml decreased the gene expression for gels synthesized with two vector dosages (Figure 5.11). Interestingly, 0.5μg gels did not show any transfection until day 4 and gene expression for these gels was lower at all the time points in comparison to gels with 1μg pDNA (Figure 5.11). Incorporation of aprotinin delayed fibrin degradation and extended the transgene expression. These results also indicated that fibrin degradation was necessary for successful gene transfection. In addition, the gels synthesized with two doses of pDNA incorporating aprotinin had no detrimental effect on cellular proliferation as shown in Figure 5.12.

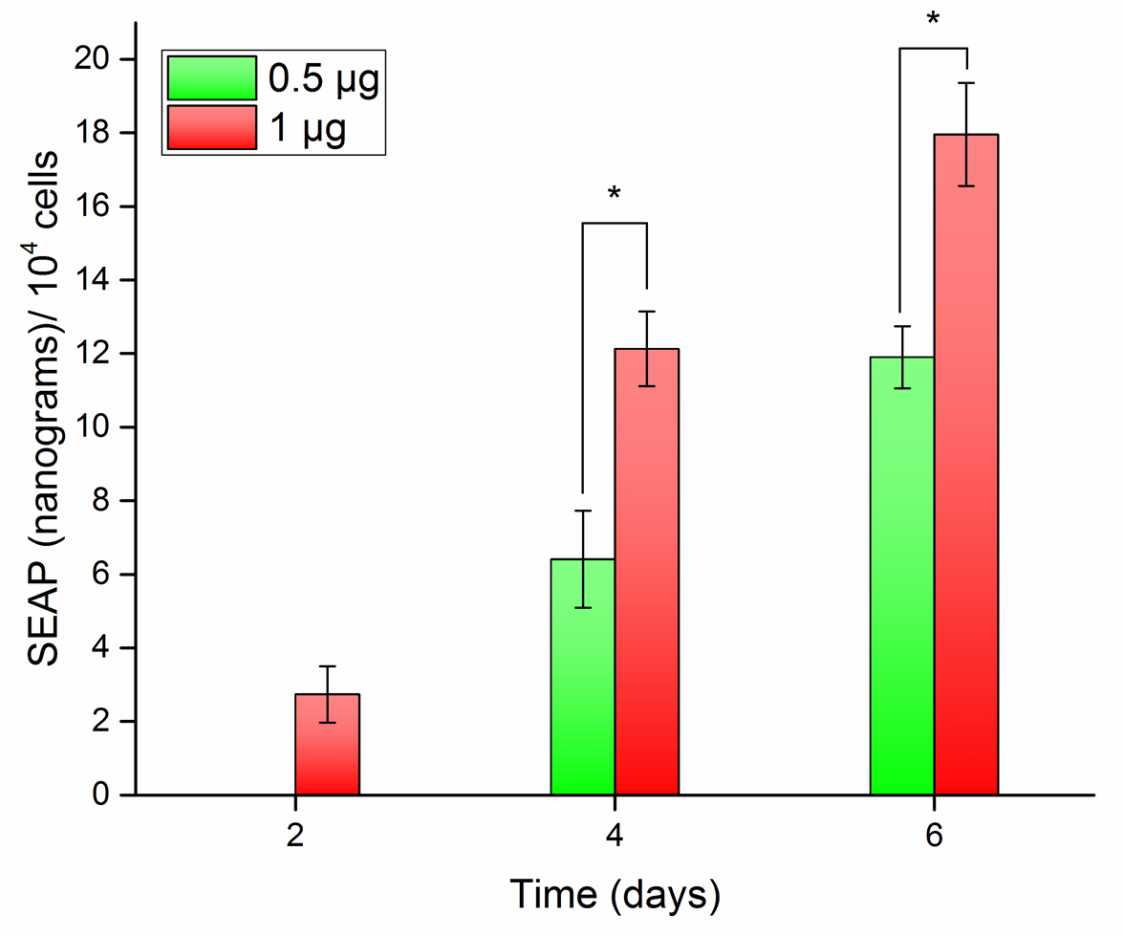

Figure 5.11. Effect of fibrinolytic inhibitor on transfection efficiency.

In-vitro transfection efficiency of HEK-293 cells showing SEAP expression at day 2, 4 and 6 by fibrin-NanoSiCaPs hydrogels synthesized incorporating 10µg/ml aprotinin. SEAP expression is normalized to cell number. Control group included gels synthesized with 10mg/ml fibrinogen (without pDNA and NanoSiCaPs complexes). The data were reported ± SD, n=6 ($p<0.05$). Post hoc analysis of statistically significant groups indicated by asterisk (*).

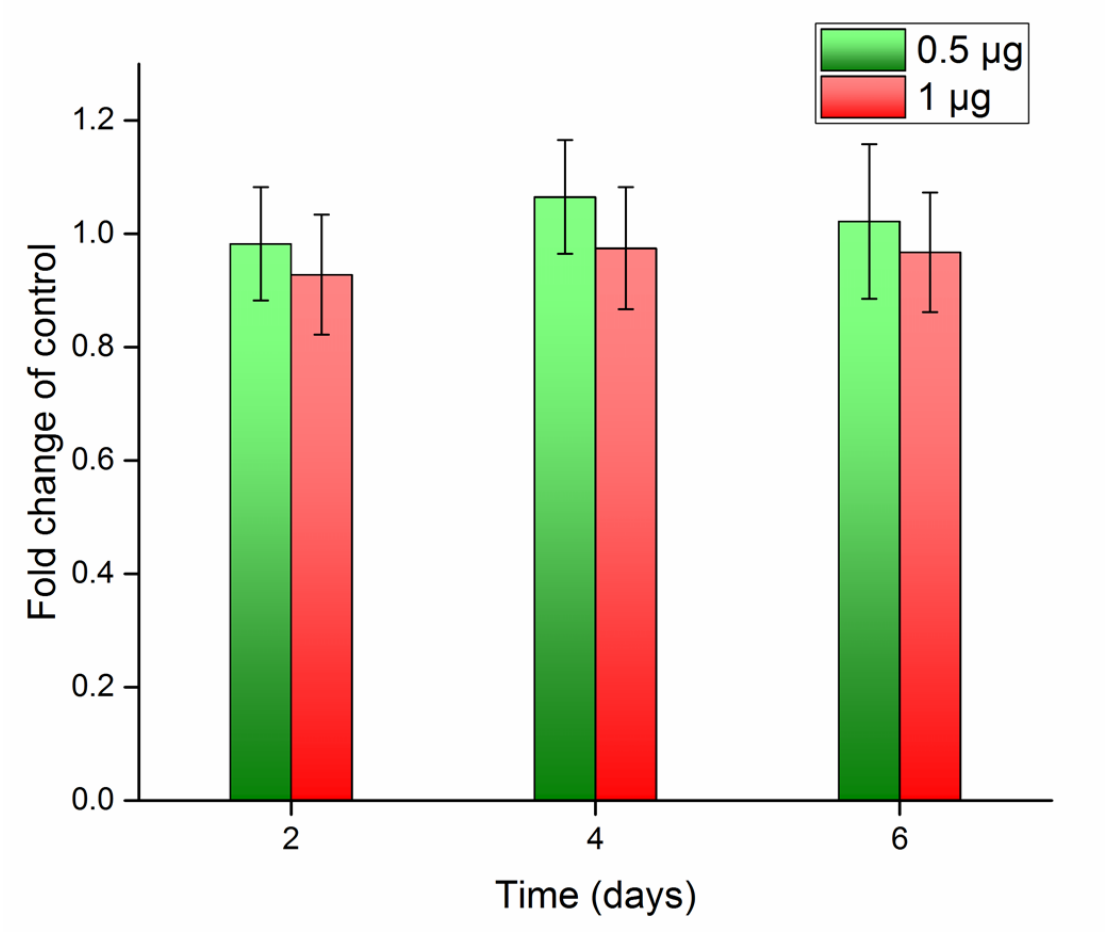

Figure 5.12. Cell proliferation analysis of Fibrin-NanoSiCaP gels.

CyQuant assay measuring HEK-293 cell proliferation at day 2, 4 and 6. Data represented as fold change of control gel, statistically not significant (without pDNA and NanoSiCaPs). The data were reported ± SD, n=6 ($p>0.05$)

5.3.5 2-D vs 3-D fibrin gene delivery systems using lyophilized and freshly prepared NanoSiCaPs

Finally, the use of lyophilized NanoSiCaPs for fibrin gel formulation was tested. Accordingly, NanoSiCaPs complexes were lyophilized in the presence of 10% sucrose and used within one week of storage for synthesizing the Fibrin-NanoSiCaPs gels, since this concentration of sucrose and storage conditions provided the highest transfection efficiency while preserving the particle stability. Additionally, two different models of gene delivery system, 2-D and 3-D models of transfection were employed (Figure 5.1). For these experiments, 300µl of gels were synthesized per well in a 24 well plate containing 200µl of freshly prepared or lyophilized NanoSiCaPs (corresponding to 5µg of pDNA coding for SEAP or GFP). The kinetics of gene expression for the fibrin gels synthesized with freshly prepared 2-D systems increased gradually from day 2 (15.4±2.55 SEAP ng/10^4 cells), to a calculated ~2.4-fold increase observed on day 6 (36.3±2.68 SEAP ng/10^4 cells and then decreasing by day 8 (18.9±1.4 SEAP ng/10^4)cells as shown by the SEAP expression analysis in Figure 5.13 and qualitative assessment of GFP expression in Figure 5.14a-d. Similar expression was observed for fibrin gels synthesized with lyophilized NanoSiCaPs that were stored no longer than 1 week and were reconstituted prior to gel formation. Gene expression for these gels for 2-D systems also increased gradually from day 2 (10.9±4.36 SEAP ng/10^4 cells), to 2-fold increase on day 6 (20.7±3.94 SEAP ng/10^4 cells) and then decreasing by day 8 (18.7±2.18 SEAP ng/10^4) cells as shown by SEAP expression analysis in Figure 5.13 and qualitative assessment of GFP expression in Figure 5.14e-h.

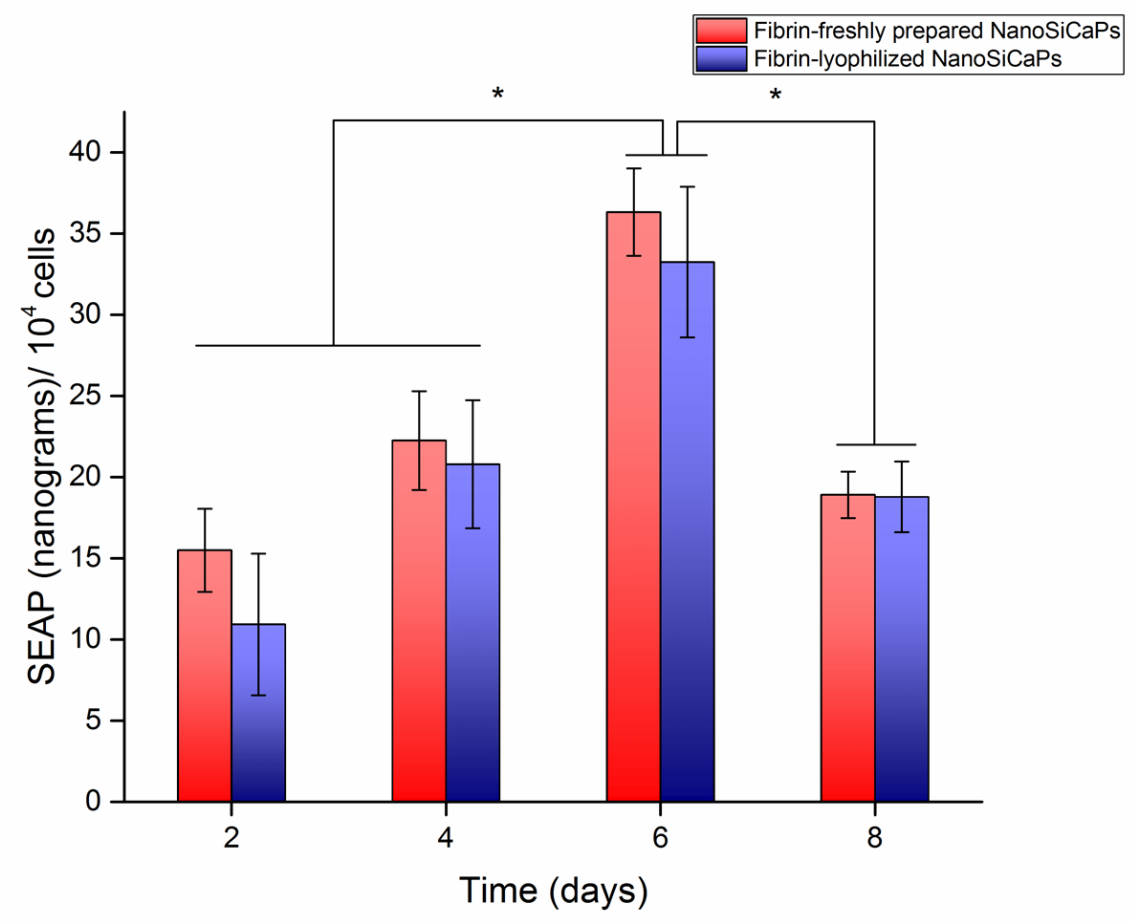

Figure 5.13. 2-D method of transfection.

In-vitro transfection efficiency of HEK-293 cells in 24-well plate showing SEAP expression at day 2, 4 and 6. 300 µl of fibrin hydrogels were synthesized with freshly prepared and lyophilized NanoSiCaPs (reconstituted prior to gel formation). Cells were plated on top of the gels for 2-D method of transfection. SEAP expression is normalized to cell number. Control group included gels synthesized with 10mg/ml fibrinogen with empty NanoSiCaPs complexes (without pDNA). The data were reported ± SD, n=3 ($p<0.05$). Post hoc analysis of statistically significant groups indicated by asterisk (*).

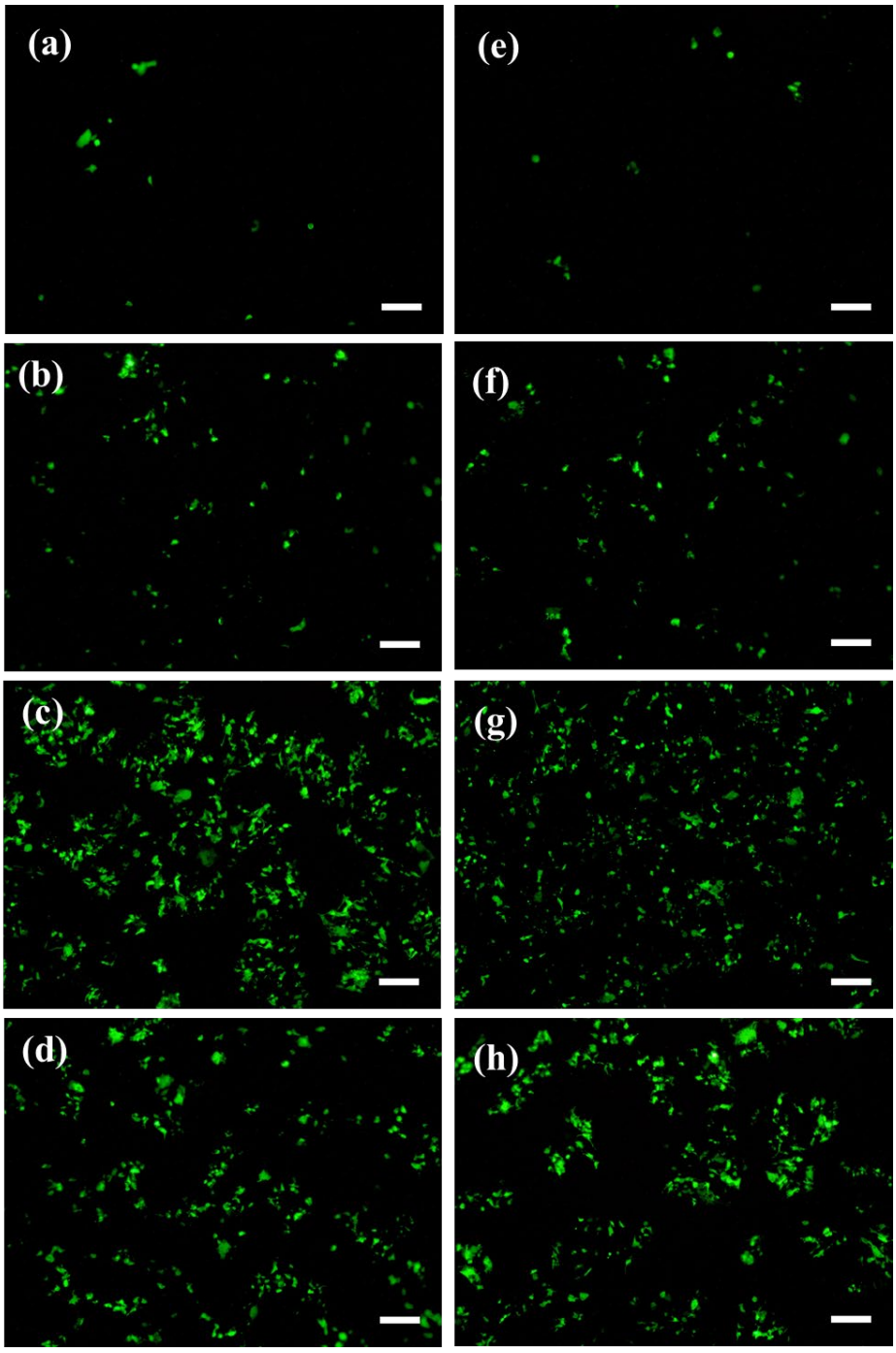

Figure 5.14. Fluorescence microscopy images by 2-D transfection method.

Qualitative assessment of GFP expression by HEK-293 cells in fibrin gels synthesized with: freshly prepared NanoSiCaPs on (a) day 2 (b) day 4 (c) day 6 and (d) day 8 (scale 200µm); lyophilized NanoSiCaPs (reconstituted prior to gel formation) on (e) day 2 (f) day 4 (g) day 6 and (h) day 8 (scale 200µm).

This duration of expression was subsequently compared to 3-D GDS with same quantities of pDNA. For 3-D GDS, there was a modest increase in gene expression during the cell culture period. As shown in Figure 5.15, 3-D GDS also had a later peak expression at day 8 (22.8±1.21 SEAP ng/10^4 cells for fibrin gels prepared with freshly prepared NanoSiCaPs complexes), with a 4-fold increase in gene expression from day 2 (5.66±1.60 SEAP ng/10^4 cells for fibrin gels prepared with freshly prepared NanoSiCaPs complexes). This was also qualitatively assessed by visualizing GFP expression using fluorescence microscopy, Figure 5.16a-d. Similar trend was observed for fibrin gels synthesized with lyophilized NanoSiCaPs, Figure 5.15 and Figure 5.16 e-h. In general, 2-D GDS displayed higher levels of gene expression than 3-D GDS at all the time points. This is partly attributed to the fact that 2-D GDS displayed higher proportion of viable cells (~100% viable cells) at 24 h and 48 h time points as compared to 3-D GDS (~80% viable cells), Figure 5.17. Incorporation of 3-D system has been proposed earlier to extend transgene expression. In our study, we do observe that the 3-D GDS has a later onset of peak expression and other factors such as optimum number of cells encapsulated and incubation time of vectors with cells will also likely play a role in kinetics of gene expression which have not been investigated here. These results nevertheless, proved that the fibrin gels can be synthesized using lyophilized NanoSiCaPs and can achieve sustained gene expression up to 1 week.

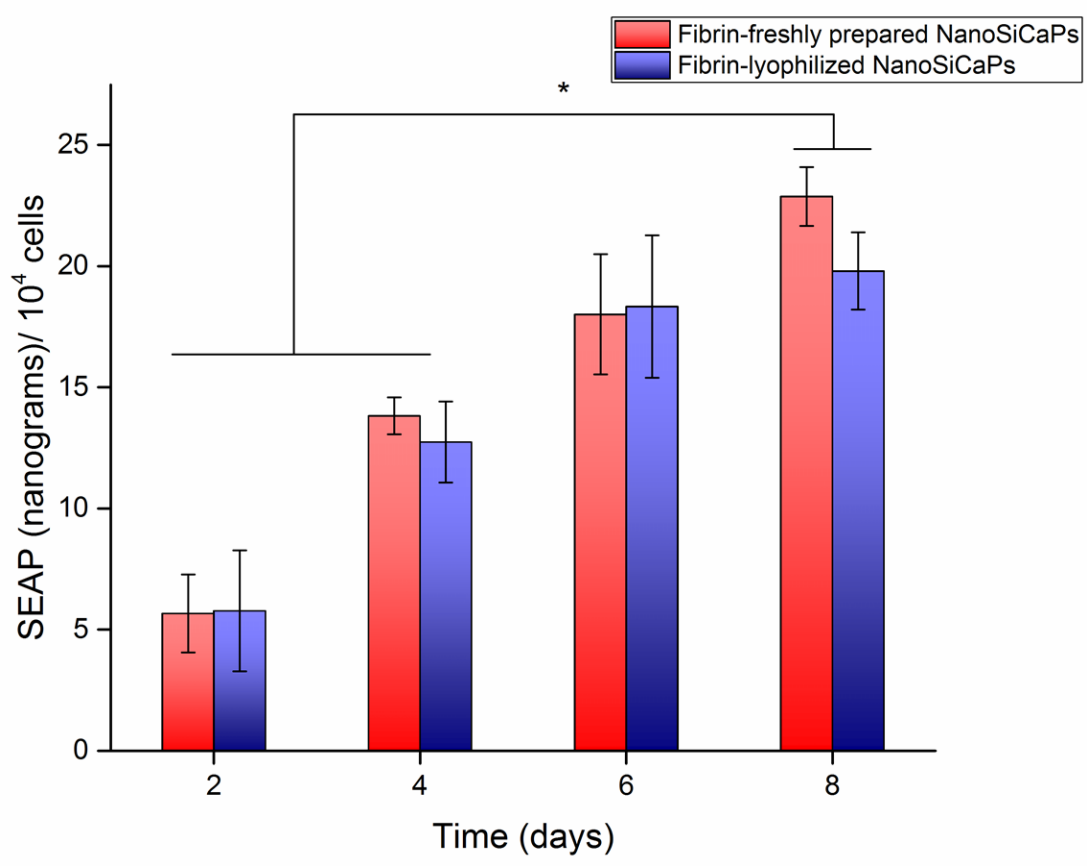

Figure 5.15. 3-D method of transfection.

In-vitro transfection efficiency of HEK-293 cells in 24-well plate showing SEAP expression at day 2, 4 and 6. 300 µl of fibrin hydrogels were synthesized with freshly prepared and lyophilized NanoSiCaPs (reconstituted prior to gel formation). For 3-D method of transfection, 50,000 cells were suspended in NanoSiCaPs solution containing thrombin and immediately mixed with fibrinogen solution for gel formation. SEAP expression is normalized to cell number. Control group included gels synthesized with 10mg/ml fibrinogen with empty NanoSiCaPs complexes (without pDNA). The data were reported as mean ± SD (n=3). Post hoc analysis of statistically significant groups indicated by asterisk (*).

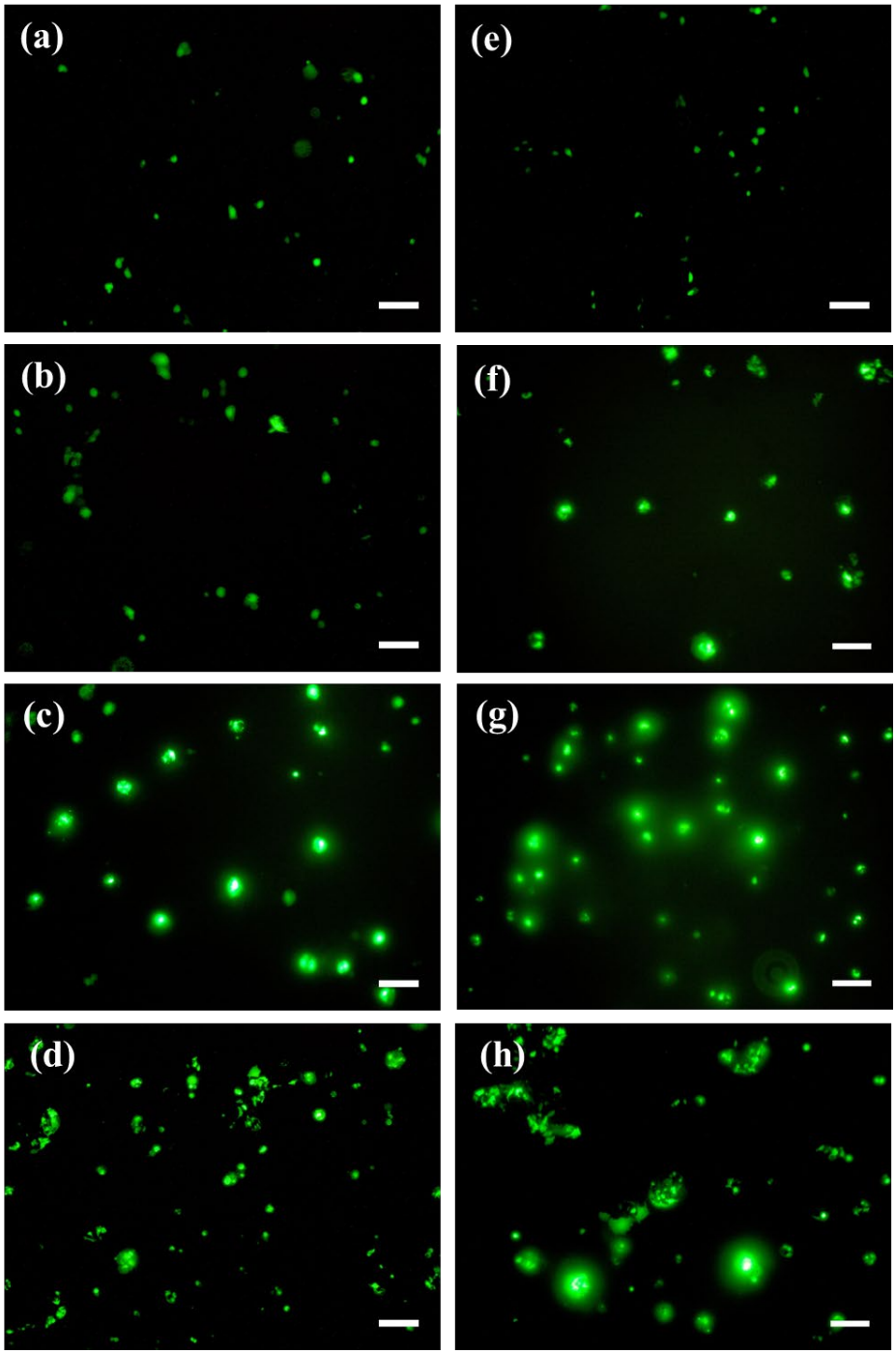

Figure 5.16. Fluorescence microscopy images by 3-D transfection method.

Qualitative assessment of GFP expression by HEK-293 cells in fibrin gels synthesized with: freshly prepared NanoSiCaPs on (a) day 2 (b) day 4 (c) day 6 and (d) day 8 (scale 200µm); lyophilized NanoSiCaPs (reconstituted prior to gel formation) on (e) day 2 (f) day 4 (g) day 6 and (h) day 8 (scale 200µm).

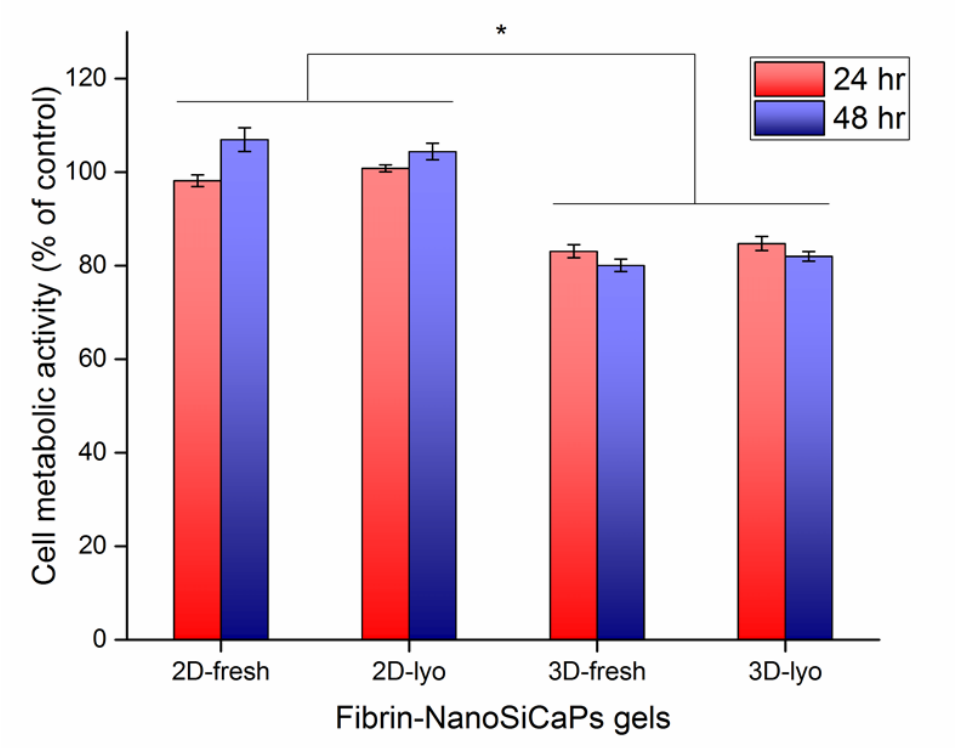

Figure 5.17. Cell viability assay using 2-D and 3-D transfection methods.

MTT assay measuring in-vitro cell metabolic activity of HEK-293 cells with 2-D and 3-D GDS at 24h and 48h. Control group included gels synthesized with 10mg/ml fibrinogen with empty NanoSiCaPs complexes (without pDNA). The data were reported as mean ± SD (n=3). Post hoc analysis of statistically significant groups indicated by asterisk (*).

5.3.6 SEM imaging of Fibrin-NanoSiCaPs

Scanning electron microscopy was used to assess the microstructure of the fibrin gels synthesized with freshly prepared and lyophilized NanoSiCaPs complexes. As evidenced in Figure 5.18a, Figure 5.18b, Figure 5.19a and Figure 5.19b there was no observable difference in the microstructure of the fibrin gels synthesized with freshly prepared or lyophilized

NanoSiCaPs (storage > 1 week). Figure 5.18b and Figure 5.19b, shows the primary particle size of encapsulated NanoSiCaPs complexes to be ~ 100nm. Specifically, SEM images of both gels shows homogenous dispersion of NanoSiCaPs complexes in the fibrin matrix with no evidence of significant aggregation.

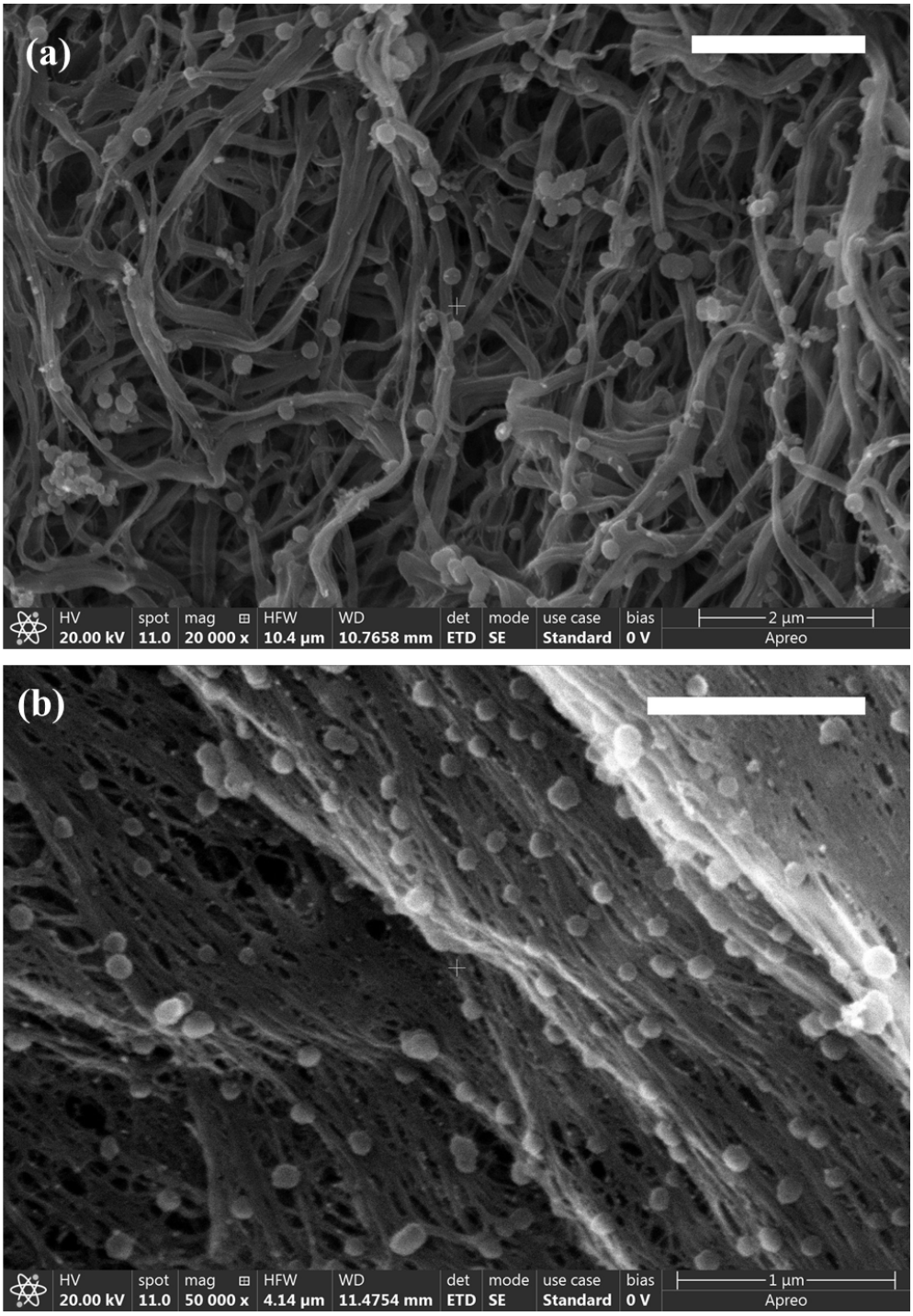

Figure 5.18. SEM images of fibrin gels synthesized with freshly prepared NanoSiCaPs.

(a) scale 2µm (b) scale 1µm.

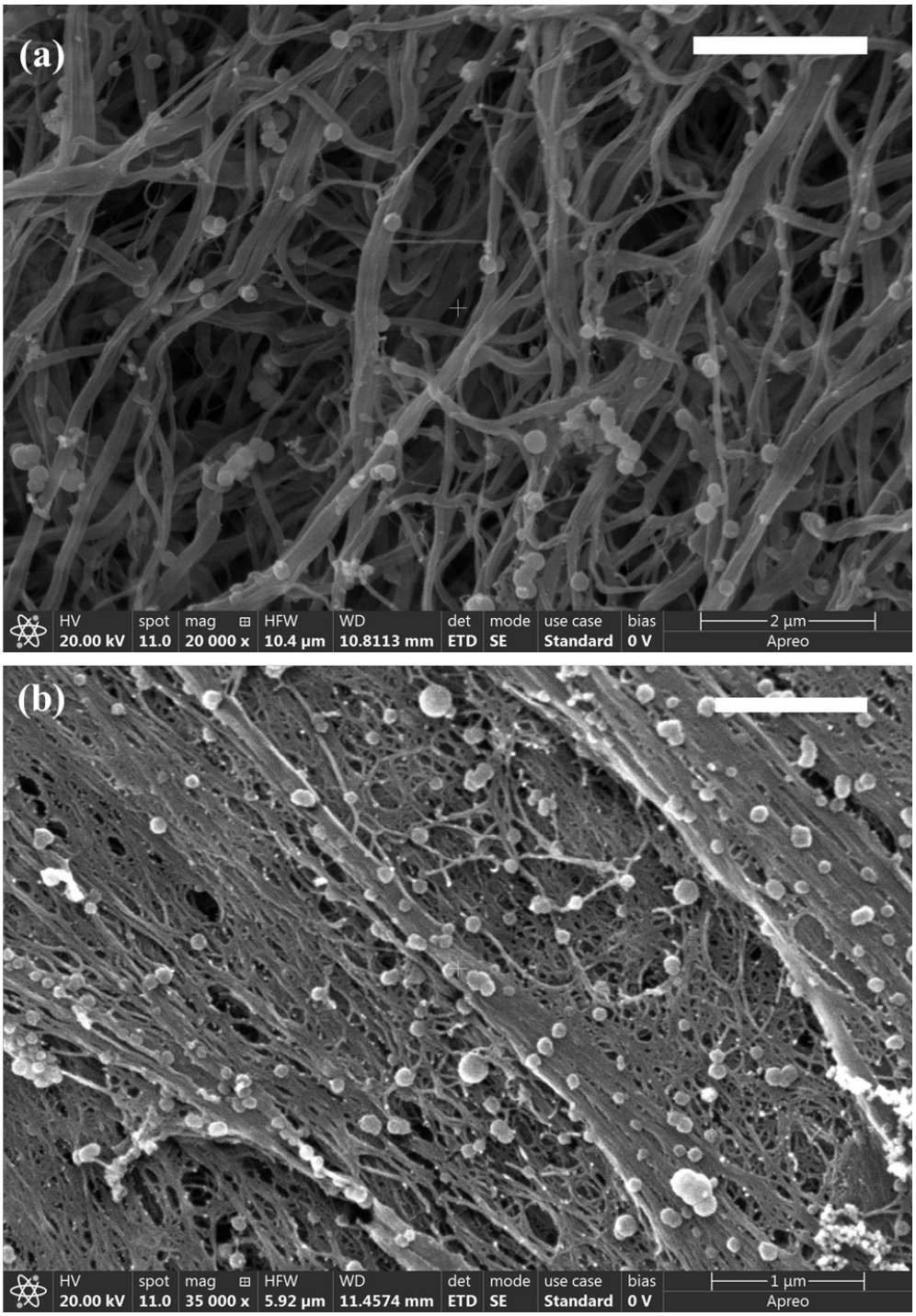

Figure 5.19. SEM images of fibrin gels synthesized with lyophilized NanoSiCaPs.

Fibrin gels synthesized with reconstituted lyophilized NanoSiCaPs after 1 week of storage (a) scale 2µm (b) scale 1µm.

5.4 DISCUSSION

The purpose of this study was to synthesize a 3-D gene delivery system (GDS) comprised of lyophilized NanoSiCaPs complexes and fibrin. The GDS was designed to facilitate sustained gene transfection of cells mediated by NanoSiCaPs complexes from the fibrin hydrogels. This was accomplished by achieving three major goals. First, developing a freeze-drying protocol for NanoSiCaPs by determining optimum sucrose concentration and storage conditions for lyophilized sucrose/NanoSiCaPs formulations. Second, synthesizing Fibrin-NanoSiCaPs hydrogels by determining the optimum fibrinogen and NanoSiCaPs concentrations. Third, determining the optimum cell transfection methodology, 2-D vs 3-D mediated via Fibrin-NanoSiCaP gels.

One of the major limitations preventing the use of CaP based vectors is the colloidal instability of these vectors, especially with prolonged storage under aqueous conditions [27]. In general, synthesis of CaP based gene delivery vectors rely on electrostatic interaction between the negatively charged pDNA and the calcium ions for condensation and subsequent particle formation by the addition of phosphates [27]. The surface charge of the synthesized complexes is approximately -20mV [67], and a minimum surface charge of ± 30mV has been shown to prevent particle aggregation [200]. Therefore, prolonged storage of synthesized NanoSiCaPs complexes in aqueous conditions results in aggregation. In addition, these complexes possess areas of charge neutrality which facilitate electrostatic interactions between the particles thus leading to particle aggregation [201]. This results in a decline in transfection efficiency of these complexes with prolonged storage as observed in the transfection experiments in this study utilizing aged samples (Figure 5.4). Overcoming this limitation was the motivation for the first part of this study to develop freeze dried formulation of NanoSiCaPs, which would enable both

withstanding the shipping and transportation related stresses and offer stability for long periods of time without exhibiting loss in transfection ability. In fact, several studies have shown that lyophilization, with the use of a lyoprotectant for example, a disaccharide, is an effective method for stabilizing lipid-DNA [113, 198] and polymer-DNA complexes [116, 197]. However, there are no reports to date, assessing the long-term stability of freeze-dried formulations comprising CaP and pDNA. Therefore, in our current work, we explored the possibility of lyophilizing NanoSiCaPs complexes, with the use of sucrose as a lyorprotectant, for achieving long-term stability of the nanoparticles.

In agreement with previous studies for lipid- and polymer-based gene delivery vectors, our data demonstrated that the gene transfection ability of the NanoSiCaPs complexes can be maintained up to 3 weeks by freeze-drying these complexes with sucrose as a lyoprotectant (Figure 5.5) [117, 197, 199]. As mentioned in Section 5.2.2.3, all the lyophilized samples were first frozen at -80 ºC for 60 minutes prior to drying. This ensured that the samples were cooled below the freezing point of sucrose solution. Cooling the samples to -80^{o}C guaranteed freezing of the sucrose/NanoSiCaPs suspension. It is believed that this process aided in the preservation of the "native" structure of the NanoSiCaPs particles with the sucrose preventing coalescence and as such helped to maintain the gene transfection abilities of the particles. Additionally, freeze-dried samples were sealed under inert conditions by purging argon gas in a glove bag as mentioned in the Section 5.2.2.4. In-vitro gene transfection of HEK-293 cells with sucrose/NanoSiCaPs formulations with different concentrations of sucrose (% weight/volume) revealed that sucrose can indeed stabilize NanoSiCaPs complexes in aqueous conditions resulting in increased SEAP expression for 10% sucrose formulation (Figure 5.2). This increase in gene expression is attributed to the colloidal stability conferred by sucrose molecules by

creation of H-bonds between hydroxyl groups on sucrose and the phosphate groups on pDNA [202] and/or NanoSiCaPs. In doing so, the sucrose molecules serve to sterically hinder the NanoSiCaPs complexes thus providing a medium for a stable dispersion of the NanoSiCaPs complexes. However, sucrose/NanoSiCaPs formulations with 20% sucrose concentrations resulted in reduced gene expression, which was attributed to the reduced cell metabolic activity for these samples, Figure 5.3. Reduced cell metabolic activity due to high sucrose concentration could be due to increasing level of tonicity resulting in cellular damage. In addition, high sucrose concentration can also influence the duration of the lyophilization cycle and significantly impact the production costs [111]. Our results indicated an optimum sucrose/NanoSiCaPs ratio offering particle stability while maintaining cell viability. Therefore, 10% sucrose was selected as the optimum concentration for lyophilization of NanoSiCaPs.

In-vitro gene transfection studies of lyophilized NanoSiCaPs on HEK-293 cells showed that the process of freeze-drying did not affect the gene transfection ability of lyophilized NanoSiCaPs as compared to freshly prepared NanoSiCaPs, Figure 5.4. In contrast, samples lyophilized without sucrose and not lyophilized (aged) samples, resulted in 40-fold less SEAP expression. These results proved that sucrose can stabilize the NanoSiCaPs during the freeze-drying process without inducing any loss in transfection abilities of these particles. However, transfection efficiency of lyophilized particles was independent of storage temperature as seen in our studies. Lyophilized sealed samples stored at 4 ºC and R.T. (under ambient conditions) had similar transfection efficiency at all time points, Figure 5.5 (statistically insignificant, $p>0.05$). Decrease in transfection efficiency with storage temperature is however, observed in other studies. It should also be noted that the decline in transfection efficiency noticed in these studies is observed at elevated temperatures, 40 ºC [117, 199]. In the current study, a steady decline in

transfection efficiency is observed with storage. Interestingly, even at week 3 the lyophilized sucrose/NanoSiCaPs formulations resulted in significant SEAP expression (Figure 5.5) as compared to samples lyophilized without sucrose and not lyophilized (aged) samples (Figure 5.4). Decline in transfection efficiency with storage was believed to be caused by the presence of water content in the freeze-dried samples. The presence of moisture could be due to two reasons. First, the sucrose/NanoSiCaPs were lyophilized in a benchtop freeze-drier, which does not possess the capability of secondary drying, which is a crucial step to completely remove the residual moisture content from the freeze-dried samples. Second, even though, extreme precautions were taken while transporting the freeze-dried samples from the lyophilizer to the glove bag, it is possible that exposure to atmospheric conditions for brief period resulted in influx of water molecules into the freeze-dried samples. This could explain the decline in transfection efficiency of lyophilized sucrose/NanoSiCaPs formulations by week 3 (Figure 5.5). In general, an increase in water content can be critical for storage stability as it is associated with a decrease in the steric hindrance ultimately leading to aggregation of complexes in the freeze dried solid [113]. Future studies, incorporating a lyophilizer capable of secondary drying step and reducing the exposure of samples to atmospheric conditions can indeed solve this problem.

In-vitro transfection results were further supported by the TEM analysis of reconstituted sucrose/NanoSiCaPs samples. Our data confirms the ability of sucrose to maintain the particle size of the lyophilized sucrose/NanoSiCaPs complexes. As confirmed by TEM analysis, sucrose/NanoSiCaPs samples yielded particle sizes that were same as positive control (freshly prepared NanoSiCaPs without sucrose), Figure 5.6a and Figure 5.6b. These particles were spherical in nature with primary particle size of ~100nm. However, with prolonged storage of sucrose/NanoSiCaPs samples there was an increase in particle aggregation, wherein week 3

samples mostly consisted of large clumps, Figure 5.8b. This explained the decline in transfection efficiency observed for these samples. Therefore, in the first part of the study, our results showed that both the particle size and transfection efficiency of the NanoSiCaPs complexes could be preserved for up to 1 week in storage under ambient conditions by freeze drying the nanoparticles with 10% sucrose.

For the second part of this study, a 3-D gene delivery system (GDS) was synthesized comprising of NanoSiCaPs complexes and fibrin. In order to achieve that, current study focused on determining the optimum fibrinogen concentration, pDNA dose (i.e. amount of NanoSiCaPs complexes), incorporation of fibrinolytic agent, and evaluating two methods of in-vitro transfection (2-D vs 3-D) for generation of Fibrin-NanoSiCaPs formulation, as outlined in Figure 5.1. Fibrin is used as a scaffold material for the current application even though it lacks the mechanical strength required for bone tissue engineering, as the long-term goal is development of a hybrid scaffold where a porous polymeric, ceramic or metallic scaffold with appropriate mechanical strength can be infiltrated with the synthesized Fibrin-NanoSiCaPs formulation.

Initially, the aim was to investigate the role of fibrinogen concentration in gene transfection abilities of fibrin gels synthesized with freshly prepared NanoSiCaPs. The thrombin concentration was fixed at 10U/ml, since the concentration of thrombin plays a more significant role in reaction kinetics of the gel formation, whereas, fibrinogen concentration has been reported to affect cell proliferation, migration and differentiation [203-205]. In our assessment, SEAP expression was observed in all Fibrin-NanoSiCaPs gel formulations. A fibrinogen concentration of 10mg/ml provided an ideal balance between cell proliferation and gel stability for the duration of cell culture, 6 days (Figure 5.9). In general, fibrin gels with high fibrinogen concentrations (70-100mg/ml) have decreased cell proliferation and migration relative to gels

with low fibrinogen concentrations (10mg/ml) [203, 204]. Based on our transfection results and other reports in literature we selected the fibrinogen concentration of 10mg/ml for the synthesis of Fibrin-NanoSiCaP gels for all other subsequent studies.

Interestingly, increasing pDNA amount (corresponding to respective amounts of NanoSiCaPs) in the fibrin gels did not yield higher gene transfection levels (Figure 5.10). This was attributed to the fact that Fibrin-NanoSiCaPs gels synthesized with 0.5µg and 1µg pDNA resulted in bulk release of complexes and did not induce sustained gene transfection for gels with high pDNA concentration. Notably, this has also been reported in other studies where increase in pDNA amount beyond a certain limit does not result in increase in transfection efficiency [194, 206]. However, incorporation of 10µg/ml aprotinin, a fibrinolytic inhibitor delayed fibrin gel degradation and resulted in reduced gene expression for both pDNA doses (Figure 5.11). This experiment showed that fibrin degradation by target cells is necessary for gene delivery. Furthermore, the effect of pDNA dose on gene expression was more pronounced with use of aprotinin, where Fibrin-NanoSiCaPs gels with 1µg pDNA resulted in higher SEAP expression at all time points (Figure 5.11). Decrease in gene transfer efficiency with increase in aprotinin concentrations has been reported by Lei et al. [194], however in the current study only one concentration of aprotinin was investigated. These results indicated that sustained gene expression can be achieved by incorporating aprotinin in the synthesis of fibrin-NanoSiCaPs gels. Additionally, the synthesized Fibrin-NanoSiCaPs gels with aprotinin and two different doses of pDNA did not elicit any adverse effect on proliferation of HEK-293 cells (Figure 5.12).

Transfection of cells using Fibrin-NanoSiCaPs gel formulations is critical to validate the activity of NanoSiCaPs following lyophilization, reconstitution in gel precursors and distribution in the 3-D environment of the hydrogel. Two primary models exist for in-vitro transfection using

hydrogel matrices: co-encapsulation of cells with vector in the gel precursor, i.e. 3-D, and initial separation of cells from the vector before gel formation, namely, 2-D. While 3-D method of transfection provides a means of early detection of gene expression due to prior incubation of complexes with cells before gelation, homogenously dispersed cells may demonstrate limited migration and only have access to complexes initially distributed near the cells [207]. In contrast, 2-D method of transfection involves separation of complexes from the cells before hydrogel formation and ensures that vector internalization occurs because of cell invasion, migration and hydrogel degradation [208]. In the current study, transfection of HEK-293 cells by 2-D method displayed higher SEAP expression at all the time points compared to the 3-D method. Reduced cell viability observed for HEK-293 cells cultured in 3-D system (Figure 5.17) can be one the predominant reason behind these lower levels of gene expression observed. However, other factors such as gel degradation due to cell invasion and migration are also likely to play a crucial role in dictating the gene transfection profile of the synthesized fibrin gels. For instance, the gene expression peaked at day 6 for 2-D method (Figure 5.13), whereas it peaked at day 8 for 3-D method (Figure 5.15). Notably, opposite results were observed by Lei et al. wherein 3-D transfection method displayed higher gene expression than 2-D methods [194]. Higher levels of gene expression in their study was also observed with increase in number of cells encapsulated in the fibrin gel. Additionally, the protocol utilized for 3-D transfection method utilized by Lei et al. incorporated incubation of lipoplexes with cell suspension for 15 minutes prior to gel formation [194], which may have resulted initial uptake of lipoplexes by the cells in suspension. In contrast, a similar study reported by Rieux et al. utilized 3-D method of transfection using fibrin-lipoplex system, where lipoplexes were incubated for 30 minutes with cell suspension prior to gel formation [206]. Interestingly, the authors observed enhanced transfection for 2-D method as

compared to 3-D method. The authors explained this difference of transfection efficiency by vector-material interactions using confocal microscopy and concluded that transfection results for the 3-D model resulted primarily from the initial cell/vector interactions, rather than uptake by cells following encapsulation within the hydrogel [206]. Following these contrasting results using similar delivery vector used by Lei et al. and Rieux et al., and the results observed in our study clearly indicates that there is need for a more systematic study to be conducted to determine the influence of number of cells encapsulated in the hydrogel matrix and the mechanisms at work therein for clearly delineating the NanoSiCaPs transfection in 2-D vs. 3-D environments.

The Fibrin-NanoSiCaPs gels exhibited the characteristic fibrillar structure in SEM micrographs. Gels synthesized with freshly prepared and lyophilized NanoSiCaPs displayed homogenous distribution of NanoSiCaPs complexes throughout the gel matrix. The morphology of the NanoSiCaPs complexes and the microstructure of the fibrin gels synthesized with either freshly prepared or lyophilized NanoSiCaPs appeared to be the same. Furthermore, NanoSiCaPs complexes in both the gels were non-aggregated and ~100nm in size. Taken together our results suggest that fibrin gels synthesized with lyophilized NanoSiCaPs complexes that yield sustained gene expression may indeed provide an effective platform for generation of gene delivery systems that has potential in bone tissue engineering.

5.5 CONCLUSIONS

In this assessment, we demonstrate use of gene delivery system using fibrin hydrogel as an encapsulation matrix to incorporate lyophilized NanoSiCaPs complexes. Our results showed that

NanoSiCaPs complexes lyophilized in the presence of sucrose can be stored for up to 1 week under ambient conditions without any change in both particle size and transfection efficiency as compared to freshly prepared samples. Preservation of transfection efficiency was only observed for nanoparticles lyophilized with sucrose. Embedding the NanoSiCaPs complexes within fibrin hydrogels allowed sustained gene expression for up to 1 week. Transfection mediated via Fibrin-NanoSiCaPs dependent on fibrinogen and pDNA concentrations (NanoSiCaPs amount). The gene expression and gel degradation can be meticulously controlled by incorporation of fibrinolytic inhibitor, like aprotinin. Gene transfection using Fibrin-NanoSiCaPs gels also depends on the method of cell transfection, on the surface i.e. 2D or within the hydrogel i.e. 3D, suggesting that gene transfer may be a function of cell-matrix interaction and the local microenvironment. Fibrin gels synthesized with lyophilized NanoSiCaPs display similar transfection levels as compared to gels synthesized with freshly prepared NanoSiCaPs. These results are indeed promising as we show for the first time that lyophilization is an excellent method for not only stabilizing NanoSiCaPs complexes but also these complexes can be reconstituted for generation of fibrin gene delivery system that are promising tools providing scope for their use in bone tissue engineering and regenerative medicine applications.

5.6 ACKNOWLEDGEMENTS

The work presented in this chapter was partially supported by the NSF (CBET-0933153) and NSF-ERC (Grant # EEC-0812348). We would also like to acknowledge the Edward R. Weidlein Chair Professorship Funds and the Center for Complex Engineered Multifunctional Materials (CCEMM), Swanson School of Engineering, and the University of Pittsburgh for providing

partial support in the form of support for graduate student, reagents, equipment and other accessories much needed for conducting and completing this research. Specifically, we would like to thank Center for Biologic Imaging (CBI) for the use of critical point dryer (CPD) utilized in this study.

6.0 CONCLUSIONS

Calcium phosphate-based nanoparticles (CaP) have demonstrated great potential as non-viral gene delivery vectors. They are widely studied biomaterials for tissue engineering applications due to their biocompatibility and non-toxicity [83]. Their use in bone tissue engineering is especially attractive owing to their structural and compositional similarity to the mineralized tissue architecture of native bone. However, despite their widespread use, several issues regarding their colloidal stability, dissolution kinetics as well as the ability for prolonged storage have stymied their success and widespread use as a non-viral gene delivery vector. Therefore, in this dissertation we crafted strategies to address these limitations by altering the materials properties of the nanostructured calcium phosphates (NanoCaP) previously developed by our group [67]. We accordingly generated the substituted version called NanoSiCaPs exhibiting much improved gene transfection and subsequently developed novel methodologies to incorporate this enhanced version of NanoCaPs (NanoSiCaPs) in scaffolds commonly employed for bone tissue engineering.

To further augment the transfection potential and thereby challenge the current accepted standard for CaP based non-viral gene delivery, we developed an enhanced version of NanoCaPs, by substituting known amounts of silicate ions for phosphate in the hydroxyapatite (HA) lattice, which we termed as NanoSiCaPs. Results discussed in the thesis indicated that in addition to excellent transfection levels exhibited by NanoCaPs alone in vitro, an additional 20-

50% increase in gene transfection was observed for NanoSiCaPs (8.3-50 mol% silicate substitution) (Figure 3.8). This increase in transfection efficiency was attributed to its rapid dissolution properties (Figure 3.7) and it was believed that this aided in pDNA escape from lysosomal degradation. The silicate substitution also limited particle aggregation (Figure 3.10a-d) which contributed to increase in transfection efficiencies of these complexes. However, high silicate substitution (>50 mol%) resulted in a drastic decline in transfection as the synthesized NanoSiCaPs deviated far from the characteristic hydroxyapatite phase formed as evidenced by the XRD and FTIR results (Figure 3.2 and Figure 3.4). Fundamental understanding of the influence of various amounts of silicate substitution on materials properties of the synthesized NanoSiCaPs utilized in this part of the study highlighted the importance of generating and maintaining a single phase of HA and its crucial role in pDNA binding and transfection.

In addition to changing the materials properties of NanoSiCaPs, we developed and assessed them as functional vectors that can be incorporated on or within scaffolds for non-viral gene delivery. First, we focused on achieving surface mediated gene delivery from implant surfaces. It is hypothesized that bio-functionalized materials will offer a unique strategy to facilitate tissue regeneration and integration around implants. Our focus was thus to develop a methodology that can be easily applied to materials with different geometries and composition. To achieve that, we developed a novel and simple coating approach using NanoSiCaPs complexes that preferentially adsorbed onto titanium (Ti) substrates coated with poly (diallyl dimethylammonium chloride) (PDADMAC) (Figure 4.1). The generated Ti-polyelectrolyte NanoSiCaPs assemblies aptly called PNA, delivered pDNA to MC3T3-E1 cells, induced reporter gene expression, without eliciting any cytotoxicity, while simultaneously encouraging cell attachment on the substrate. Interestingly, the coated substrates that lacked NanoSiCaPs as a

delivery agent (pDNA only) did not result in efficient gene transfection (Figure 4.8), although these samples also supported cell attachment, without eliciting any cytotoxicity (Figure 4.9and Figure 4.10). This observation clearly suggested that it is indeed crucial to incorporate a transfecting agent in the coatings for successful delivery of pDNA to the cells and subsequently obtain the desired gene expression. Nevertheless, the reporter gene expression achieved from PNA could not be sustained for a week, since the peak gene expression was observed on day 3 (Figure 4.8). It can also be construed that the adsorption of NanoSiCaPs complexes on Ti-surfaces largely relies on the electrostatic interaction between the negatively charged NanoSiCaPs complexes and the positively charged polyelectrolyte, PDADMAC. This interaction while beneficial may have led to charge compensation with limited adsorption of the NanoSiCaPs complexes beyond a certain limit. Although, the methodology developed is simple, it lacked the desired control over the amount of NanoSiCaPs complexes needed for effective incorporation onto the substrate to achieve the sustained gene transfection warranting further studies.

In order to overcome these challenges for the reasons discussed above, we developed a methodology that can provide precise control over the amount NanoSiCaPs complexes that can be incorporated in a scaffold. To achieve this goal, we focused on achieving gene delivery through the bulk of the scaffold, in contrast to the surface mediated gene delivery described in the previous approach. It was therefore, hypothesized that entrapping and distributing NanoSiCaPs complexes over a 3-D volume would serve two main purposes, First, the aggregation of NanoSiCaPs complexes can potentially be reduced or eliminated since the interactions between the individual NanoSiCaPs particles are less likely to occur if quickly incorporated in a hydrogel matrix after their formation. Second, the scaffold would serve as a

template for the infiltration, attachment and proliferation of cells, and subsequent transfection through the incorporated NanoSiCaPs complexes in the gel. To achieve that, we developed a gene delivery system comprised of NanoSiCaPs complexes and fibrin gels. For production of the Fibrin-NanoSiCaPs formulation, effect of fibrinogen concentration, vector dosage and incorporation of fibrinolytic inhibitor (aprotinin) on the gene transfer ability of the NanoSiCaPs complexes was investigated. We observed that gene transfection abilities of the gels can be meticulously controlled by modulating the fibrinogen concentration (Figure 5.9), vector dosage and incorporation of aprotinin (Figure 5.11). In our assessment, the Fibrin-NanoSiCaPs formulation synthesized in 96-well plates with 10mg/ml fibrinogen, 1µg pDNA and 10µg/ml aprotinin resulted in optimum gene expression during the in-vitro cell culture period of 6 days. Furthermore, for the Fibrin-NanoSiCaPs to be used in a clinical setting we also developed a lyophilization protocol for NanoSiCaPs complexes that would allow long-term storage of synthesized complexes.

We hypothesized that development of a technique that could enable storage and shipment of pre-made NanoSiCaPs complexes would eliminate the need of having trained personnel for synthesizing the NanoSiCaPs complexes prior to its use. With respect to the fibrin gel study, reconstitution of the lyophilized NanoSiCaPs complexes prior to gel formation would further advance the feasibility of utilizing Fibrin-NanoSiCaPs formulations in a clinical setting. To achieve this goal, we developed a lyophilizing technique for preservation of NanoSiCaPs complexes in the presence of sucrose. In vitro transfection results of HEK-293 cells showed that 10% sucrose (% weight/volume) can preserve transfection efficiency and particle morphology of NanoSiCaPs complexes through the freeze-drying process (Figure 5.4). Notably complexes that were lyophilized in the absences of sucrose and complexes that were aged (without

lyophilization) resulted in reduced transfection efficiency. Furthermore, lyophilized NanoSiCaPs complexes (with 10% sucrose) can be stored under ambient conditions for up to 1 week without any loss in transfection efficiency and observed measurable change in the particle size when compared to freshly prepared NanoSiCaPs complexes (Figure 5.5 and Figure 5.7). Finally, use of lyophilized NanoSiCaPs in the generation of fibrin gene delivery systems was assessed. The lyophilized NanoSiCaPs complexes (stored up to 1 week) were reconstituted for generation of fibrin hydrogels. In-vitro transfection efficiency employing 2-D and 3-D methods of transfection displayed similar gene expression profile in HEK-293 cells between gels synthesized with freshly prepared and lyophilized NanoSiCaPs complexes (Figure 5.13 and Figure 5.15). Similar microstructure of both gels was observed using SEM imaging (Figure 5.18 and Figure 5.19). These results thus indicated the successful generation of a gene delivery system comprised of fibrin gels that can be synthesized in the presence of reconstituted lyophilized NanoSiCaPs complexes and effectively displayed transfection ability comparable to the gels synthesized with freshly prepared NanoSiCaPs complexes.

Overall in summary, the work presented in this dissertation describes the creation of next generation of CaP vectors, called NanoSiCaPs that display enhanced transfection abilities due to superior materials properties achieved through silicate substitution into the HA lattice. For these complexes to be utilized in bone tissue engineering applications, we also developed methodologies to achieve scaffold mediated non-viral gene delivery through NanoSiCaPs complexes. The methodologies developed in this study can achieve gene delivery both from the surfaces and the bulk of the scaffolds. Furthermore, sincere effort was made in crafting methodologies that would enable easy translation of these techniques towards a clinical setting.

However, further studies are clearly warranted to enable this seamless transition into the clinical setting which are discussed in the following chapter.

7.0 FUTURE DIRECTIONS

In order to exploit the advantageous traits of NanoSiCaPs based non-viral vectors discussed in all the chapters discussed above which include, enhanced dissolution kinetics, high transfection efficiency and minimal cytotoxicity, additional strategies can be employed to exhibit higher therapeutic effect. One of the crucial intracellular barriers is the entry of pDNA to the nucleus of the cells. pDNA once released from the endosome must make its pathway into the cell nucleus for successful transcription and subsequent protein expression in the cytosol. This barrier as is ubiquitously known poses a significant challenge for achieving successful gene transfection of primary stem cells and terminally differentiated cells. Therefore, the use of messenger RNA (mRNA) can be an attractive strategy over the pDNA delivery discussed in this dissertation, since mRNA does not need to enter the nucleus of the cells to be functional, thereby being effective for both dividing and non-diving cells [209]. In theory, the formation of NanoSiCaPs-mRNA complexes should be straight forward since it will employ the same principle of DNA/RNA condensation in the presence of calcium ions and subsequent precipitation in the presence of phosphate and silicate ions, as observed for the NanoSiCaPs-pDNA complex formation. Systemic studies would be required for chemical modification of the mRNA complexes for achieving higher stability and their subsequent use in the generation of NanoSiCaPs-mRNA complexes.

To further prove the efficacy and feasibility of polyelectrolyte NanoSiCaPs assembly (PNA), the fabrication methodology should be applied to other ceramic, metallic and polymeric biomaterials. Since the PNA methodology can be achieved in 30 minutes, it opens up the possibilities to achieve similar surface modifications on degradable substrates in addition to inert substrates. This would enable the creation of PNA on degradable metallic implants such as magnesium-based alloys that exploits the useful traits of biodegradability and mechanical strength for orthopedic applications. Additionally, to exploit the advantageous traits of nanoceramic coating obtained on the surfaces through PNA generation, such as creation of rougher surfaces in the nanoscale range, additional research would be required to understand the influence of these topographies on the differentiation of mesenchymal stem cells (MSCs) and/or osteoblasts. Osteogenic differentiation of hMSCs is guided by various physical and biochemical factors. Controlled nanotopographies created on the biomaterial surfaces, such as pits, grooves, rods, and pores, have already been shown to regulate bone cell adhesion, spreading, proliferation, and differentiation [210]. Therefore, it is important to study the effect of nanoceramic coating on the osteoconductive properties of the modified surfaces by carrying out gene expression analysis of the relevant cells attached to the substrates.

Fibrin gels synthesized with lyophilized NanoSiCaPs complexes displayed encouraging results in the current study. Based on the results observed in the current study there is clearly scope for further development of the synthesized GDS by developing a systematic study, to determine the influence of number of cells encapsulated in the hydrogel matrix for the 3-D method of transfection as well as investigate the optimum incubation time of NanoSiCaPs with cells prior to gel formation. These studies will help in understanding the mechanisms at work therein for clearly delineating the NanoSiCaPs transfection in both 2-D vs. 3-D environments.

The immediate next step for showcasing its efficacy for bone tissue engineering applications would be to utilize the gel formulation for infiltration of porous ceramic, polymeric or metallic bone implant materials. Additionally, 3-D printed scaffolds with desired dimensions can be effectively utilized for the generation of functional gel-implant hybrid scaffolds.

Finally, for any biomaterials to be clinically effective, it needs to be tested in relevant animal models proving its efficacy. The synthesized NanoSiCaPs, lyophilized NanoSiCaPs, PNA, and Fibrin-NanoSiCaPs formulations should be tested in relevant animal models with specific gene of interest to show the efficacy of this gene delivery vector. Ideally first, the studies should incorporate testing these scaffolds for the induction of ectopic bone formation, since this is an effective way to demonstrate bone inducing capability of vector/scaffolds [20]. Additionally, attention should be given to the animal models utilized for testing these scaffolds. Currently, most of the *in-vivo* experiments conducted for testing synthetic biomaterials utilize young rodent models. However, orthopedic biomaterials are implanted more frequently in geriatric patients suffering from other major health problems which interfere with the natural healing response around implants. Aging is also associated with up-regulation of ROS, inflammatory cytokines, and accompanying tissue damage. Therefore, it is crucial to establish new *in-vitro* and *in-vivo* experiments to test the efficacy of fabricated scaffolds. Establishing suitable animal models that can closely mimic the aging-induced deterioration of immune system and stem cells observed in humans would not only lead to successful clinical outcomes, but also reduce the burden on healthcare costs.

APPENDIX A

MISCELLANEOUS EXPERIMENTS FOR CHAPTER 3: IN-VITRO TRASNFECTION EFFICIENCY OF NANOSICAPS IN COMPARISON TO OTHER COMMERCIAL NON-VIRAL VECTORS

A.1 SUMMARY

In Chapter 3.0 , we investigated the influence of silicate ion substitution on NanoCaPs gene transfection abilities. 8.3 mol% Si substitution, termed as NanoSiCaPs displayed the highest transfection efficiency and was selected as the gene delivery agent for subsequent studies. We also compared the transfection efficiency of NanoSiCaPs (with 8.3 mol% substitution) with a few commercially available non-viral agents. In addition, influence of non-viral agents on cell metabolic activity was also assessed.

A.2 METHODS

For this experiment, NIH-3T3 fibroblasts cells were used to determine the transfection efficiency and cell viability. For the transient transfection experiments, the cells were seeded in 12-well

plates at cell-density of about 1.0 x 10^5 cells per well. The gWiz GFP was complexed with NanoSiCaPs as described above in Section 3.2.3, and immediately transferred drop by drop into each well. Commercially available non-viral agents used for this study included polymer-based transfection reagents namely, X-tremeGENE 9 and X-tremeGENE HP, and cationic-lipid based reagent, Lipofectamine 2000. The transfection complexes were made by using optimum complex:pDNA ratio (1:1) as per manufactures protocol so that each well received same amounts of pDNA as used for NanoSiCaPs complexes i.e. 2.11µg gWiz GFP pDNA per well. The complexes were prepared in Opti-MEM Reduced serum media and incubated for 5 minutes for complex formation. The complexes were incubated with the cells for 24 hours after which transfection efficiency was measured by counting the GFP positive cells using the Accuri C6 Flow Cytometer (n=3). Cell metabolic activity was measured using MTT assay as described in Section 5.2.2.5(n=3).

A.3 RESULTS AND DISCUSSION

As shown in Figure A. 1, transfection efficiency of X-tremeGene HP and Lipofectamine 2000 was comparable~ 55% GFP expression, whereas NanoSiCaPs displayed a lower transfection efficiency than these samples with 47% GFP positive cells. On the other hand, X-tremeGene 9 had the lowest transfection efficiency with only 13% GFP positive cells. Commercially available transfection reagents undergo self-assembly with negatively charged pDNA to from particles or complexes that are small enough for cellular uptake. Due to the positive charge of the complexes for polymer-based and cationic lipid-based reagents, the synthesized particles are able to interact with cellular membranes which is negatively charged, and thus be internalized by cells [211].

However, due to the high surface charge these complexes are known to cause cytotoxic effects [212, 213], which was also seen in this study. MTT assay measuring cell metabolic activity did show cytotoxic effect of these complexes on NIH-3T3 fibroblast cells, Figure A. 2. Cells treated with NanoSiCaPs complexes displayed highest viability with 83% viable cells, followed by X-tremeGENE 9 with 80% viable cells. In contrast, X-tremeGENE HP and Lipofectamine 2000 had only about 42% viable cells. Even though the gene transfection efficiency of these samples were higher than NanoSiCaPs complexes, the induced cytotoxicity observed for these complexes was significant. These results suggested that, depending on the type of tissue engineering application, choice of non-viral reagent will play a crucial role in determining the ultimate outcome.

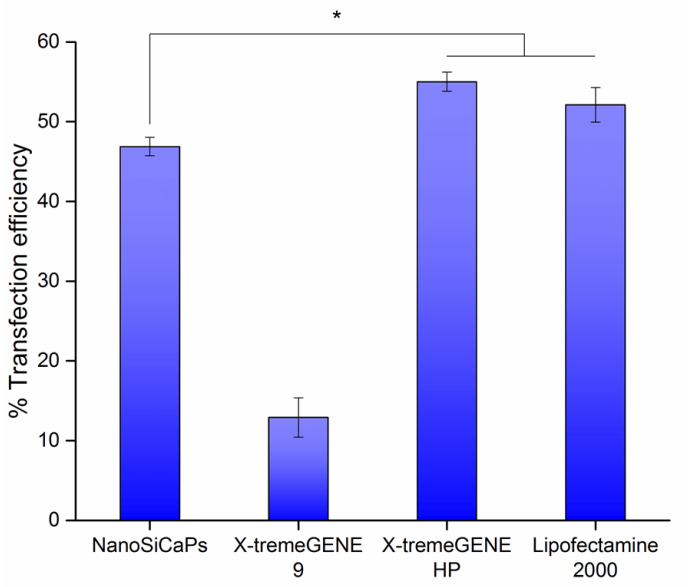

Figure A. 1. Transfection efficiency of NanoSiCaPs and commercial non-viral agents.

Flow cytometry analysis (at 24hours) of GFP transfected NIH-3T3 cells by different transfection reagents. The control used for the flow analysis included GFP negative cells receiving no treatment. The data were reported ± SD, n=3 ($p<0.05$). Post hoc analysis of the cell metabolic activity showed statistical significance between groups, indicated by the asterisk (*).

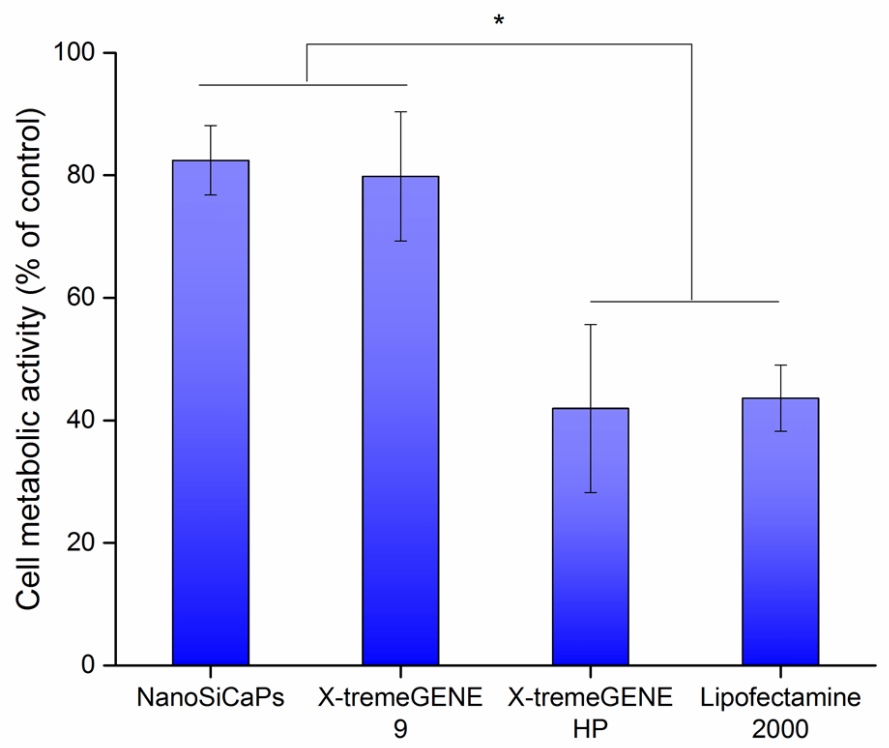

Figure A. 2. MTT assay showing cell metabolic activity.

MTT assay measuring in-vitro cell metabolic activity of NIH-3T3 cells by different transfection reagents at 24h. Data is normalized to control group that received no treatment. The data were reported ± SD, n=3 ($p<0.05$). Post hoc analysis of the cell metabolic activity showed statistical significance between groups, indicated by the asterisk (*).

BIBLIOGRAPHY

1. Rodan, G.A., *Introduction to bone biology.* Bone, 1992. **13**: p. S3-S6.

2. Berendsen, A.D. and B.R. Olsen, *Bone development.* Bone, 2015. **80**: p. 14-18.

3. O'Keefe, R.J. and J. Mao, *Bone Tissue Engineering and Regeneration: From Discovery to the Clinic—An Overview.* Tissue Engineering Part B: Reviews, 2011. **17**(6): p. 389-392.

4. Atala, A., F.K. Kasper, and A.G. Mikos, *Engineering Complex Tissues.* Science Translational Medicine, 2012. **4**(160): p. 160rv12-160rv12.

5. Williams, D.F., *To engineer is to create: the link between engineering and regeneration.* Trends in Biotechnology, 2006. **24**(1): p. 4-8.

6. Langer, R. and J. Vacanti, *Tissue engineering.* Science, 1993. **260**(5110): p. 920-926.

7. Raftery, R.M., et al., *Delivering Nucleic-Acid Based Nanomedicines on Biomaterial Scaffolds for Orthopedic Tissue Repair: Challenges, Progress and Future Perspectives.* Adv Mater, 2016. **28**(27): p. 5447-69.

8. Elaine, Q., et al., *Controlled release of vascular endothelial growth factor from spray-dried alginate microparticles in collagen–hydroxyapatite scaffolds for promoting vascularization and bone repair.* Journal of Tissue Engineering and Regenerative Medicine, 2017. **11**(4): p. 1097-1109.

9. Moncion, A., et al., *Controlled release of basic fibroblast growth factor for angiogenesis using acoustically-responsive scaffolds.* Biomaterials, 2017. **140**: p. 26-36.

10. Bao, X., et al., *3D biomimetic artificial bone scaffolds with dual-cytokines spatiotemporal delivery for large weight-bearing bone defect repair.* Scientific Reports, 2017. **7**(1): p. 7814.

11. S., M.F., et al., *Cytokine Secreting Microparticles Engineer the Fate and the Effector Functions of T-Cells.* Advanced Materials, 2018. **30**(7): p. 1703178.

12. Raftery, R.M., et al., *Development of a gene-activated scaffold platform for tissue engineering applications using chitosan-pDNA nanoparticles on collagen-based scaffolds.* Journal of Controlled Release, 2015. **210**: p. 84-94.

13. Tomas, G.-F., et al., *Gene Delivery of TGF-β3 and BMP2 in an MSC-Laden Alginate Hydrogel for Articular Cartilage and Endochondral Bone Tissue Engineering.* Tissue Engineering Part A, 2016. **22**(9-10): p. 776-787.

14. Bleich, N.K., et al., *Gene therapy approaches to regenerating bone.* Advanced drug delivery reviews, 2012. **64**(12): p. 1320-1330.

15. D'Mello, S., et al., *Bone Regeneration Using Gene-Activated Matrices.* Aaps j, 2017. **19**(1): p. 43-53.

16. Kumar, P., B. Vinitha, and G. Fathima, *Bone grafts in dentistry.* Journal of Pharmacy & Bioallied Sciences, 2013. **5**(Suppl 1): p. S125-S127.

17. Friedlaender, G.E., et al., *Osteogenic protein-1 (bone morphogenetic protein-7) in the treatment of tibial nonunions.* J Bone Joint Surg Am, 2001. **83-A Suppl 1**(Pt 2): p. S151-8.

18. McKay, W.F., S.M. Peckham, and J.M. Badura, *A comprehensive clinical review of recombinant human bone morphogenetic protein-2 (INFUSE Bone Graft).* Int Orthop, 2007. **31**(6): p. 729-34.

19. Shimer, A.L., F.C. Öner, and A.R. Vaccaro, *Spinal reconstruction and bone morphogenetic proteins: Open questions.* Injury, 2009. **40**: p. S32-S38.

20. Rose, L. and H. Uludağ, *Realizing the potential of gene-based molecular therapies in bone repair.* Journal of Bone and Mineral Research, 2013. **28**(11): p. 2245-2262.

21. Hill, A.B., et al., *Overcoming Gene-Delivery Hurdles: Physiological Considerations for Nonviral Vectors.* Trends Biotechnol, 2016. **34**(2): p. 91-105.

22. Finer, M. and J. Glorioso, *A brief account of viral vectors and their promise for gene therapy.* Gene Ther, 2017. **24**(1): p. 1-2.

23. Coelho-Castelo, A., et al., *Tissue distribution of a plasmid DNA encoding Hsp65 gene is dependent on the dose administered through intramuscular delivery.* Genetic Vaccines and Therapy, 2006. **4**(1): p. 1.

24. Hengge, U.R., B. Dexling, and A. Mirmohammadsadegh, *Safety and Pharmacokinetics of Naked Plasmid DNA in the Skin: Studies on Dissemination and Ectopic Expression11Presented in part at the 28th Annual Meeting of the European Society for Dermatological Research, Montpellier, France, September 22–25, 1999.* Journal of Investigative Dermatology, 2001. **116**(6): p. 979-982.

25. Bonadio, J., *Tissue engineering via local gene delivery:: Update and future prospects for enhancing the technology.* Advanced Drug Delivery Reviews, 2000. **44**(2): p. 185-194.

26. Oliver, B., et al., *Gene transfer strategies in tissue engineering.* Journal of Cellular and Molecular Medicine, 2007. **11**(2): p. 206-223.

27. Lee, D., K. Upadhye, and P.N. Kumta, *Nano-sized calcium phosphate (CaP) carriers for non-viral gene delivery.* Materials Science and Engineering B-Advanced Functional Solid-State Materials, 2012. **177**(3): p. 289-302.

28. Zhu, L. and R.I. Mahato, *Lipid and polymeric carrier-mediated nucleic acid delivery.* Expert Opinion on Drug Delivery, 2010. **7**(10): p. 1209-1226.

29. Gao, X., K.S. Kim, and D.X. Liu, *Nonviral gene delivery: What we know and what is next.* Aaps Journal, 2007. **9**(1): p. E92-E104.

30. Escoffre, J.M., J. Teissie, and M.P. Rols, *Gene Transfer: How Can the Biological Barriers Be Overcome?* Journal of Membrane Biology, 2010. **236**(1): p. 61-74.

31. Jafari, M., et al., *Nonviral Approach for Targeted Nucleic Acid Delivery.* Current Medicinal Chemistry, 2012. **19**(2): p. 197-208.

32. Mehier-Humbert, S. and R.H. Guy, *Physical methods for gene transfer: Improving the kinetics of gene delivery into cells.* Advanced Drug Delivery Reviews, 2005. **57**(5): p. 733-753.

33. Mahvi, D.M., M.J. Sheehy, and N.S. Yang, *DNA cancer vaccines: A gene gun approach.* Immunology and Cell Biology, 1997. **75**(5): p. 456-460.

34. Prud'homme, G.J., et al., *Electroporation-enhanced nonviral gene transfer for the prevention or treatment of immunological, endocrine and neoplastic diseases.* Current Gene Therapy, 2006. **6**(2): p. 243-273.

35. Andre, F. and L.M. Mir, *DNA electrotransfer: its principles and an updated review of its therapeutic applications.* Gene Therapy, 2004. **11**: p. S33-S42.

36. Muramatsu, T., A. Nakamura, and H.M. Park, *In vivo electroporation: A powerful and convenient means of nonviral gene transfer to tissues of living animals (Review).* International Journal of Molecular Medicine, 1998. **1**(1): p. 55-62.

37. Yin, H., et al., *Non-viral vectors for gene-based therapy.* Nat Rev Genet, 2014. **15**(8): p. 541-55.

38. Keeler, A.M., M.K. ElMallah, and T.R. Flotte, *Gene Therapy 2017: Progress and Future Directions.* Clinical and Translational Science, 2017. **10**(4): p. 242-248.

39. Oyane, A., et al., *Calcium phosphate composite layers for surface-mediated gene transfer.* Acta Biomaterialia, 2012. **8**(6): p. 2034-2046.

40. M. C. Hung, L.H., and E. Wagner, *Nonviral Vectors for Gene Therapy*. 1st ed. 1999: Academic Press, Washington, D.C.

41. Lemarchand, P., et al., *Adenovirus-mediated transfer of a recombinant human alpha-1-antitrypsin cdna to human endothelial-cells.* Proceedings of the National Academy of Sciences of the United States of America, 1992. **89**(14): p. 6482-6486.

42. Harris, J.D. and N.R. Lemoine, *Strategies for targeted gene therapy.* Trends in Genetics, 1996. **12**(10): p. 400-405.

43. Miller, N. and R. Vile, *Targeted vectors for gene-therapy.* Faseb Journal, 1995. **9**(2): p. 190-199.

44. R., F.T., *Gene and Cell Therapy in 2018: A Look Ahead.* Human Gene Therapy, 2018. **29**(1): p. 1-1.

45. Zhang, X. and W.T. Godbey, *Viral vectors for gene delivery in tissue engineering.* Advanced Drug Delivery Reviews, 2006. **58**(4): p. 515-534.

46. Pack, D.W., et al., *Design and development of polymers for gene delivery.* Nature Reviews Drug Discovery, 2005. **4**: p. 581.

47. Lipchina, I., et al., *Genome-wide identification of microRNA targets in human ES cells reveals a role for miR-302 in modulating BMP response.* Genes Dev, 2011. **25**(20): p. 2173-86.

48. Jose, L.S., et al., *Non-Viral Gene Delivery to Mesenchymal Stem Cells: Methods, Strategies and Application in Bone Tissue Engineering and Regeneration.* Current Gene Therapy, 2011. **11**(1): p. 46-57.

49. Zhang, X.X., T.J. McIntosh, and M.W. Grinstaff, *Functional lipids and lipoplexes for improved gene delivery.* Biochimie, 2012. **94**(1): p. 42-58.

50. Xu, L. and T. Anchordoquy, *Drug Delivery Trends in Clinical Trials and Translational Medicine: Challenges and Opportunities in the Delivery of Nucleic Acid-Based Therapeutics.* Journal of Pharmaceutical Sciences, 2011. **100**(1): p. 38-52.

51. Tros de Ilarduya, C., Y. Sun, and N. Duzgunes, *Gene delivery by lipoplexes and polyplexes.* European journal of pharmaceutical sciences : official journal of the European Federation for Pharmaceutical Sciences, 2010. **40**(3): p. 159-70.

52. Midoux, P., et al., *Chemical vectors for gene delivery: a current review on polymers, peptides and lipids containing histidine or imidazole as nucleic acids carriers.* British Journal of Pharmacology, 2009. **157**(2): p. 166-178.

53. Abdallah, B., L. Sachs, and B.A. Demeneix, *Non-viral gene transfer: Applications in developmental biology and gene therapy.* Biology of the Cell, 1995. **85**(1): p. 1-7.

54. Godbey, W.T., et al., *Poly(ethylenimine)-mediated transfection: A new paradigm for gene delivery.* Journal of Biomedical Materials Research, 2000. **51**(3): p. 321-328.

55. Neu, M., D. Fischer, and T. Kissel, *Recent advances in rational gene transfer vector design based on poly(ethylene imine) and its derivatives.* Journal of Gene Medicine, 2005. **7**(8): p. 992-1009.

56. Kichler, A., *Gene transfer with modified polyethylenimines.* Journal of Gene Medicine, 2004. **6**: p. S3-S10.

57. Wong, S.Y., J.M. Pelet, and D. Putnam, *Polymer systems for gene delivery-past, present, and future.* Progress in Polymer Science, 2007. **32**(8-9): p. 799-837.

58. Thomas, M. and A.M. Klibanov, *Non-viral gene therapy: polycation-mediated DNA delivery.* Applied Microbiology and Biotechnology, 2003. **62**(1): p. 27-34.

59. De Smedt, S.C., J. Demeester, and W.E. Hennink, *Cationic polymer based gene delivery systems.* Pharmaceutical Research, 2000. **17**(2): p. 113-126.

60. Chen, C. and H. Okayama, *High-efficiency transformation of mammalian-cells by plasmid dna.* Molecular and Cellular Biology, 1987. **7**(8): p. 2745-2752.

61. Chen, C.A. and H. Okayama, *Calcium phosphate-mediated gene-transfer - a highly efficient transfection system for stably transforming cells with plasmid dna.* Biotechniques, 1988. **6**(7): p. 632-&.

62. Roy, I., et al., *Calcium phosphate nanoparticles as novel non-viral vectors for targeted gene delivery.* International Journal of Pharmaceutics, 2003. **250**(1): p. 25-33.

63. Welzel, T., et al., *Transfection of cells with custom-made calcium phosphate nanoparticles coated with DNA.* Journal of Materials Chemistry, 2004. **14**(14): p. 2213-2217.

64. Sokolova, V.V., et al., *Effective transfection of cells with multi-shell calcium phosphate-DNA nanoparticles.* Biomaterials, 2006. **27**(16): p. 3147-3153.

65. Sokolova, V. and M. Epple, *Inorganic nanoparticles as carriers of nucleic acids into cells.* Angewandte Chemie-International Edition, 2008. **47**(8): p. 1382-1395.

66. Olton, D.Y.E., et al., *Intracellular trafficking pathways involved in the gene transfer of nano-structured calcium phosphate-DNA particles.* Biomaterials, 2011. **32**(30): p. 7662-7670.

67. Olton, D., et al., *Nanostructured calcium phosphates (NanoCaPs) for non-viral gene delivery: Influence of the synthesis parameters on transfection efficiency.* Biomaterials, 2007. **28**(6): p. 1267-1279.

68. Kumta, P.N., et al., *Nanostructured calcium phosphates for biomedical applications: novel synthesis and characterization.* Acta Biomaterialia, 2005. **1**(1): p. 65-83.

69. Narayan, R.J., et al., *Nanostructured ceramics in medical devices: Applications and prospects.* Jom, 2004. **56**(10): p. 38-43.

70. Yamano, S., J. Dai, and A.M. Moursi, *Comparison of transfection efficiency of nonviral gene transfer reagents.* Mol Biotechnol, 2010. **46**(3): p. 287-300.

71. Hickman, M.A., et al., *Gene expression following direct injection of DNA into liver.* Hum Gene Ther, 1994. **5**(12): p. 1477-83.

72. Bisht, S., et al., *pDNA loaded calcium phosphate nanoparticles: highly efficient non-viral vector for gene delivery.* Int J Pharm, 2005. **288**(1): p. 157-68.

73. Batard, P., M. Jordan, and F. Wurm, *Transfer of high copy number plasmid into mammalian cells by calcium phosphate transfection.* Gene, 2001. **270**(1-2): p. 61-68.

74. Cheng, L., P.R. Ziegelhoffer, and N.S. Yang, *In vivo promoter activity and transgene expression in mammalian somatic tissues evaluated by using particle bombardment.* Proceedings of the National Academy of Sciences of the United States of America, 1993. **90**(10): p. 4455-4459.

75. Fillion, P., et al., *Encapsulation of DNA in negatively charged liposomes and inhibition of bacterial gene expression with fluid liposome-encapsulated antisense oligonucleotides.* Biochim Biophys Acta, 2001. **1515**(1): p. 44-54.

76. Jiao, S., et al., *Particle bombardment-mediated gene transfer and expression in rat brain tissues.* Biotechnology (N Y), 1993. **11**(4): p. 497-502.

77. Maurer, N., et al., *Lipid-based systems for the intracellular delivery of genetic drugs.* Mol Membr Biol, 1999. **16**(1): p. 129-40.

78. McKenzie, D.L., K.Y. Kwok, and K.G. Rice, *A potent new class of reductively activated peptide gene delivery agents.* J Biol Chem, 2000. **275**(14): p. 9970-7.

79. Sikes, M.L., et al., *In-Vivo Gene-Transfer into Rabbit Thyroid Follicular Cells by Direct DNA Injection.* Human Gene Therapy, 1994. **5**(7): p. 837-844.

80. Somiari, S., et al., *Theory and in vivo application of electroporative gene delivery.* Mol Ther, 2000. **2**(3): p. 178-87.

81. Trentin, D., J. Hubbell, and H. Hall, *Non-viral gene delivery for local and controlled DNA release.* J Control Release, 2005. **102**(1): p. 263-75.

82. Sokolova, V. and M. Epple, *Inorganic nanoparticles as carriers of nucleic acids into cells.* Angew Chem Int Ed Engl, 2008. **47**(8): p. 1382-95.

83. Wang, P., et al., *Bone tissue engineering via nanostructured calcium phosphate biomaterials and stem cells.* Bone Res, 2014. **2**: p. 14017.

84. Kanazawa, T., ed. *Inorganic phosphate materials: Materials Science Monographs # 52.* 1989, Elsevier Science Publishers, Amsterdam. 304.

85. K. Groot, C.P.A.T.K., J.G.C. Wolke, and J.M.A. de Blieck-Hogervorst, ed. *Chemistry of Calcium Phosphate Bioceramics*. CRC Handbook of Bioactive Ceramics: Volume II; Calcium Phosphate and Hydroxylapatite Ceramics, ed. a.L.L.H. T. Yamamuro, and J. Wilson. Vol. II, Ch. 1. 1990, CRC Press, Boca Raton, FL.

86. Legeros, R.Z., *Calcium phosphates in oral biology and medicine. Monographs in Oral Science.* Vol. 15. 1991: Basel, Karger.

87. Elliot, J.C., *Structures and Chemistry of the Apatites and Other Calcium Orthophosphates. Studies in Inorganic Chemistry*. Vol. 18. 1994: Elsevier; Amsterdam.

88. Constantz, P.W.B.a.B., *Hydroxyapatite and related materials*. 1994, Boca Raton : CRC. p. 343.

89. Olszta, M.J., et al., *Bone structure and formation: A new perspective.* Materials Science & Engineering R-Reports, 2007. **58**(3-5): p. 77-116.

90. Young, J.L., J.N. Benoit, and D.A. Dean, *Effect of a DNA Nuclear Targeting Sequence on Gene Transfer and Expression of Plasmids in the Intact Vasculature.* Gene therapy, 2003. **10**(17): p. 1465-1470.

91. Mesika, A., et al., *Enhanced intracellular mobility and nuclear accumulation of DNA plasmids associated with a karyophilic protein.* Hum Gene Ther, 2005. **16**(2): p. 200-8.

92. Hoare, M., et al., *Enhanced lipoplex-mediated gene expression in mesenchymal stem cells using reiterated nuclear localization sequence peptides.* J Gene Med, 2010. **12**(2): p. 207-18.

93. Jordan, M., A. Schallhorn, and F.M. Wurm, *Transfecting Mammalian Cells: Optimization of Critical Parameters Affecting Calcium-Phosphate Precipitate Formation.* Nucleic Acids Research, 1996. **24**(4): p. 596-601.

94. Rejman, J., et al., *Size-dependent internalization of particles via the pathways of clathrin- and caveolae-mediated endocytosis.* Biochem J, 2004. **377**(Pt 1): p. 159-69.

95. Li, J., et al., *Biodegradable calcium phosphate nanoparticle with lipid coating for systemic siRNA delivery.* J Control Release, 2010. **142**(3): p. 416-21.

96. Lee, K., et al., *Stabilized calcium phosphate nano-aggregates using a dopa-chitosan conjugate for gene delivery.* Int J Pharm, 2013. **445**(1-2): p. 196-202.

97. Chowdhury, E.H. and T. Akaike, *High performance DNA nano-carriers of carbonate apatite: multiple factors in regulation of particle synthesis and transfection efficiency.* Int J Nanomedicine, 2007. **2**(1): p. 101-6.

98. Chowdhury, E.H., et al., *High-efficiency gene delivery for expression in mammalian cells by nanoprecipitates of Ca–Mg phosphate.* Gene, 2004. **341**(0): p. 77-82.

99. Chowdhury, E.H., et al., *pH-sensing nano-crystals of carbonate apatite: effects on intracellular delivery and release of DNA for efficient expression into mammalian cells.* Gene, 2006. **376**(1): p. 87-94.

100. Chowdhury, E.H., et al., *Dramatic effect of Mg2+ on transfecting mammalian cells by DNA/calcium phosphate precipitates.* Analytical Biochemistry, 2004. **328**(1): p. 96-97.

101. Chowdhury, E.H., et al., *Fibronectin in collaboration with Mg2+ enhances transgene expression by calcium phosphate coprecipitates.* Analytical Biochemistry, 2004. **335**(1): p. 162-164.

102. Hanifi, A., M.H. Fathi, and H. Mir Mohammad Sadeghi, *Effect of strontium ions substitution on gene delivery related properties of calcium phosphate nanoparticles.* Journal of Materials Science: Materials in Medicine, 2010. **21**(9): p. 2601-2609.

103. Wiethoff, C.M. and C.R. Middaugh, *Barriers to nonviral gene delivery.* J Pharm Sci, 2003. **92**(2): p. 203-17.

104. Chowdhury, E.H., *Fluoride enhances transfection activity of carbonate apatite by increasing cytoplasmic stability of plasmid DNA.* Biochem Biophys Res Commun, 2011. **409**(4): p. 745-7.

105. Chowdhury, E.H., et al., *High-efficiency gene delivery for expression in mammalian cells by nanoprecipitates of Ca-Mg phosphate.* Gene, 2004. **341**(0): p. 77-82.

106. Hanifi, A., M.H. Fathi, and H. Mir Mohammad Sadeghi, *Effect of strontium ions substitution on gene delivery related properties of calcium phosphate nanoparticles.* J Mater Sci Mater Med, 2010. **21**(9): p. 2601-9.

107. Hanifi, A., et al., *Mg2+ substituted calcium phosphate nano particles synthesis for non viral gene delivery application.* J Mater Sci Mater Med, 2010. **21**(8): p. 2393-401.

108. LeGeros, R.Z., *Calcium phosphates in oral biology and medicine.* Monogr Oral Sci, 1991. **15**: p. 1-201.

109. Hing, K.A., et al., *Effect of silicon level on rate, quality and progression of bone healing within silicate-substituted porous hydroxyapatite scaffolds.* Biomaterials, 2006. **27**(29): p. 5014-5026.

110. Allison, S.D. and T.J. Anchordoquy, *Lyophilization of nonviral gene delivery systems.* Methods Mol Med, 2001. **65**: p. 225-52.

111. Anchordoquy, T.J. and G.S. Koe, *Physical stability of nonviral plasmid-based therapeutics.* J Pharm Sci, 2000. **89**(3): p. 289-96.

112. Abdelwahed, W., et al., *Freeze-drying of nanoparticles: formulation, process and storage considerations.* Adv Drug Deliv Rev, 2006. **58**(15): p. 1688-713.

113. Allison, S.D., M.C. Molina, and T.J. Anchordoquy, *Stabilization of lipid/DNA complexes during the freezing step of the lyophilization process: the particle isolation hypothesis.* Biochim Biophys Acta, 2000. **1468**(1-2): p. 127-38.

114. Molina, M., et al., *The stability of lyophilized lipid/DNA complexes during prolonged storage.* J Pharm Sci, 2004. **93**(9): p. 2259-73.

115. Cherng, J.Y., et al., *Freeze-drying of poly((2-dimethylamino)ethyl methacrylate)-based gene delivery systems.* Pharm Res, 1997. **14**(12): p. 1838-41.

116. Talsma, H., et al., *Stabilization of gene delivery systems by freeze-drying.* Int J Pharm, 1997. **157**(2): p. 233-238.

117. Kasper, J.C., et al., *Development of a lyophilized plasmid/LPEI polyplex formulation with long-term stability--A step closer from promising technology to application.* J Control Release, 2011. **151**(3): p. 246-55.

118. Owens, B.D., et al., *Combat wounds in operation Iraqi freedom and operation enduring freedom.* Journal of Trauma-Injury Infection and Critical Care, 2008. **64**(2): p. 295-299.

119. Stevens, M.M. and J.H. George, *Exploring and engineering the cell surface interface.* Science, 2005. **310**(5751): p. 1135-8.

120. Civantos, A., et al., *Titanium Coatings and Surface Modifications: Toward Clinically Useful Bioactive Implants.* ACS Biomaterials Science & Engineering, 2017. **3**(7): p. 1245-1261.

121. Narayanan, R., et al., *Calcium phosphate-based coatings on titanium and its alloys.* J Biomed Mater Res B Appl Biomater, 2008. **85**(1): p. 279-99.

122. Oyane, A., et al., *Controlled superficial assembly of DNA-amorphous calcium phosphate nanocomposite spheres for surface-mediated gene delivery.* Colloids Surf B Biointerfaces, 2016. **141**: p. 519-527.

123. Yazaki, Y., et al., *Area-specific cell stimulation via surface-mediated gene transfer using apatite-based composite layers.* Int J Mol Sci, 2015. **16**(4): p. 8294-309.

124. Shen, H., J. Tan, and W.M. Saltzman, *Surface-mediated gene transfer from nanocomposites of controlled texture.* Nature Materials, 2004. **3**: p. 569.

125. Fasbender, A., et al., *Incorporation of adenovirus in calcium phosphate precipitates enhances gene transfer to airway epithelia in vitro and in vivo.* Journal of Clinical Investigation, 1998. **102**(1): p. 184-193.

126. Endo, M., et al., *Bone regeneration by modified gene-activated matrix: Effectiveness in segmental tibial defects in rats.* Tissue Engineering, 2006. **12**(3): p. 489-497.

127. Ng, J., et al., *Biomimetic Approaches for Bone Tissue Engineering.* Tissue Eng Part B Rev, 2017.

128. Lavik, E. and R. Langer, *Tissue engineering: current state and perspectives.* Applied Microbiology and Biotechnology, 2004. **65**(1): p. 1-8.

129. Ramaswamy, S., et al., *An analysis of the integration between articular cartilage and nondegradable hydrogel using magnetic resonance imaging.* Journal of Biomedical Materials Research Part B: Applied Biomaterials, 2006. **77B**(1): p. 144-148.

130. Williams, C.G., et al., *In Vitro Chondrogenesis of Bone Marrow-Derived Mesenchymal Stem Cells in a Photopolymerizing Hydrogel.* Tissue Engineering, 2003. **9**(4): p. 679-688.

131. Raisin, S., E. Belamie, and M. Morille, *Non-viral gene activated matrices for mesenchymal stem cells based tissue engineering of bone and cartilage.* Biomaterials, 2016. **104**(Supplement C): p. 223-237.

132. Orrantia, E. and P.L. Chang, *Intracellular-Distribution of DNA Internalized through Calcium-Phosphate Precipitation.* Experimental Cell Research, 1990. **190**(2): p. 170-174.

133. Jordan, M., A. Schallhorn, and F.M. Wurm, *Transfecting mammalian cells: optimization of critical parameters affecting calcium-phosphate precipitate formation.* Nucleic Acids Res, 1996. **24**(4): p. 596-601.

134. Hing, K.A., et al., *Effect of silicon level on rate, quality and progression of bone healing within silicate-substituted porous hydroxyapatite scaffolds.* Biomaterials, 2006. **27**(29): p. 5014-26.

135. Marchat, D., et al., *Accurate characterization of pure silicon-substituted hydroxyapatite powders synthesized by a new precipitation route.* Acta Biomater, 2013. **9**(6): p. 6992-7004.

136. Hayakawa, S., et al., *Heterogeneous structure and in vitro degradation behavior of wet-chemically derived nanocrystalline silicon-containing hydroxyapatite particles.* Acta Biomater, 2013. **9**(1): p. 4856-67.

137. Porter, A.E., et al., *Comparison of in vivo dissolution processes in hydroxyapatite and silicon-substituted hydroxyapatite bioceramics.* Biomaterials, 2003. **24**(25): p. 4609-20.

138. Choi, D. and P.N. Kumta, *An alternative chemical route for the synthesis and thermal stability of chemically enriched hydroxyapatite.* Journal of the American Ceramic Society, 2006. **89**(2): p. 444-449.

139. Olton, D., et al., *Nanostructured calcium phosphates (NanoCaPs) for non-viral gene delivery: influence of the synthesis parameters on transfection efficiency.* Biomaterials, 2007. **28**(6): p. 1267-79.

140. Chen, J.J., et al., *Solubility and structure of calcium silicate hydrate.* Cement and Concrete Research, 2004. **34**(9): p. 1499-1519.

141. Bang, L.T., B.D. Long, and R. Othman, *Carbonate hydroxyapatite and silicon-substituted carbonate hydroxyapatite: synthesis, mechanical properties, and solubility evaluations.* ScientificWorldJournal, 2014. **2014**: p. 969876.

142. Yu, P., et al., *Structure of Calcium Silicate Hydrate (C-S-H): Near-, Mid-, and Far-Infrared Spectroscopy.* Journal of the American Ceramic Society, 1999. **82**(3): p. 742-748.

143. Porter, A.E., *Nanoscale characterization of the interface between bone and hydroxyapatite implants and the effect of silicon on bone apposition.* Micron, 2006. **37**(8): p. 681-8.

144. Pietak, A.M., et al., *Silicon substitution in the calcium phosphate bioceramics.* Biomaterials, 2007. **28**(28): p. 4023-32.

145. Pietak, A.M., J.W. Reid, and M. Sayer, *Electron spin resonance in silicon substituted apatite and tricalcium phosphate.* Biomaterials, 2005. **26**(18): p. 3819-30.

146. Camire, C.L., et al., *Material characterization and in vivo behavior of silicon substituted alpha-tricalcium phosphate cement.* J Biomed Mater Res B Appl Biomater, 2006. **76**(2): p. 424-31.

147. Porter, A.E., S.M. Best, and W. Bonfield, *Ultrastructural comparison of hydroxyapatite and silicon-substituted hydroxyapatite for biomedical applications.* J Biomed Mater Res A, 2004. **68**(1): p. 133-41.

148. Zou, S., et al., *Crystal imperfection studies of pure and silicon substituted hydroxyapatite using Raman and XRD.* J Mater Sci Mater Med, 2005. **16**(12): p. 1143-8.

149. Gibson, I.R., S.M. Best, and W. Bonfield, *Chemical characterization of silicon-substituted hydroxyapatite.* J Biomed Mater Res, 1999. **44**(4): p. 422-8.

150. Vandiver, J., et al., *Silicon addition to hydroxyapatite increases nanoscale electrostatic, van der Waals, and adhesive interactions.* J Biomed Mater Res A, 2006. **78**(2): p. 352-63.

151. Bianco, A., et al., *Thermal stability and sintering behaviour of hydroxyapatite nanopowders.* Journal of Thermal Analysis and Calorimetry, 2007. **88**(1): p. 237-243.

152. Xu, G., I.A. Aksay, and J.T. Groves, *Continuous crystalline carbonate apatite thin films. A biomimetic approach.* Journal of the American Chemical Society, 2001. **123**(10): p. 2196-203.

153. Leeuwenburgh, S.C.G., et al., *Influence of precursor solution parameters on chemical properties of calcium phosphate coatings prepared using Electrostatic Spray Deposition (ESD).* Biomaterials, 2004. **25**(4): p. 641-649.

154. Kumta, P.N., et al., *Nanostructured calcium phosphates for biomedical applications: novel synthesis and characterization.* Acta Biomaterialia, 2005. **1**(1): p. 65-83.

155. Sadat-Shojai, M., et al., *Synthesis methods for nanosized hydroxyapatite with diverse structures.* Acta Biomaterialia, 2013. **9**(8): p. 7591-7621.

156. Liou, S.-C., et al., *Structural characterization of nano-sized calcium deficient apatite powders.* Biomaterials, 2004. **25**(2): p. 189-196.

157. Palazzo, B., et al., *Amino acid synergetic effect on structure, morphology and surface properties of biomimetic apatite nanocrystals.* Acta Biomaterialia, 2009. **5**(4): p. 1241-1252.

158. Koutsopoulos, S., *Synthesis and characterization of hydroxyapatite crystals: A review study on the analytical methods.* Journal of Biomedical Materials Research, 2002. **62**(4): p. 600-612.

159. Shepard, J.A., et al., *Balancing cell migration with matrix degradation enhances gene delivery to cells cultured three-dimensionally within hydrogels.* Journal of controlled release : official journal of the Controlled Release Society, 2010. **146**(1): p. 128-135.

160. Shekhar, S., et al., *Nanostructured silicate substituted calcium phosphate (NanoSiCaPs) nanoparticles — Efficient calcium phosphate based non-viral gene delivery systems.* Materials Science and Engineering: C, 2016. **69**: p. 486-495.

161. Anderson, J.M., A. Rodriguez, and D.T. Chang, *Foreign body reaction to biomaterials.* Semin Immunol, 2008. **20**(2): p. 86-100.

162. Mitragotri, S. and J. Lahann, *Physical approaches to biomaterial design.* Nat Mater, 2009. **8**(1): p. 15-23.

163. Hench, L.L. and J.M. Polak, *Third-generation biomedical materials.* Science, 2002. **295**(5557): p. 1014-7.

164. Jewell, C.M. and D.M. Lynn, *Multilayered polyelectrolyte assemblies as platforms for the delivery of DNA and other nucleic acid-based therapeutics.* Adv Drug Deliv Rev, 2008. **60**(9): p. 979-99.

165. Shen, H., J. Tan, and W.M. Saltzman, *Surface-mediated gene transfer from nanocomposites of controlled texture.* Nat Mater, 2004. **3**(8): p. 569-74.

166. Rao, R.R., J. He, and J.K. Leach, *Biomineralized composite substrates increase gene expression with nonviral delivery.* Journal of Biomedical Materials Research Part A, 2010. **94A**(2): p. 344-354.

167. Hu, Y., et al., *Surface mediated in situ differentiation of mesenchymal stem cells on gene-functionalized titanium films fabricated by layer-by-layer technique.* Biomaterials, 2009. **30**(21): p. 3626-3635.

168. Civantos, A., et al., *Titanium Coatings and Surface Modifications: Toward Clinically Useful Bioactive Implants.* ACS Biomaterials Science & Engineering, 2017.

169. Qiu, Z.Y., et al., *Advances in the surface modification techniques of bone-related implants for last 10 years.* Regen Biomater, 2014. **1**(1): p. 67-79.

170. Junker, R., et al., *Effects of implant surface coatings and composition on bone integration: a systematic review.* Clin Oral Implants Res, 2009. **20 Suppl 4**: p. 185-206.

171. Olton, D., et al., *Nanostructured calcium phosphates (NanoCaPs) for non-viral gene delivery: Influence of the synthesis parameters on transfection efficiency.* Biomaterials, 2007. **28**(6): p. 1267-1279.

172. Kunjukunju, S., et al., *A layer-by-layer approach to natural polymer-derived bioactive coatings on magnesium alloys.* Acta Biomaterialia, 2013. **9**(10): p. 8690-8703.

173. Li, H. and C.P. Tripp, *Infrared study of the interaction of charged silica particles with TiO2 particles containing adsorbed cationic and anionic polyelectrolytes.* Langmuir, 2005. **21**(6): p. 2585-90.

174. Zhao, X.Y., et al., *Calcium phosphate hybrid nanoparticles: self-assembly formation, characterization, and application as an anticancer drug nanocarrier.* Chem Asian J, 2013. **8**(6): p. 1306-12.

175. Lavenus, S., et al., *Cell interaction with nanopatterned surface of implants.* Nanomedicine (Lond), 2010. **5**(6): p. 937-47.

176. Michna, A., et al., *Formation of PDADMAC monolayers evaluated in situ by QCM and streaming potential measurements.* Journal of Colloid and Interface Science, 2014. **428**: p. 170-177.

177. Wandrey, C., J. Hernández-Barajas, and D. Hunkeler, *Diallyldimethylammonium Chloride and its Polymers*, in *Radical Polymerisation Polyelectrolytes*, I. Capek, et al., Editors. 1999, Springer Berlin Heidelberg: Berlin, Heidelberg. p. 123-183.

178. Han, Z.-P., et al., *A general strategy for protein immobilization in layered titanates: Polyelectrolyte-assisted self-assembly.* Enzyme and Microbial Technology, 2013. **53**(2): p. 79-84.

179. Killmann, E., et al. *Adsorption of polyelectrolytes on colloidal particles — Electrostatic interactions and stability behaviour*. 1998. Darmstadt: Steinkopff.

180. Liu, L., et al., *Fabrication, characterization, and biological assessment of multilayer DNA coatings on sandblasted-dual acid etched titanium surface.* J Biomed Mater Res A, 2011. **97**(3): p. 300-10.

181. Yamauchi, F., et al., *Layer-by-layer assembly of cationic lipid and plasmid DNA onto gold surface for stent-assisted gene transfer.* Biomaterials, 2006. **27**(18): p. 3497-3504.

182. Shekhar, S., et al., *Surface mediated non-viral gene transfection on titanium substrates using polymer electrolyte and nanostructured silicate substituted calcium phosphate pDNA (NanoSiCaPs) composites.* Materials Today Communications, 2018. **16**: p. 169-173.

183. Balmayor, E.R. and M. van Griensven, *Gene Therapy for Bone Engineering.* Frontiers in Bioengineering and Biotechnology, 2015. **3**(9).

184. Brown, A.C. and T.H. Barker, *Fibrin-based biomaterials: modulation of macroscopic properties through rational design at the molecular level.* Acta Biomater, 2014. **10**(4): p. 1502-14.

185. Spotnitz, W.D., *Fibrin Sealant: The Only Approved Hemostat, Sealant, and Adhesive-a Laboratory and Clinical Perspective.* ISRN Surg, 2014. **2014**: p. 203943.

186. Whelan, D., N.M. Caplice, and A.J. Clover, *Fibrin as a delivery system in wound healing tissue engineering applications.* J Control Release, 2014. **196**: p. 1-8.

187. Sacchi, V., et al., *Long-lasting fibrin matrices ensure stable and functional angiogenesis by highly tunable, sustained delivery of recombinant VEGF164.* Proc Natl Acad Sci U S A, 2014. **111**(19): p. 6952-7.

188. Fujioka-Kobayashi, M., et al., *An in vitro study of fibrin sealant as a carrier system for recombinant human bone morphogenetic protein (rhBMP)-9 for bone tissue engineering.* J Craniomaxillofac Surg, 2017. **45**(1): p. 27-32.

189. van Esterik, F.A., et al., *Enhanced Osteogenic and Vasculogenic Differentiation Potential of Human Adipose Stem Cells on Biphasic Calcium Phosphate Scaffolds in Fibrin Gels.* Stem Cells Int, 2016. **2016**: p. 1934270.

190. Isogai, N., et al., *Experimental use of fibrin glue to induce site-directed osteogenesis from cultured periosteal cells.* Plast Reconstr Surg, 2000. **105**(3): p. 953-63.

191. Balmayor, E.R., et al., *Modified mRNA for BMP-2 in Combination with Biomaterials Serves as a Transcript-Activated Matrix for Effectively Inducing Osteogenic Pathways in Stem Cells.* Stem Cells Dev, 2017. **26**(1): p. 25-34.

192. Schek, R.M., S.J. Hollister, and P.H. Krebsbach, *Delivery and protection of adenoviruses using biocompatible hydrogels for localized gene therapy.* Mol Ther, 2004. **9**(1): p. 130-8.

193. Kidd, M.E., S. Shin, and L.D. Shea, *Fibrin hydrogels for lentiviral gene delivery in vitro and in vivo.* J Control Release, 2012. **157**(1): p. 80-5.

194. Lei, P., R.M. Padmashali, and S.T. Andreadis, *Cell-controlled and spatially arrayed gene delivery from fibrin hydrogels.* Biomaterials, 2009. **30**(22): p. 3790-9.

195. Lee, T.C., et al., *Bone morphogenetic protein gene therapy using a fibrin scaffold for a rabbit spinal-fusion experiment.* Neurosurgery, 2006. **58**(2): p. 373-80; discussion 373-80.

196. Kulkarni, M., et al., *Fibrin-lipoplex system for controlled topical delivery of multiple genes.* Biomacromolecules, 2009. **10**(6): p. 1650-4.

197. Cherng, J.Y., et al., *Stabilization of polymer-based gene delivery systems.* International Journal of Pharmaceutics, 1999. **183**(1): p. 25-28.

198. Anchordoquy, T.J., J.F. Carpenter, and D.J. Kroll, *Maintenance of Transfection Rates and Physical Characterization of Lipid/DNA Complexes after Freeze-Drying and Rehydration.* Archives of Biochemistry and Biophysics, 1997. **348**(1): p. 199-206.

199. Cherng, J.-Y., et al., *Long Term Stability of Poly((2-dimethylamino)ethyl Methacrylate)-Based Gene Delivery Systems.* Pharmaceutical Research, 1999. **16**(9): p. 1417-1423.

200. Aguilar, Z.P., *Chapter 5 - Targeted Drug Delivery*, in *Nanomaterials for Medical Applications*, Z.P. Aguilar, Editor. 2013, Elsevier. p. 181-234.

201. Allison, S.D. and T.J. Anchordoquy, *Mechanisms of protection of cationic lipid-DNA complexes during lyophilization.* J Pharm Sci, 2000. **89**(5): p. 682-91.

202. Maitani, Y., et al., *Effect of sugars on storage stability of lyophilized liposome/DNA complexes with high transfection efficiency.* Int J Pharm, 2008. **356**(1-2): p. 69-75.

203. Ho, W., et al., *The Behavior of Human Mesenchymal Stem Cells in 3D Fibrin Clots: Dependence on Fibrinogen Concentration and Clot Structure.* Tissue Engineering, 2006. **12**(6): p. 1587-1595.

204. Cox, S., M. Cole, and B. Tawil, *Behavior of Human Dermal Fibroblasts in Three-Dimensional Fibrin Clots: Dependence on Fibrinogen and Thrombin Concentration.* Tissue Engineering, 2004. **10**(5-6): p. 942-954.

205. Catelas, I., et al., *Human Mesenchymal Stem Cell Proliferation and Osteogenic Differentiation in Fibrin Gels in Vitro.* Tissue Engineering, 2006. **12**(8): p. 2385-2396.

206. des Rieux, A., A. Shikanov, and L.D. Shea, *Fibrin hydrogels for non-viral vector delivery in vitro.* Journal of Controlled Release, 2009. **136**(2): p. 148-154.

207. Wieland, J.A., T.L. Houchin-Ray, and L.D. Shea, *Non-viral vector delivery from PEG-hyaluronic acid hydrogels.* J Control Release, 2007. **120**(3): p. 233-41.

208. Herbert, C.B., G.D. Bittner, and J.A. Hubbell, *Effects of fibinolysis on neurite growth from dorsal root ganglia cultured in two- and three-dimensional fibrin gels.* J Comp Neurol, 1996. **365**(3): p. 380-91.

209. Sahin, U., K. Karikó, and Ö. Türeci, *mRNA-based therapeutics — developing a new class of drugs.* Nature Reviews Drug Discovery, 2014. **13**: p. 759.

210. Dalby, M.J., et al., *Osteoprogenitor response to semi-ordered and random nanotopographies.* Biomaterials, 2006. **27**(15): p. 2980-2987.

211. Dalby, B., et al., *Advanced transfection with Lipofectamine 2000 reagent: primary neurons, siRNA, and high-throughput applications.* Methods, 2004. **33**(2): p. 95-103.

212. Chen, D.J., et al., *Structure-function relationships of gene delivery vectors in a limited polycation library.* J Control Release, 2005. **103**(1): p. 273-83.

213. Choksakulnimitr, S., et al., *In vitro cytotoxicity of macromolecules in different cell culture systems.* Journal of Controlled Release, 1995. **34**(3): p. 233-241.